Relating phase separation and thickness mismatch in model lipid membranes.

Joan V. Bleecker

A dissertation submitted in partial fulfillment
of the requirements for the degree of

Doctor of Philosophy

University of Washington

2015

Reading Committee:

Sarah L. Keller, Chair

David S. Ginger Jr.

Lutz Maibaum

Program Authorized to Offer Degree:

Department of Chemistry

University of Washington

Abstract

Relating phase separation and thickness mismatch in model lipid membranes.

Joan V. Bleecker

Chair of Supervisory Committee:

Professor Sarah L. Keller
Department of Chemistry

Membrane lipids can spontaneously undergo a process called phase separation wherein they organize into domains with different compositions. Phase separation has been proposed as a mechanism in the formation of heterogeneous lipid regions (e.g. rafts) in cell membranes. The activity and partitioning of membrane proteins vary depending on the local lipid environment due both to hydrophobic thickness matching between the protein and lipids and to lipid packing (also known as lipid order). A major question is how these two parameters, thickness and order, vary with lipid composition. Many previous studies have treated membrane order and thickness as inextricably linked; thicker regions always have higher order. Other studies have attributed membrane thickness to properties of phase separation, including the temperature below which phases appear, T_{mix}, and the size of phase domains. In this thesis we present two studies that test whether the previously observed relationships among phase thickness, order, and T_{mix} are as straightforward as previously thought.

For the first study, we investigate whether in liquid-liquid phase separated membranes the more ordered phase need be thicker than the less ordered phase. We use non-canonical ternary lipid mixtures designed to produce thicker Ld than Lo phases and measure mixing temperatures in fluorescence. We find that few of these candidate systems produce coexisting liquid phases in vesicles. We also directly measure membrane thickness by atomic force microscopy and find that none of the systems produce thicker Ld than Lo phases under standard experimental conditions, although one system does after photo-oxidation. Interestingly, we find no simple monotonic relationship exists between the physical parameters of single-component lipid membranes and the highest demixing temperature of the corresponding ternary membranes. These results highlight the surprisingly robust propensity for the Lo phase to be thicker than the Ld phase, regardless of lipid composition.

In our second study, we provide an experimental counterpoint to the previously found trend that mixing temperatures depend strongly on the thickness mismatch of the two phases. We use measure mixing temperatures and thickness differences of membranes composed of different mole ratios of DiPhyPC/DPPC/chol in fluorescence microscopy and atomic force microscopy. We show trends in which membrane thickness differences do not uniquely predict mixing temperatures. Our results highlight the importance of membrane composition on the physical properties of phase separation.

ACKNOWLEDGMENTS

Thank you Sarah Keller, my incredible advisor.

Thank you to my lab mates, past and present.

Thank you to my family for all your encouragement. Especially to Eve Bleecker for putting up with me as I worked on my thesis.

To members of Women in the Chemical Sciences at UW for being the support I needed when I needed it. Thank you also to STEM OUT UW for the opportunity to serve my community.

To Motter, Britt and the rest of my non-department friends. Thank you for keeping me grounded.

To Colleen, Phil, Cynthia, Jake, and everyone else who helped me realize my dream to teach.

Funding:

I thank the Molecular Biophysics Training grant at UW (T32 GM008268) for funding my

fellowship proposal.

This research was supported by NSF MCB-1402059 and NSF MCB-0744852.

DEDICATION

To my parents, Stephen Bleecker and Elizabeth Harasek
who taught me to always be curious.

To Women in the Chemical Sciences at UW and STEM OUT
for allowing me to be of service.

TABLE OF CONTENTS

LIST OF FIGURES

LIST OF TABLES

Chapter 1

INTRODUCTION

1.1 Lipids, lipid bilayers, and vesicles

1.1.1 Lipid structure

Lipids are one of the fundamental building blocks of life (1). Lipids are amphiphiles, meaning a portion of their structure is hydrophilic ("water loving") while another portion is hydrophobic ("water hating"). (Figure 1-3).

The hydrophilic portion of the lipid is the head group. For our studies we use only phosphatidylcholine, PC, head groups, which have no net charge (zwitterionic) under standard conditions, as seen in Figures 1-3. The hydrophobic portion is the lipid tails, which are typically fatty acids between 14-22 carbons long (1). All the lipids in our studies have two tails with the same structure, although in nature the two tails may be different (2). For our studies, the tails are either saturated acyl chains, branched with methylated chains, or mono-unsaturated chains (Figure 1). For PC lipids, the two fatty acid tails are connected by ester linkages to a glycerol backbone. The final -OH in the glycerol is connected via a phosphate ester linkage to the phosphatidylcholine head groups.

We use two naming conventions for our PC lipids in this thesis. The first convention is capital D for "di" (two of the same tail), followed by a one-letter abbreviation of name of the fatty acid tail, and finally "PC" for the phosphocholine head group. For example 1,2-dipalmitoyl-sn-glycero-3-phosphocholine is DPPC (Di + palmitoyl + PC). The other convention is the

number of carbons in the tail, followed by a colon, then the number of unsaturated bonds, a space or a dash, and the PC head group (Figure 1). With this notation DPPC is 16:0 PC.

Our lipid bilayers also contain cholesterol (Figure 1). Cholesterol is also amphiphilic, but has a much smaller head group (-OH group) than PC lipids. Because of its ring structure, cholesterol is more rigid than PC lipids. Cholesterol is part of a larger family of sterols and is found in animal cells. Plants and yeast have sterols with slightly different structures (1).

1.1.2 Lipid bilayers and vesicles

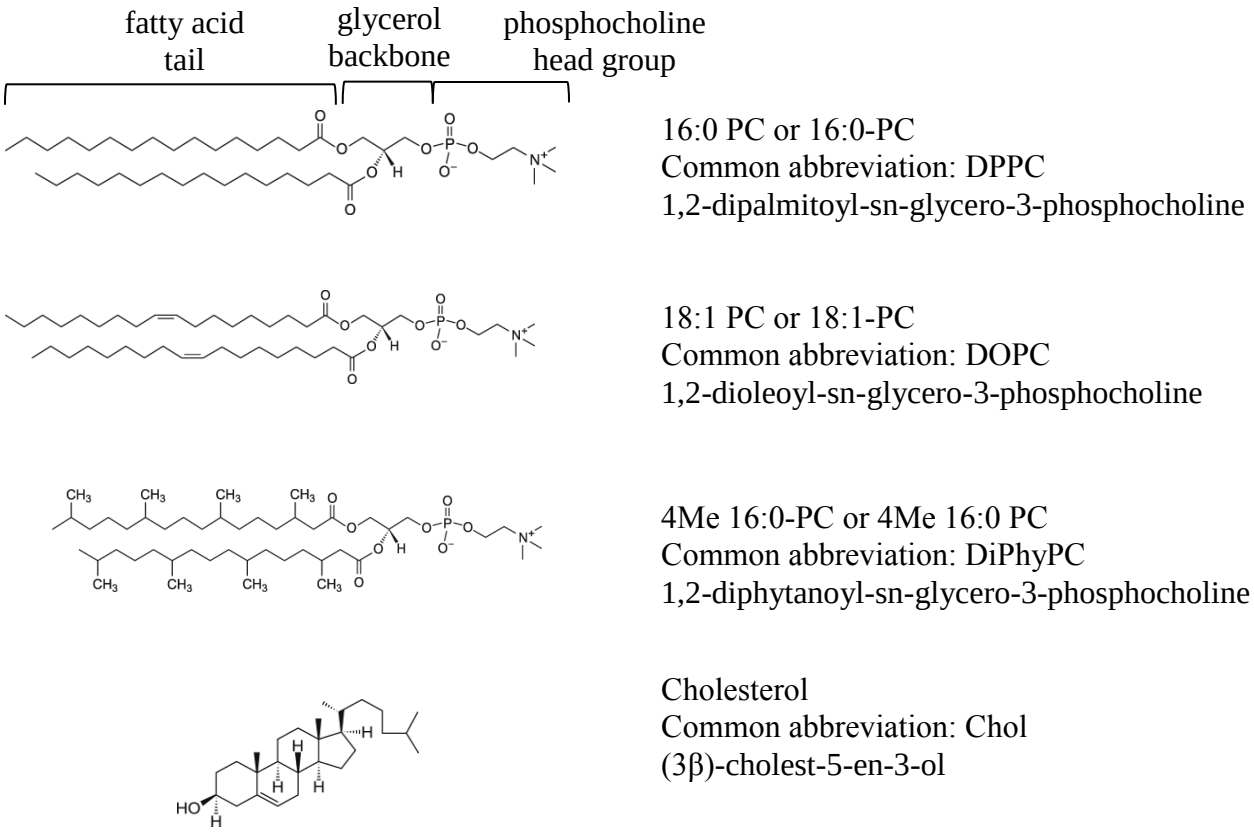

Figure 1 Lipid structure and nomenclature. Images are from http://avantilipids.com/

To shield the hydrophobic tails from water, lipids can self-assemble into lipid bilayers (Figure 2 A and B). The bilayer is composed of two lipid monolayers with the hydrophobic tails facing inward. Lipids are constrained from moving out of the plane of the bilayer by the hydrophobic effect, but lipids can diffuse laterally and rotate within the bilayer and to a lesser extent can flip from leaflet to leaflet. The bilayer thickness is typically listed between 3 and 10 nm (1). The oily interior of the bilayer is impermeable to most hydrophilic compounds, and so acts a barrier to hydrophilic and charged compounds. A bilayer in a closed spherical shell is called a vesicle (Figure 2 C) (1).

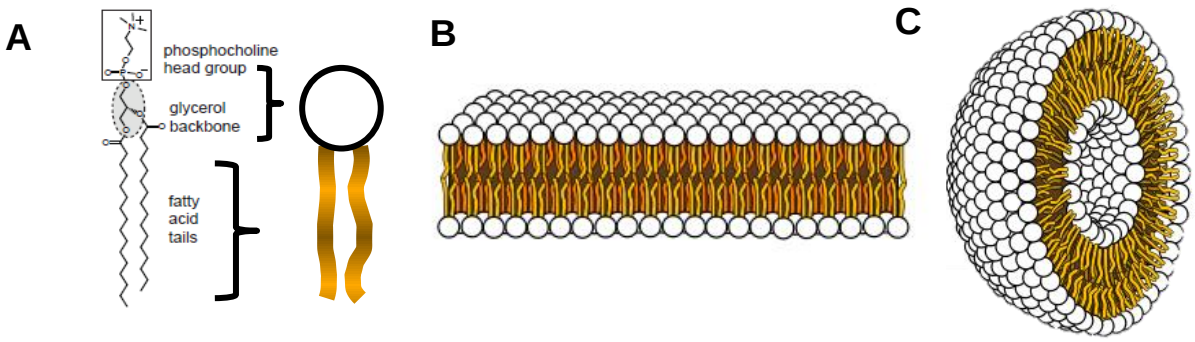

Figure 2 Lipids self-assemble into lipid bilayers. (A) In the schematic the lipid head group is shown as a white circle and the lipid tails are two orange lines. (B) A lipid bilayer composed of two monomers with tails facing inward. (C) Cross section of a vesicle. The bilayer and vesicle images are from Mariana Ruiz Villarreal, https://commons.wikimedia.org/wiki/File: Phospholipids_aqueous_solution_structures.svg.

1.1.3 Bilayer melting temperatures

The melting temperature, T_{melt}, also called the main chain transition temperature of a lipid bilayer, is the temperature at which the specific heat of the bilayer is at its highest. It is called the main chain transition because the major entropic change is the added degrees of freedom of the flexible fatty acid tails (1). Below T_{melt}, the lipid bilayer is in the gel phase, which is characterized by ordered, tightly packed lipid chains and slow lipid diffusion, (~0.01 $\mu m^2/s$) (3).

Above T_{melt}, the bilayer is in the liquid phase. The lipid tails are more disordered: they are more loosely packed and lipid diffusion is around 100 times faster than in gel (3). Almost all biological membranes are in the liquid phase, although gel phase biological membranes exist on the outermost layer of dead skin cells (1).

For our work we distinguish between high-T_{melt} and low-T_{melt} lipids. High-T_{melt} lipids are usually in the gel phase at room temperature. Structurally, high-T_{melt} lipids have long saturated carbon tails. An example is DPPC or 16:0-PC which has two saturated 16-carbon tails and a T_{melt} of 41°C (4) (Figure 3). Low-T_{melt} lipids and are in the liquid phase at room temperature. They typically feature short, unsaturated or branched chains. An example is DOPC, 18:1 PC, which has two 18 carbon tails with one double bond on the 9^{th} carbon down from the carbonyl group and has a melting temperature of 12°C (Figure 3). A lipid's T_{melt} is a useful way to characterize its packing ability in the bilayer: the higher the T_{melt}, the better the lipids are able to pack together into the gel phase, the more energy (measured by temperature) is required to disrupt the packing.

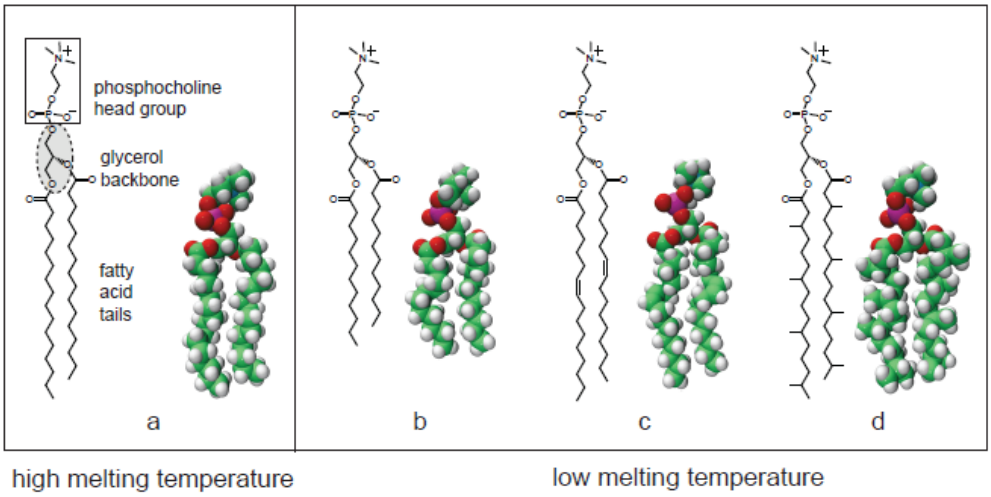

Figure 3 Lipid structures and melting temperatures. The lipids in our studies are composed of a hydrophilic phosphatidylcholine head group, a glycerol backbone, and a hydrophobic tail (a). High melting temperature lipids like DPPC tend to have long, saturated tails (a). Structural elements of lipids that lead to low melting temperatures include short tails (b), unsaturated tails (c), and methylated tails (d). Lipid images are from Avanti Polar Lipids. The image was made by Aurelia Honerkamp-Smith (110).

1.1.4 Bilayer thicknesses

The structure of lipids and their packing affects the bilayer's T_{melt} as well as the bilayer thickness. Bilayer thicknesses are typically experimentally measured in x-ray or neutron scattering (5-7). For our studies we employ atomic force microscopy, or AFM, which directly images the height of the upper surface of a lipid bilayer that is deposited on a solid surface the bilayer of interest (See AFM Methods Section). Bilayer thickness increases with increasing lipid tail length (8) and with increasing mole % cholesterol (up to 50 mole %) (9-10). These trends were employed to find candidate mixtures of lipids for Study 1.

1.2 Lipids in biology

Cell membranes are 2D solutions of proteins and lipids (Figure 4) (11). Approximately a third of the human genome encodes for membrane proteins and others proteins that interact with the membrane at various times (12). In a proposal by Singer and Nicholson on how lipids and proteins organize within cell membranes, the lipids form a semipermeable membrane in which transmembrane proteins diffuse freely (Figure 4 A) (13). Since this model was introduced, thousands of different lipids species have been found in cell membranes and biochemists have found that lipid complexity is highly regulated within the cell (14-15). A natural question from these results is why do cells need such a complex array of lipids? One proposed explanation is that lipids in the bilayer form heterogeneous regions of different lipid compositions (Figure 4 B). These regions possess different physical properties depending on the structure of the lipids and the overall lipid composition. This type of inhomogeneous distribution of lipids across the surface of a cell membrane is thought to impact cell signaling, membrane transport, protein

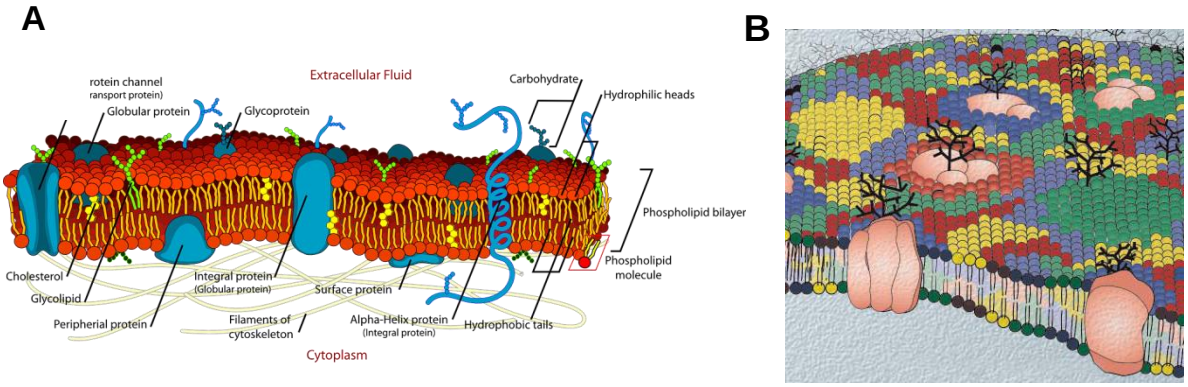

Figure 4 Two models of cell plasma membranes. (A) In the fluid mosaic model from Singer and Nicolson (13) lipids in the bilayer serve as a barrier and as a substrate for membrane proteins (blue blobs). The model distinguishes only between lipids bordering proteins and bulk lipids in the membrane. (B) Newer model of the plasma membrane with coexisting regions of different lipid composition (here shown in different colors). The branched structures are sugars. The actin skeleton is not shown. Image used with permission from (109).

trafficking, and virus pathogenesis (15) The most widely cited example of heterogeneous lipid regions is the lipid raft. The keystone definition of rafts are "small (10-200 nm), heterogeneous, highly dynamic, sterol- and sphingolipid-enriched domains that compartmentalize cellular processes" (16), where sphingolipids are usually high-T_{melt} lipids with slightly different head groups than PC lipids. Rafts have been linked to diseases like Alzheimer's, influenza, and diabetes (17). However the lipid raft theory remains controversial (18). Among the many unanswered questions is why these heterogeneous regions do not coalesce coalesce into domains that are large enough to image above the diffraction limit. There is also a lack of agreement among different technique like FRET, neutron scattering, and NMR about the size of rafts, their lipid content, and time scales for which they exist (15). For example in 2013 Frisz et al. used nano secondary ion mass spectrometry measurements to measure lipid content on the plasma membrane of fixed fibroblast cells (19). They found ~200 nm domains that were sphingomyelin-enriched, but NOT cholesterol-enriched (19-20), which goes against one of the key definitions for lipid rafts.

Membrane thickness has been shown to strongly affect transmembrane protein function. For example, the activity of a sodium potassium pump is strongly dependent on the number of tails on the lipids and whether or not the membrane contains cholesterol, both of which directly affect membrane thickness (10, 21-22). For heterogeneous lipid regions, the thickness differences between the two regions affects protein sorting, possibly through hydrophobic thickness matching between the bilayer and the hydrophobic domain (15, 23).

Membrane biophysicists are still working to discover the physical mechanism for heterogeneity within cell membranes. Our lab studies one possible mechanism, in which the

heterogeneous regions are the result of phase separation. To study how lipid structure affects properties of phase separation, we use reductionist ternary model membranes composed of a high-T_{melt} lipid, a low-T_{melt} lipid, and cholesterol. These ternary membranes have the potential to exhibit coexisting liquid ordered exhibit liquid-liquid coexistence into liquid ordered (Lo) and liquid disordered (Ld) domains. In the next section we will give a brief introduction to liquid-liquid phase separation in model membranes and connect this phenomenon with domains in biological membranes.

1.3 Bilayer membrane miscibility

1.3.1 Phase separation

Bilayers that exhibit liquid-liquid phase separation have at minimum three components: a high-T_{melt} lipid, a low-T_{melt} lipid, and cholesterol. At high temperatures, the lipids in the bilayer mix uniformly. Below the miscibility transition temperature (T_{mix}), the entropy of mixing is outweighed by lipid-lipid interactions, and two distinct phases appear: liquid ordered (Lo) and

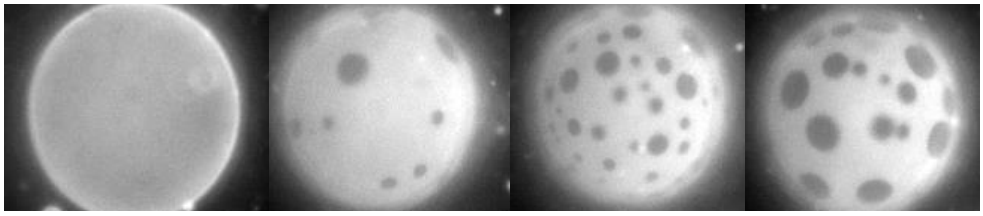

A: 40.0°C B: 39.0°C C: 37.0°C D: 35.0°C

Figure 5 Phase separation of GUVs. A) A GUV above the transition temperature T_{mix} (39.5°C) shows no phase separation. B, C, D) Below T_{mix}, two phases appear, a dark L_o phase and a bright L_d phase. The area fraction of the L_o phase increases as the temperature is lowered. The vesicle is made of 40/20/40 mole % 14:0-PC/DiPhyPC/cholesterol and is ~40μm in diameter.

liquid disordered (Ld). This phenomenon is observed with fluorescence microscopy, on Giant Unilamellar Vesicles (GUVs) tagged with a dye that partitions preferably into the Ld phase (Figure 5) (24).

Cholesterol is a necessary component for liquid-liquid coexistence in our membranes. Binary systems of the high-T_{melt} and low-T_{melt} lipids can exhibit only gel-liquid phase coexistence. The Lo phase is enriched in high-T_{melt} lipids and slightly enriched in cholesterol (Figure 6). The Lo phase is more ordered, has a lower area per lipid, and is commonly thicker than the Ld phase. The Ld phase has enriched in low-T_{melt} lipids and slightly depleted in cholesterol, is more disordered, and thinner compared to the Lo phase (Figure 6) (24).

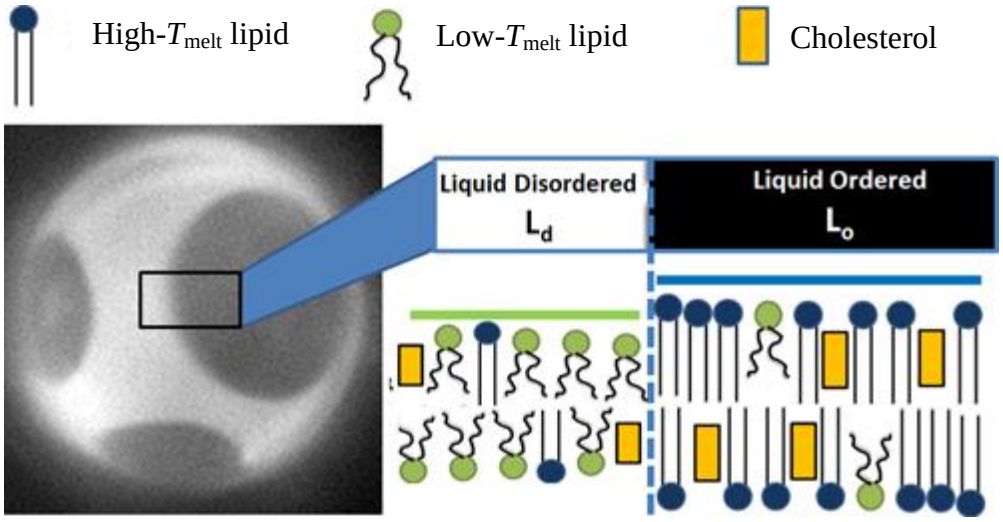

Figure 6 Phase separation in a model lipid membrane. A three-component vesicle below its miscibility transition temperature, T_{mix}, can phase separate into two liquid phases: the liquid ordered (Lo) phase rich in high-T_{melt} lipids, and the liquid disordered (Ld) phase rich in low-T_m lipids. For fluorescently labeled giant vesicles (left image) the fluorescent dye partitions more into the Ld phase, making it brighter. The GUV is between 20 and 40 μm in diameter.

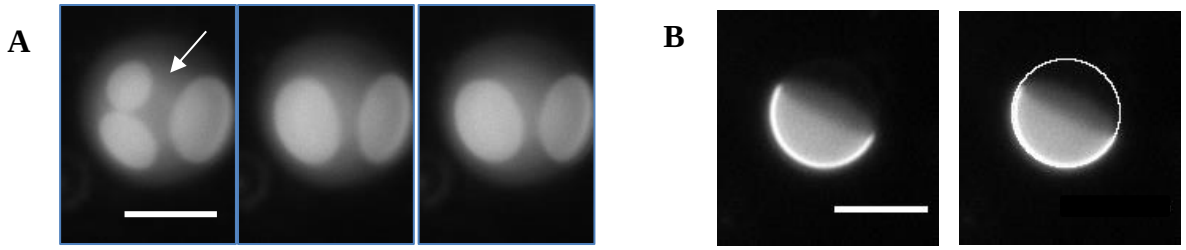

Figure 7 Effects of line tension on domains. All micrographs are of vesicles composed of 27/23/50 mole % DiPhyPC/DPPC/chol at 22.0 °C. (A) Liquid-liquid domains are circular to minimize Lo/Ld perimeter. When two domains encounter one another, they merge into one circular domain. Frame to frame is 300 microseconds. (B) Vesicle after all small domains have merged into one bright and one dark domain. The vesicle outline is drawn for clarity. Scale bars are 20 μm.

"There is an energy penalty associated with line tension at the Lo/Ld interface. This energy scales with the length of the interface (24-25). We observe GUVs minimizing the Lo/Ld interface in two ways: 1) Domains of the minority phase are circular are circular, so they minimize the perimeter for a given domain area (26). 2) when two domains collide, they coalesce to form a larger circular domain (Figure 7 A). Domains merge until there is one large domain of the minority phase (Figure 7 B).

1.3.2 Miscibility phase diagrams

Phase diagrams document all possible phase states of a membrane at thermodynamic equilibrium (24). Figure 8 shows a binary system in which components α and β are miscible at high temperatures (above the solid black line) and immiscible at low temperatures (below the solid black line). Above the miscibility temperature, T_{mix}, there is one uniform liquid phase. Below T_{mix}, the system demixes along a tie line to two phases: α', which is rich in component α, and β', which is rich in component β. Compositions along the same tie line (black dots 1-5) will

all demix to α' and β', but they will have different mole fractions of the two phases. The mole fraction is inversely related to the distance from the quench point to the end of the tie line in α (Figure 8 B) (24). For example, halfway along the tie-line, half of the system should have mole fraction α' and half mole fraction β'.

The phase behavior of a three-component system is traditionally displayed in a Gibbs phase triangle, where each point in the triangle represents a different ratio of the three components as seen in Figure 9. At a given temperature there is a 2 a 2D surface that bounds the 3D volume of the liquid-liquid coexistence region. The dashed lines in Figure 10A and B are tie lines which terminate into two compositions, one rich in the high-T_{melt} lipid and one rich in the low-T_{melt} lipid. Tie lines on a plane must be determined experimentally using NMR, EPR, x-ray

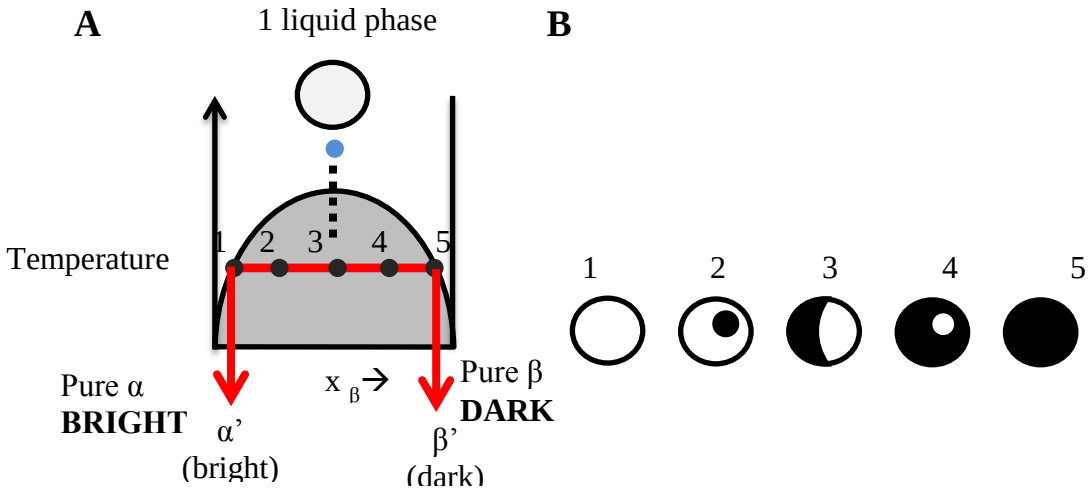

Figure 8 Binary phase diagram of components α and β. The x-axis is mole fraction of β. (A) At high temperatures, α and β mix completely in one uniform liquid phase (top blue dot). When the temperature is quenched (top dashed line), the miscibility phase boundary is crossed and the system demixes into two coexisting liquid phases along the tie-line (horizontal red line). The resulting phases, α' and β' are rich in components α and β respectively. The black dots (1-5) correspond to different starting compsitions. (B) Vesicles of compositions 1-5 vary in their area fractions according to the lever rule. Images are by Cynthia Stanich.

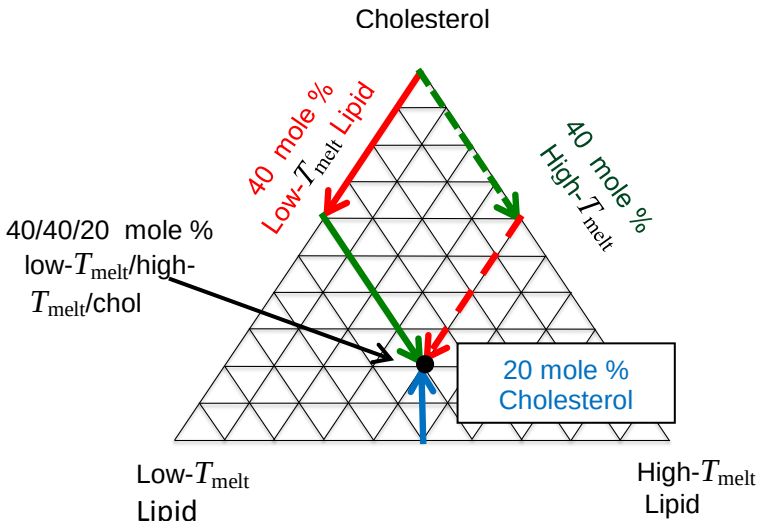

Figure 10 Reading compositions on a Gibbs phase triangle. A system containing only low-T_{melt} lipids is represented by a point at the vertex labeled Low-T_{melt} lipids. Binary mixtures are represented by points along the Low-T_{melt}/High-T_{melt}, Low-T_{melt}/chol and High-T_{melt}/chol axes. From any point in the triangle, the sum of all perpendicular lines to the axes is a constant.

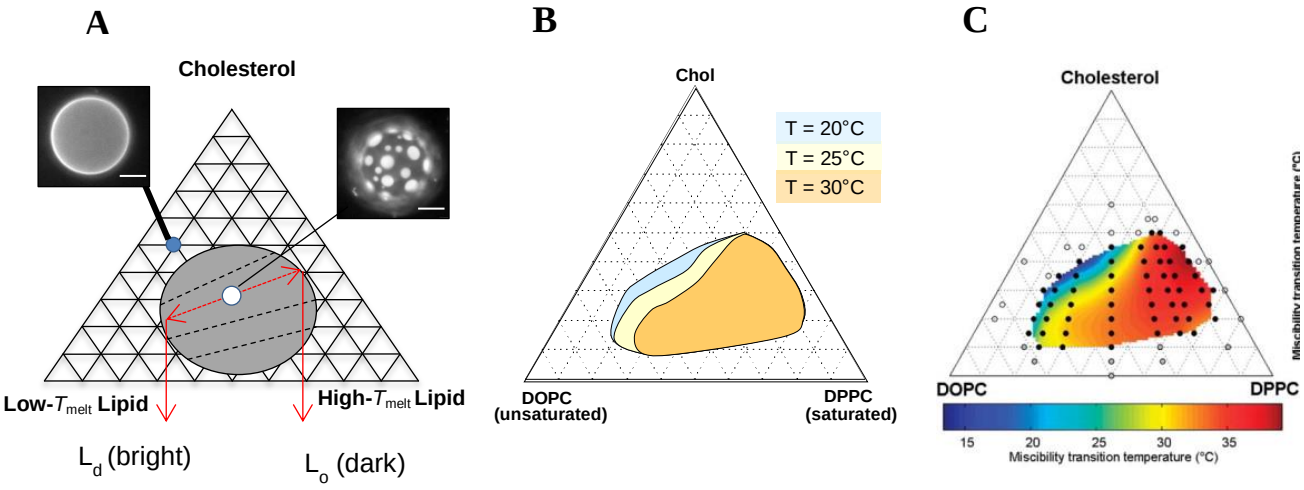

Figure 9 Phase separation in ternary membranes. (A) Phase boundary at a fixed temperature. A composition within the liquid-liquid phase boundary (white dot) will demix along the tie lines (dashed lines) to the phase boundaries, resulting in two phases: one rich in the low-T_{melt} lipids, Ld, and one rich in high-T_{melt} lipids, Lo. Scale bars are 20 μm. (B) The liquid-liquid phase boundary for DOPC/DPPC/chol changes as a function of temperature (each slice). (C) A map of all T_{mix} for liquid-liquid phase separation of DOPC/DPPC/chol. Black dots are the experimentally measured compositions. Phase diagrams from (B) and (C) are from (105).

diffraction, or fluorescence (24, 27). Phase separation occurs over a wide range of compositions and temperatures (Figure 10 C) (24).

A key advantage of studying phase separation in model systems is that the composition of bilayers can be tightly controlled. Biological membranes have more complex and dynamic compositions (28). Despite these and other differences, recent work has linked large domains in biological membranes to phase separation. Veatch et al. studied giant plasma membrane vesicles (GPMVs) derived from cells. The GPMV membranes exhibit two-phase coexistence like 3-component GUVs (Figure 11) (29). In GPMVs, the plasma membrane is removed from the cell's actin skeleton, so it may be that the actin is preventing large-scale domains from appearing within unperturbed cell membranes (29). Recently large domains similar to domains on our GUVs have been seen in vacuoles of living yeast (30).

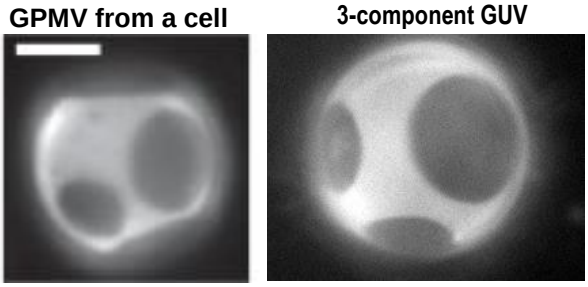

Figure 11 Phase separation in biological membranes versus model membranes. Fluorescently labeled giant plasma membrane vesicles from chemically-treated living rat basophil leukemia cells exhibit large scale phase separation with domains like the ones we observe in in phase separated of 3-component GUVs. The GPMV image is from (29). The GPMV scale bar is 5 μm. The GUV is between 20 and 40 μm in diameter.

In this thesis we examine how changing the structure of the lipids and the ratio of lipids affect the membrane thickness mismatch between the Lo and Ld phases. For both projects I measure transition temperatures of giant unilamellar vesicles using fluorescence microscopy and the thickness mismatch of the Lo and Ld phases within supported lipid bilayers using atomic force microscopy.

Chapter 2

EXPERIMENTAL METHODS

2.1 Making and observing lipid membranes

2.1.1 Electroformation of giant unilamellar vesicles, GUVs

Giant unilamellar vesicles (GUVs) are spherical lipid bilayers 10-100s of microns in diameter Micron scale domains within phase-separated, fluorescently labeled GUVs can by imaged by fluorescence microscopy (Figure 12) (24). The ability to observe phase behavior in real time and space lends itself well to studying different properties of phase behavior, including the transition temperature, T_{mix}, of model membranes and the area fractions of the different phases (31).

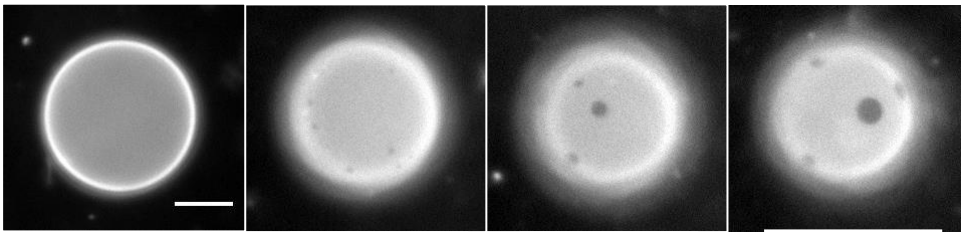

A: 41.6°C B: 38.7°C C: 37.4°C D: 35.7°C

Figure 12 A single GUV composed of 48/32/20 mole % DiPhyPC/DPPC/chol and 0.8% Texas Red DHPE imaged by fluorescence microscopy. A: Above T_{mix} (40.7°C), all lipids mix uniformly; no phase separation is observed. B, C, D: Below $T_{mix,}$ two phases appear, a dark Lo phase and a bright L_d phase. Scale bar is 20 μm.

We make GUVs through a process called electroformation (32). A detailed method for electroforming GUVs is provided in the Appendix. Briefly, lipids dissolved in chloroform are mixed to the desired molar ratios and dried on the conducting side of an indium tin oxide (ITO) coated glass slide (Figure 13 A and B). The lipid film is dried under vacuum to eliminate any

remaining chloroform, and then a chamber is formed by assembling Teflon spacers between two ITO slides coated with dried lipids (Figure 13 B). The chamber is filled with the desired aqueous solution, sealed, clipped to two metal conducting bars, and a 1V 10Hz AC field is applied across the two plates for 1 hour (Figure 13 D). Vesicles are extracted from the chamber, diluted and kept above T_{mix} until viewing. All visualized bilayers contain 0.8 mole % Texas Red DHPE fluorescent dye. Fluorescence microscopy is performed on Nikon Microscopes with air objectives and captured using charged coupled device (CCD) cameras. The specific microscopes used are described in the chapters relating to each project.

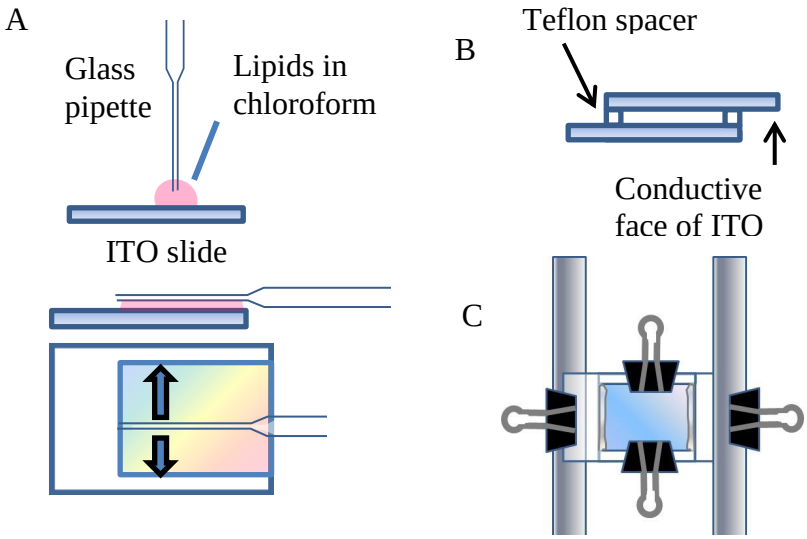

Figure 13 Schematic of preparing the electroformation chamber. (A) Lipids dissolved in chloroform are pipetted onto the conductive face of an ITO slide and spread into an even layer until all the chloroform has evaporated. (B) Two ITO slides with dried lipids are assembled face to face to form a capacitor. (C) The assembled growth chamber is attached to two thin aluminum bus bars and an AC field is applied across the bar. GUVs swell in water in the electric field.

Determining miscibility transition temperatures, T_{mix}

To determine T_{mix} a solution of electroformed vesicles is sealed between two coverslips and thermally coupled with heat-sink grease to a home-built temperature stage under a fluorescence microscope. The temperature of the stage is lowered until large-scale domains appear (Figure 12 B-D) on at least one vesicle. From there, the temperature is lowered in decrements of ~0.5 °C. At each temperature point, ~30 vesicles are evaluated to find the percent of phase separated vesicles in the population for that temperature. The temperature is lowered until over 90% of vesicles are phase separated. This process is repeated at least once more with a different batch of vesicles to account for any variations in the preparation and electroformation process. The data of % phase separated vesicles vs. temperature is fit with a sigmoid (Figure 14). The T_{mix} is defined as the temperature at which 50% of the population is phase separated based on a sigmoid fit of % phase separated vs. temperature as described by Gray et. al. (33). The T_{mix} errors are 95% confidence intervals of the fit at 50% (Figure 14).

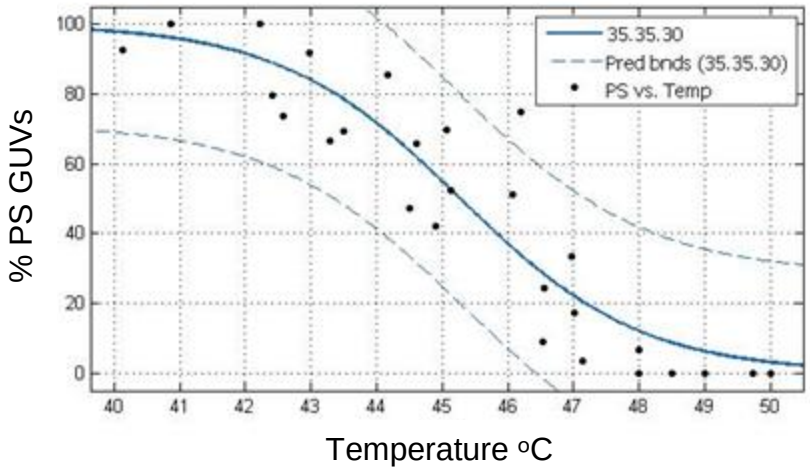

Figure 14 Determining T_{mix} for 35/35/30 mole % DiPhyPC/DPPC/chol. The percent phase separated GUVs (% PS) are plotted versus temperature (black dots). The data are fit with a sigmoid curve (blue line) and the 95% confidence intervals (dashed blue line). T_{mix} is defined as the temperature at which 50 % of the vesicles are phase separated on the fit. For 35/35/30 this is at 45.3 °C. The reported uncertainty is the range of confidence intervals at 50% phase separation, in this case ± 0.5°C. Data points are from three different batches of vesicles.

1.1.2 Supported Lipid Bilayers

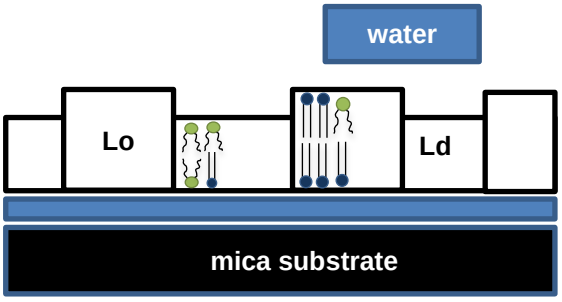

Figure 15 Schematic of a supported lipid bilayer on mica under water (not to scale).

For Study 1 and 2, we measure bilayer thicknesses of supported lipid bilayers (SLBs) on a mica substrate with atomic force microscopy (AFM). In an SLB, the bilayer is separated from the mica by a water layer that is approximately 1 nm thick (34-35). Although the schematic in Figure 15 shows all lipid headgroups on the bottom leaflet of the bilayer aligning the same distance from the mica, it is still unclear exactly how two phases on a supported bilayer align. (Further analysis of this topic appears in the discussion section of Study 1) (36). Diffusion coefficients measured for individual lipids in an SLB are only slightly lower than coefficients measured in a free bilayer far from a solid surface (36). However, the collective motion of groups of lipids is hindered on length scales larger than the 1 nm water layer, such that micron-scale domains do not coalesce into larger domains. Compare Figure 16a to Figure 17 (37-38). We employ two methods for making SLBs:

SLBs from GUVs ruptured on mica substrates.

For Study 1, we electroformed GUVs in 200 mM sucrose and sank the GUVs over mica in a solution of 200 mM glucose and 5 mM $CaCl_2$. The $CaCl_2$ was added because divalent cations have been shown to induce vesicle rupture, possibly through increasing the bending moduli (39). We found that vesicles added in glucose without $CaCl_2$ sank but did not rupture. We

and others (40) found that vesicle rupturing does not cause a discernable change in the area fractions of the Lo and Ld phases phases. Instead the rupturing process captures a "snapshot" of the domains just before rupture (Figure 16), which makes it an excellent technique for measuring area fractions of the two phases. However if a ruptured phase separated vesicle is heated above T_{mix} and then cooled below T_{mix}, large domains do not reappear, due to the hydrodynamic suppression of collective motion. As a result, it was crucial to keep the temperature stable. We verified that the surface area of the pre-ruptured GUV and the area of the supported bilayer were the same, which confirmed that the ruptured GUVs is one bilayer thick. Because domains are large (tens of μms) on GUVs, rupturing phase separated GUVs on mica surfaces allowed us to directly and easily Lo vs. Ld phases as identified by fluorescence microscopy with thicker vs. thinner phases identified by atomic force microscopy in Study 1.

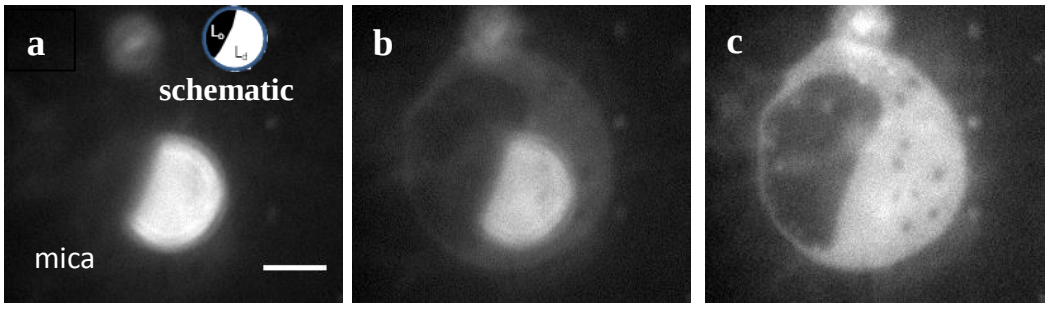

Figure 16 Phase separated vesicle rupturing on mica. a) A vesicle on mica b) ruptures to c) form a supported lipid bilayer. After rupturing, the position and size of Lo and Ld phases appears static within the supported bilayer, as long as there are no changes in temperature (not shown). The surface area of the spherical vesicle in panel a corresponds to the area of the ruptured vesicle in panel c, indicating that the resulting supported lipid bilayer is only one bilayer thick. The bright specks around the vesicle are floating aggregates of labeled lipid that are produced during the electroformation process, and are washed off before the supported bilayer is scanned in the AFM. The vesicle is 40/40/20 mole % 18:1 PC/16:0 PC/chol at 23°C. Scale bar is 20 μm. Exposure and acquisition time is 400 ms.

SLBs from small unilamellar vesicles ruptured on mica surfaces.

For Study 2, bilayers were formed from ruptured small unilamellar vesicles (SUVs, < 100 nm in diameter) in the presence 5 mM $CaCl_2$. SUVs can be made in a variety of ways, including sonication and extrusion. For Study 2 we employed sonication. We and others (41) found that it is important to deposit SUVs above the transition temperature to ensure that the supported bilayer composition is the same as the bulk lipid composition. As the temperature is lowered through the miscibility transition, domains of Lo and Ld phases appear. These domains are smaller than observed in taut, free-floating GUVs because the domains do not coarsen significantly on time scales of the experiment (Figure 17). Depositing and rupturing SUVs created large patches of bilayer across the mica. We employed the SUV method for Study 2 because bilayers produced from SUVs were easier to find and scan in the AFM than from ruptured GUVs, and, and because the Lo phase was always taller for the systems we study, so there was no need to identify the Lo and Ld phases by fluorescence microscopy.

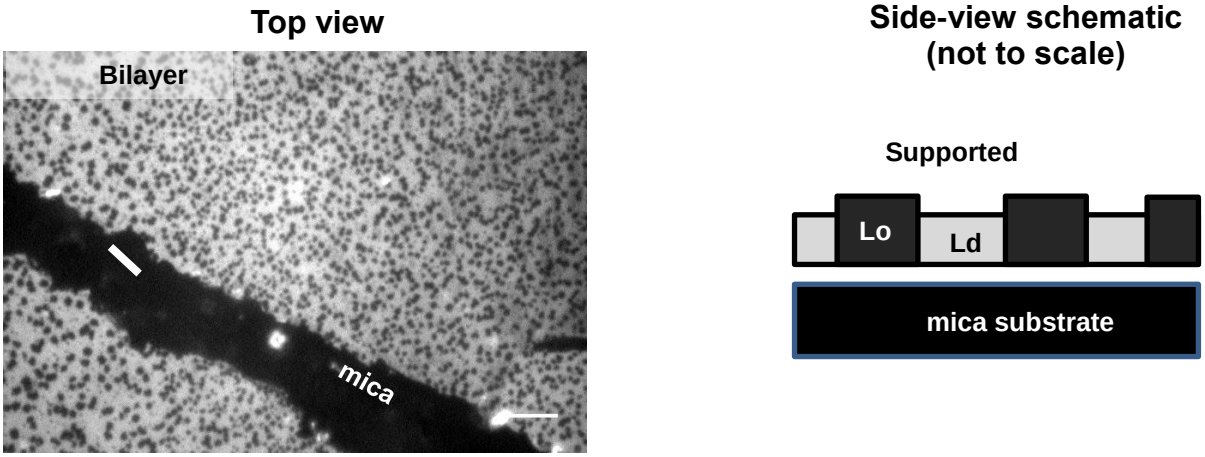

Figure 17 Supported lipid bilayer from rupturing SUVS. (Left) Fluorescence micrograph of domains in a supported lipid bilayer made by rupturing small unilamellar vesicles of 48/32/20 mole % DiPhyPC/DPPC/chol and 0.8% Texas Red DHPE on a mica substrate at 60 ˚C. The bilayer is then rinsed and cooled to 22 ˚C before scanning. The bilayer surface is scratched to reveal the mica to enable comparison of the bilayer with the substrate. Dark spots are Lo-phase membranes. The scale bar is 20 μm. (Right) Schematic of the supported lipid bilayer. For this system the Lo phase is thicker.

2.2 Using AFM to determine thicknesses of supported lipid bilayers

2.2.1 Introduction

. We use AFM to measure bilayer thicknesses, specifically the thickness difference between the Lo and liquid Ld of bilayers (Figure 18).

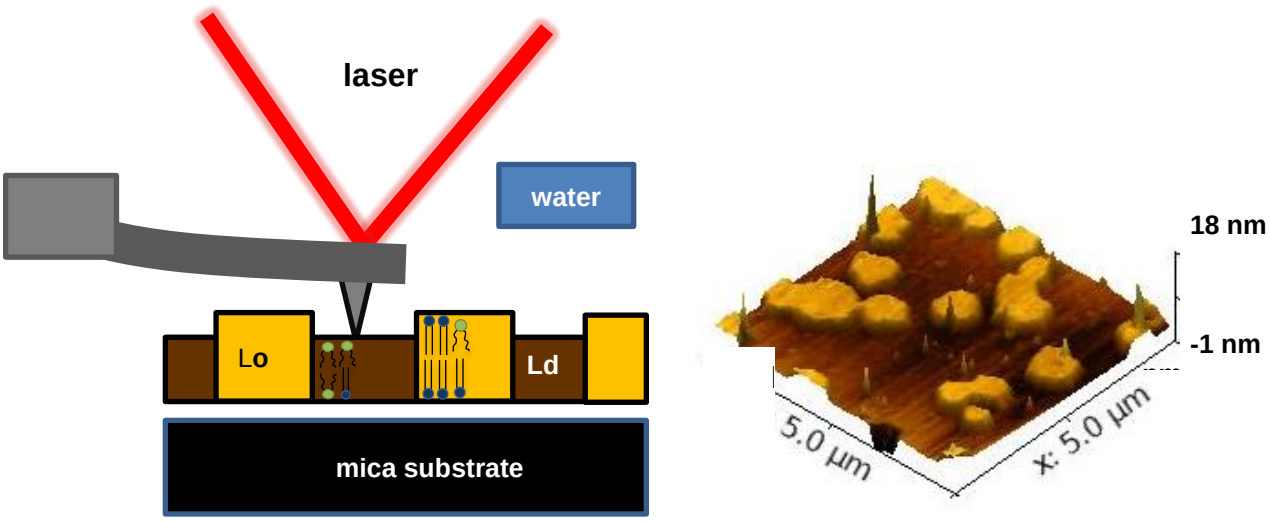

Figure 18 AFM of supported lipid bilayers. (A) Schematic of an AFM tip scanning across a phase separated supported lipid bilayer under water. (B) Topography of 48/32/20 mole % supported lipid bilayer. Tall spikes are impurities. The Lo phase (yellow spots) is ~1.4 nm taller than the Ld phase (brown background).

AFM has sub-nanometer (< 10^{-9} m) vertical resolution and lateral resolution that is roughly the same order as the diameter of the tip, typically tens of nanometers (43, 44). (42)(43)High vertical resolution is essential for measuring differences in bilayer thicknesses, which are commonly 0.1-2 nanometers (6-7, 41, 44-49). AFM directly images the sample of interest in real time, compared to sample-averaging and time-averaging techniques like x-ray diffraction or neutron scattering (43). For our work, direct visualization allows us to compare AFM images with fluorescence microscopy images to identify which thickness corresponds to the Lo and Ld phase in Project 1. Unlike x-ray diffraction, which requires measuring bilayers in

humidity chambers, AFM can be performed on samples underwater at ambient conditions (50). A drawback of AFM is the sensitivity of measured height values to scanning conditions, including obtaining non-physical height results, and issues with reproducible height measurements for a given system, which we address later (51). Another challenge is that the AFM probe can act as a "molecular broom", which pushes aside and/or damages soft membranes (43).

Here we present a brief introduction to the AFM instrument and the AFM modes we use for our studies: low-force contact mode, Peak Force Quantitative Nanomechanical Mapping® mode, and blueDrive™ Photothermal Excitation tapping mode. We address how these modes provide solutions to common challenges in AFM. Lastly we discuss how AFM scans are processed and we present future challenges for the field.

2.2.2 AFM instrumentation

The basic components of an AFM are a probe, detector, scanner, sample chamber, and electronic control system (Figure 19) (42, 52).

The AFM probe is a sharp tip connected to the end of a cantilever that is scanned over the sample. Probes are sensitive to surface interactions and the magnitude of interaction varies with distance from probe to sample in a precise controlled way (51-52). The probes for our projects are summarized in Table 1 and depend on the method of scanning.

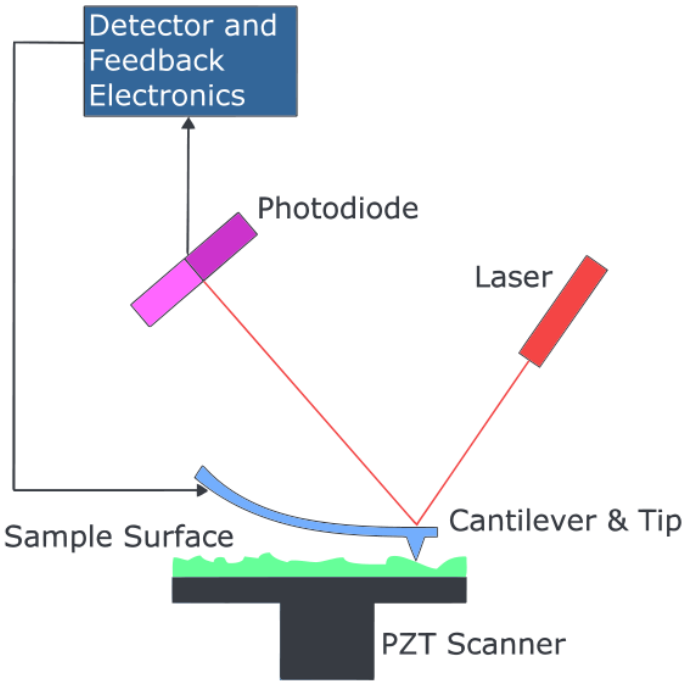

Figure 19 Basic AFM instrumentation with beam deflection detection.

Table 1 Summary of AFM instruments and scanning modes for each study			
AFM Instrument	Scanning Mode	Tip	Study
Veeco Dimension Icon-PT AFM	Peak Force Tapping Mode	Scan Asyst Fluid+ (0.7 N/m, 150 kHz, Si tip, 2 nm, Bruker)*	Chapter 3
Asylum MFP3D Bio AFM	Contact Mode (0.2 - 0.4 nN force set point)	DNP-10, Triangle B (0.12 N/m, 23 kHz, Si_3N_4 tip, 20 nm, Bruker)	Chapter 3
Asylum Cypher ES Environmental AFM system SLD-DD	Tapping Mode blueDrive™ Photothermal Excitation	Arrow UHFAuD tip (6 N/m, 850 kHz, Si tip, 10 nm, NanoWorld)	Chapter 4
*(average cantilever spring constant, average cantilever resonance frequency, tip material, average tip radius, tip manufacturer)			

The scanner is a piezoelectric ceramic material that changes geometry in a predictable manner with applied voltage. The x-y piezo moves the probe across the sample. A z-piezo is responsible for changing the vertical position of the cantilever (52). The deflection detector detects the interaction between probe and sample. These interactions include long range electrostatic repulsion from the charged double layer on the tip and on the zwitterionic head groups of the lipids and short range attractive Van der Waals interactions (often modeled as proportional to $1/r^6$) between the tip and the membrane (49). These interaction cause the cantilever to bend, and the bending is measured with a laser beam that is focused on the end of the cantilever. The reflected beam hits a photodiode detector that is positioned a set distance from the cantilever. Changes of the position of the beam in the detector start a feedback loop using an electronic control system. The electronic control system is a z-feedback loop that ensures that the probe tracks the surface. It compares the detected signal to a given set point and applies a voltage to the z-piezo to bring the signal back to the set point (42). The ratio of path length between the cantilever and detector vs. cantilever length amplifies signal so that very small vertical distances (down to <0.1nm) can be measured (52).

Sample chambers hold the sample in position while it is being scanned. Our samples had to remain submerged in water for the entire scanning process. For low-force contact mode, we used an Asylum scanning chamber. For Peak Force Quantitative Nanomechanical Mapping® mode, we used a perfusion cell from Bruker. Both chambers kept the samples submerged under water. For blueDrive™ Photothermal Excitation tapping mode we pipetted a large droplet of water over the sample.

2.2.3 AFM modes

Contact mode

In contact mode, the tip is in constant contact with the surface, and maps the topography of the sample by changing the z-position to maintain constant tip deflection (52-53). Contact mode cantilevers have low spring constants relative to the intermolecular forces within the sample and repulsive interactions between tip and sample cause the cantilever to bend (52). The feedback loop keeps the cantilever deflection constant (51). Contact mode is easier to understand and less complex to interpret than tapping mode, the other common AFM mode for topography. Simon Connell et al. found that low force contact mode (< 0.2nN set point) led to consistent height results for Lo/Ld height differences compared to tapping, such they were able to formulate an entire phase diagram from height differences of different bilayer compositions (41). A disadvantage of contact mode is that it applies high lateral forces and can easily destroy the sample and/or the tip if the set point is too high (52). We found that using a 0.2nN constant scanning force did not destroy samples and led to consistent thickness measurement (Project 1) (41). We used low-force contact mode to scan bilayers that were also imaged in fluorescence for Study 1 (Chapter 3).

Tapping mode

In traditional tapping mode, the cantilever is driven such that it oscillates near its resonance frequency. The oscillating tip is scanned across the sample and moves in to and out of contact with the sample. When the sample and tip are in contact, the sample exerts short-range forces on the probe, which cause shifts in the cantilever's resonance frequency and amplitude. The feedback loop monitors the amplitude and moves the z-piezo to maintain constant tip amplitude,

and through this process maps the sample's topography. Because the tip is only intermittently in contact with sample, the forces exerted on the sample are greatly reduced compared to contact mode (52-53). Tapping mode commonly gives sharper images than contact (41) and is more stable. One major drawback is that in practice the process of cantilever tuning is not straightforward. A cantilever typically does not behave like a straightforward damped-driven harmonic oscillator. Commonly the cantilever is piezo driven and piezo excitation has a complicated resonance. The piezo's movement can also activate resonances in the water and in the instrument itself leading to a "forest of peaks" (Figure 20). It is often not clear which peak in this forest will give a clear topographic image. We found non-physical bilayer thicknesses using tapping mode to drive a cantilever under water, possibly due to selecting the wrong tuning peak (Table 2). Tapping is also susceptible to drift from changes in temperature and surrounding volume under water which leads to changes in measured topography over time (53). For our experiments we noticed the deflection set point drifted significantly for up to 30 minutes after the cantilever and tip were submerged in water, which led to changes in measured heights within the same scan (e.g. Table 2, Image 1).

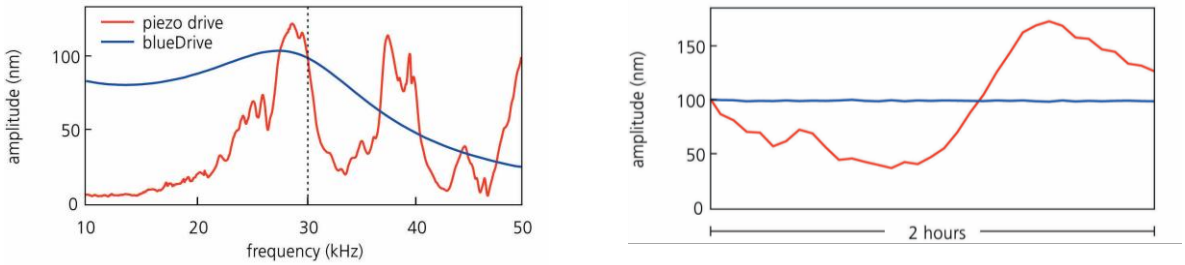

Figure 20 (Left) Representative possible tuning peaks for AFM cantilevers in tapping mode under water. The red line represents traditional piezo-driven cantilevers, which exhibit "a forest of peaks" under water. The blue lines represent blueDrive Photothermal Excitation from Asylum in which there is one clear tuning peak. (Right) The amplitude is not stable over time in piezo-driven cantilevers, but is for blueDrive cantilevers (53).

Table 2 Non-physical bilayer thickness results in tapping mode						
#	Fluorescence and AFM scans	Tip	Amp. Set Point (V)	Drive Freq. (kHz)	Heights (nm)	Non-physical result
1	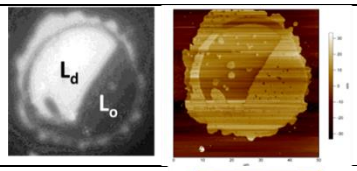	Veeco	N/A	N/A	Lo: 39.0+3.9 Ld: 27.5+6.3 Δh:12.9+5.3	Δh >> 1 nm
2	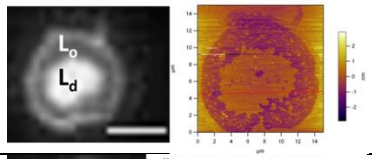	Olympus TR400PB 0.02 N/m 10 kHz	0.25	67.2	Lo: -1.1+0.1 Ld: -0.6+0.2 Δh: -0.5+0.1	Bilayer lower than mica Δh < 1 nm
3	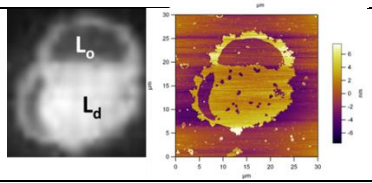	Olympus TR400PB 0.02 N/m 10 kHz	0.36	66	Lo: 2.1+0.7 Ld: 7.8+0.4 Δh: -5.7+0.5	Δh < 1 nm

All images were taken on an Asylum MFP3D Bio AFM in tapping mode. Left are fluorescence micrographs of the ruptured vesicles on mica surfaces. Right are the AFM scans. Vesicles are 35/35/30 % DiPhyPC/DPPC/chol. Heights of bilayers zeroed to mica are in the table above. AFM images have not been zeroed. In reality the Lo phase is thicker for this system, which is the case for vesicle 1. Vesicles 2 or 3 show the artifact that the Ld phase is thicker. The heights of phases for vesicle 1 are much larger than the expected range of 3-6nm (See Table 3). In vesicle 2, AFM scans indicate the mica is taller than the bilayer, which cannot be true. Switching to a new tip reversed the heights (data not shown). To see whether the scanning solution affected observed heights, scan 3 is done in a buffer as described in Marques et al. (54), however the heights are still outside of the expected range of 3-6nm and the Ld phase appears taller. The large variation in heights may be due to tuning the driving frequencies for the cantilever much higher than the resonance frequency.

Below we present two forms of tapping mode we use in our studies. These methods address challenges in traditional tapping mode.

Peak Force Quantitative Mechanical Mapping (Project 1)

How about "In peak Force tapping mode (developed by Bruker), the probe periodically taps the sample far below the resonance frequency (e.g. 2 kHz for a 150 kHz resonance tip) and at very low forces (down to 10 pN as opposed to 0.1-1nN in typical tapping). In Peak Force, the set point is the maximum applied force on the tip as opposed to the amplitude. Because the set point is based on a difference in force (Figure 21 (i) A to C), peak forces can be measured even when the interaction is dominated by attractive or repulsive interactions, which makes scanning more stable across different environments (e.g. Lo vs. Ld bilayers) (Figure 21 (ii)). Since the scanning forces are low, Peak Force taping is an excellent technique for scanning soft bilayer samples. It also does not require tuning the cantilever (55). We used Peak Force tapping to scan ruptured GUVs in Project 1.

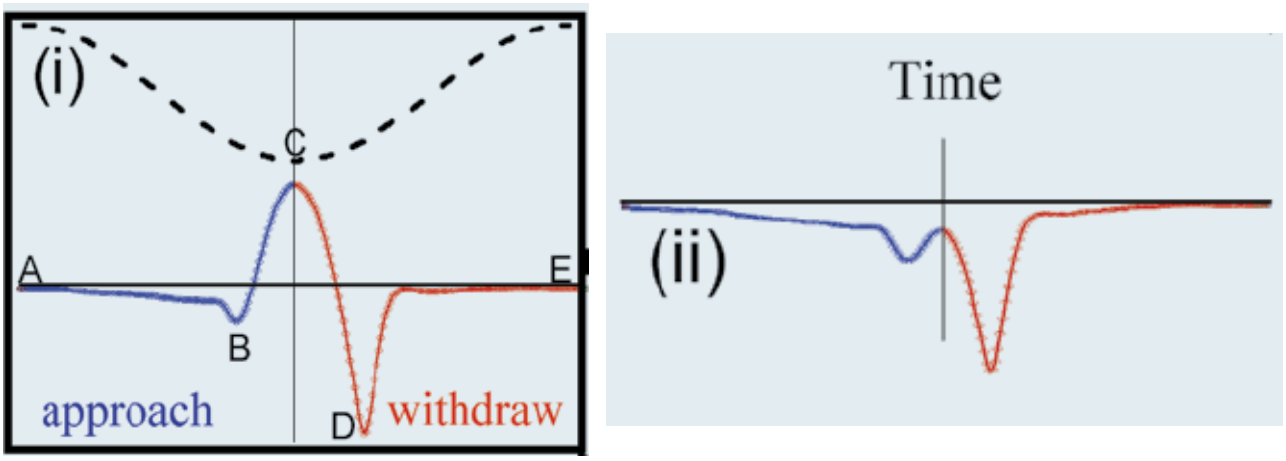

Figure 21 Tip trajectory and force curves for Peak Force tapping mode. (i) Plot of force (filled lines) and z-position (dashed line) versus time. (A) pre-contact (B) jump to contact (C) peak force (distance from A to C) set by the user. (D) adhesion. (ii) Example of small peak force in a system dominated by attractive interactions. (55)

blueDrive™ Photothermal Excitation tapping mode (Project 2)

In blueDrive™ Photothermal Excitation tapping mode, the cantilever is driven by modulating the power of a blue laser (405 nm) focused at the base of the cantilever (Figure 22). This modulating power induces thermal stresses on the cantilever that cause it to vibrate in a well-controlled manner. The laser point is very narrow (4 um diameter on a 42 um-wide cantilever) so that very little laser light spills over onto the sample. The heat from the laser conducts mostly through the chip that the cantilever is connected to. Asylum the company that developed blueDrive , tested the effects of the laser with DOPC/DPPC phase separated bilayers. They found that the laser did not affect phase separation (53). Because only the laser drives the cantilever, there is a very clean resonance response and no forest of peaks (Figure 20). There is also almost no drift, even after hours of imaging times (Figure 20) (56). Another advantage is that scans are fast, with images taking around 5 minutes, as opposed to 15 – 40 minutes with the other modes.

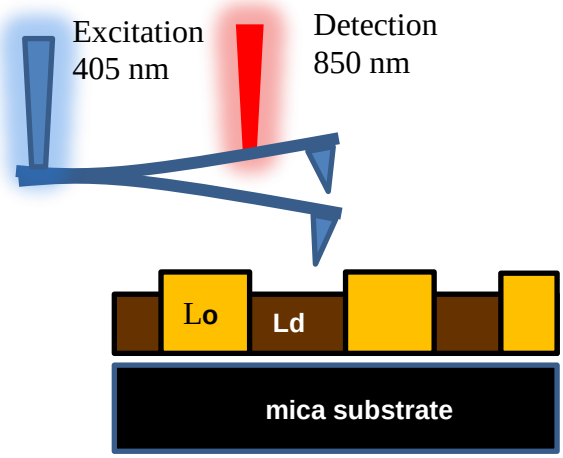

Figure 22 Schematic of scanning a supported lipid bilayer under water using a Cypher ES Environmental AFM system SLD-DD (Asylum Research). The blueDrive™ Photothermal Excitation tapping mode uses a blue laser to drive oscillation of an Arrow UHFAuD tip (6 N/m, Nanoworld) (53).

2.2.4 Challenges with AFM of bilayers

One of the current challenges of measuring bilayer properties with AFM is a lack of consistent height values in the literature compared to other techniques like x-ray diffraction. Reported AFM measurements can vary widely, even for simple supported lipid bilayer systems composed of only one lipid type (Table 3). Measured thicknesses may depend on the bilayer preparation, scanning mode, scan settings, post-processing procedures, and method for evaluating thicknesses. In the literature quantitative details about these methods are underreported.

Table 3 AFM thicknesses of pure DPPC bilayers at room temperature in the literature

Height (nm)	Temp (°C)	AFM Mode	Reference
4.7	RT	Contact (< 500 pN)	(44)
5.0 ± 0.2	RT	Contact (< 500 pN)	(57)
5.5	22	Tapping (MAC mode)	(58)
~ 6	~ 23	Contact (0.5 nN)	(59)
6.15 ± 0.93 (29 cross sections)	20	Contact (< 100 pN)	(60)

RT denotes that the value of room temperature was not specifically given. MAC is magnetically driven tapping mode.

Almost all AFM images require post processing to remove background so that features can be measured (61). Here we discuss two of the most common post-processing procedures: leveling and median line scan. AFM measures height features, but changes in the height of the background from a tilt in the sample can mask out small height differences (Figure 23 A). There

can also be scanner bow, which is a result of a swinging motion of the x-y piezo. For both issues, a sample plane is computed from all the image points and is subtracted from the data (first order for the tilt and second order for the scanner bow) (62). Another common method is median line subtraction. Profiles taken in the fast scanning axis (usually x-axis) can be mutually shifted by some amount or have slightly different slopes, which will not be corrected with just plane subtraction. In median line subtraction, the image is corrected line by line so that all lines share the same median height (Figure 23 B and C). We outline how images are processed in the supplement, however few published AFM papers give clear methods for their image processing. It is very likely that different processing method lead to different height results.

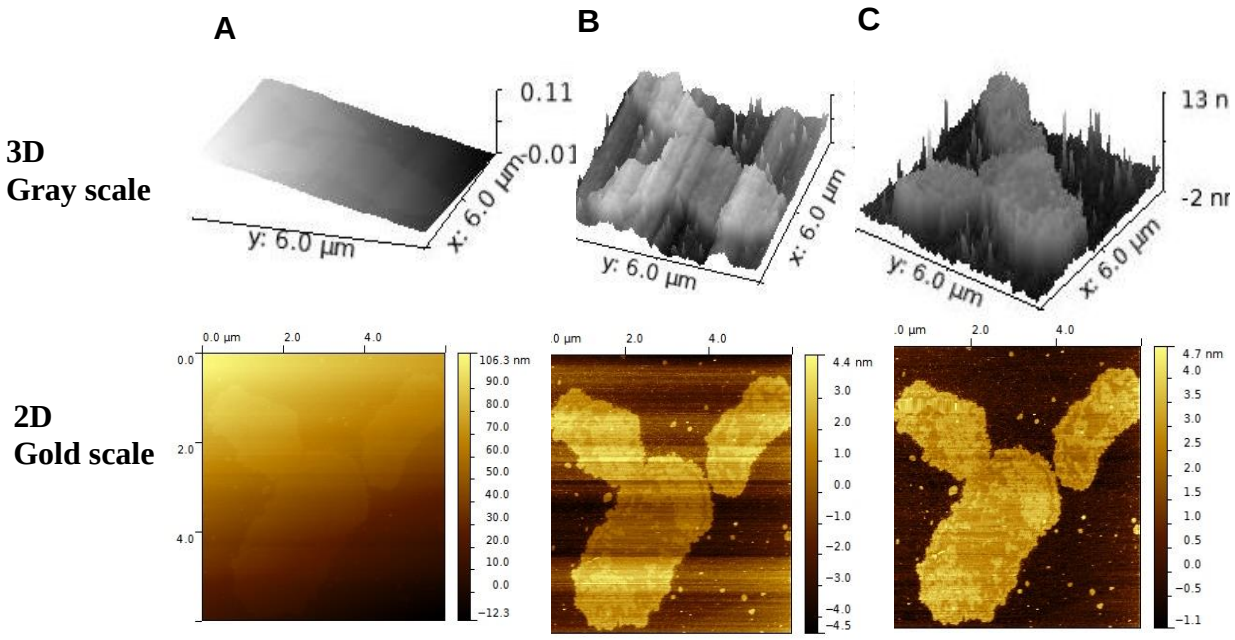

Figure 23 Processing a raw AFM image of supported bilayers of 30/40/30% 4Me-16:0 PC/13:0 PC/chol on mica. AFM scans are shown axiometrically in gray (top) and 2-dimensionally in gold (bottom). (A) Image before processing. (B) Image after plane correction, median line scan correction, and horizontal scar correction. (C) Image after median line corrections of the bilayer and mica layer and after zeroing the mica layer. The height histogram of this final image is processed in Matlab peak-fitting software.

Another important consideration is how to measure heights from the processed images. These methods are also seldom addressed in detail in the AFM bilayer literature. It is often unclear how many scans were used to determine heights for bilayers or how much of the AFM image is analyzed for height difference. For example, only one of the five papers in Table 3 gave what data they used to find heights (in that case 29 line cross sections). Probably the most common method of determining heights in AFM is through a line profile (61), which gives the height as a function of distance along the selected line. Line profiles are simple way to measure thicknesses, but they give data only for the selected pixels in the line, and so may not represent

the height changes across the entire scan. There is also noise for each height level (Figure 24) and it is often unclear how an operator chooses how they define the height for each feature. With these limitations in mind, we developed a method to determine height differences using every pixel in the AFM scan. We fit the height histograms of the entire image with peak fitting software in Matlab. Our reported experimental uncertainty is a standard deviation from a 100 trial bootstrap peak fit of the data, which tells how stable the mean of the peak is to random noise (Figure 24). This uncertainty is usually much smaller than the scan-to-scan variation in heights. In the supplement of this thesis, we give the AFM images, height profiles, and peak fits for all AFM values.

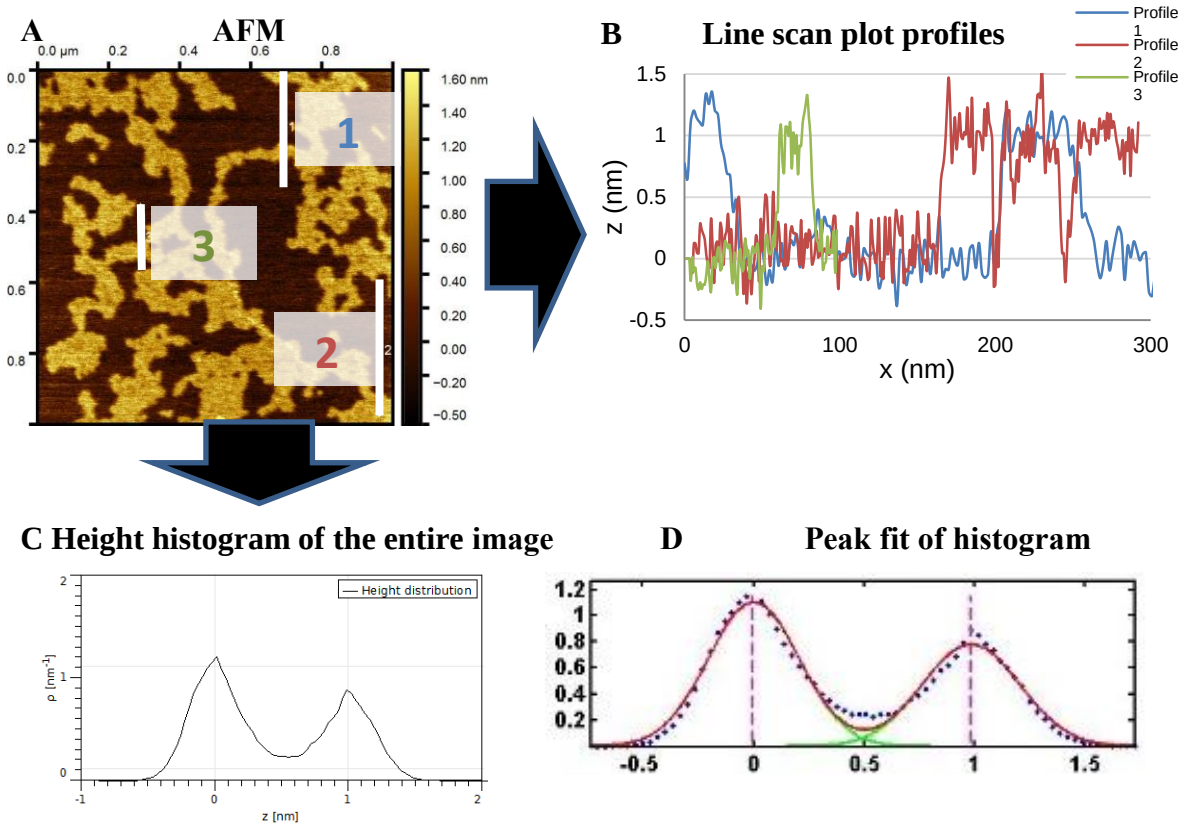

Figure 24 Line scan and height histograms. (A) An AFM scan in Peak Force QNM Mode with a silicon nitride SCANASYST FLUID+ tip (Bruker) of 50/30/20 mole % 20:1 PC/16:0 PC/chol at room temperature. (B) Line scans of the three white lines in (A). Line scans are only 1 pixel thick, the white lines in (A) are drawn thicker for clarity. (C) A height histogram of the entire AFM scan shows two peaks representing the two height populations. (D) A typical peak fit trial of the height histogram in a 100 trial bootstrap fit. Blue dots are data, the dark red line is the total peak fit, light green lines are the component peaks, and magenta dashed lines are the first guess at peak position from the previous trial. The height difference between the two populations is 0.985 ± 0.002 nm.

Chapter 3

THICKNESS MISMATCH OF NON-CANONICAL LO-LD LIPID MEMBRANES

3.0 Contributions

This chapter is slightly modified from a manuscript of the same title by Joan V. Bleecker, Phillip A. Cox, Rami N. Foster, Jonathan P. Litz, Matthew C. Blosser, David G. Castner and Sarah L. Keller, in preparation for submission to the Journal of the American Chemical Society.

3.1 Introduction

The activity of a membrane protein can vary dramatically with local lipid composition (22, 63). Because lipid composition dictates many physical properties of a membrane including thickness, lateral pressure, order, and elasticity (64), isolation of the impact of an individual physical parameter on protein activity is difficult. This difficulty is exacerbated when the protein can explore different regions of the membrane with distinct compositions. Here we study the relationship between composition and membrane thickness in model membranes with micron-scale heterogenities. Heterogeneities in cell membrane thickness have been proposed to influence membrane trafficking (11, 65).

For a typical lipid bilayer, thickness positively correlates with both lipid tail order and lipid gel-to-liquid melting temperature (T_{melt}) (8). All of these parameters increase when the length or degree of saturation of the composite lipid tails are increased (66). However, when there is a simultaneous increase in lipid tail length and decrease in bond saturation, the correlation between order, thickness, and T_{melt} breaks down. Namely, single-component membranes comprised of monounsaturated phosphatidylcholine (PC)-lipids are thicker than membranes composed of

saturated PC-lipids containing two fewer carbons per tail, despite the fact that the monounsaturated lipids are less ordered and have a lower T_{melt} than the saturated lipids (8, 67).

Demixing of model membranes into micron-scale regions of coexisting liquid phases occurs below a threshold temperature (T_{mix}) for some ternary systems comprised of a high T_{melt} lipid, a low T_{melt} lipid, and cholesterol (24). The two resulting phases are termed the liquid-ordered (Lo) and liquid-disordered (Ld) phases in reference to the linearity of the lipid tails within each phase (24). Canonically, the Lo phase, which is enriched in saturated low-T_{melt} lipids, is assumed to be thicker than the Ld phase (68).

Here we examine a series of non-canonical ternary systems composed of short-tailed ordered lipids and long-tailed disordered lipids. In particular, we study systems in which a single-component membrane made of the disordered lipid is *thicker* than a single-component membrane made of the ordered lipid. The lipids used in the ternary systems we studied are listed in Table 4, along with the previously reported thickness differences between the corresponding single-component membranes (5, 69). Because the Ld phase is enriched in low-T_{melt} lipids, we hypothesized that these systems would produce membranes with thicker Ld than Lo phases.

We study these systems because we seek to provide model systems for future studies on thickness-modulated protein activity and to provide physical boundaries for computational models that incorporate thickness mismatches between the Lo and Ld phases (25, 70-71). We constrain our systems to those that are biologically relevant, readily replicable, and amenable to study by both fluorescence microscopy and room-temperature AFM. These constraints translate into five specific actions. ***1.*** To maximize reproducibility, we use lipids with at most one degree of unsaturation in each acyl chain, thereby minimizing the potential for photo-oxidation (72- 73).

2. To visualize the Lo and Ld phases by fluorescence microscopy, we choose membranes that demix into domains that are larger than the diffraction limit of red light (> 1 μm). 3. To assess membrane thickness via room-temperature AFM, we study vesicles that demix above room temperature. 4. To maximize biological relevance, we investigate systems containing coexisting liquid phases and not those with coexisting gel and liquid phases (24). 5. To avoid preferential interactions between the AFM tip and different headgroups, we use only PC-lipids with glycerol-ester linkages. We determine if each system is capable of liquid-liquid phase separation by fluorescence microscopy. For those that demix into coexisting liquid phases, we measure the thickness difference between the two phases by atomic force microscopy (AFM). In doing so, we

Table 4 Physical parameters of low-T_{melt} and high-T_{melt} lipids; Phase behavior of ternary lipid membranes

high-T_{melt} lipid tail	low-T_{melt} lipid tail	$d_{high} - d_{low}$ (Å) [a]	Lo/Ld coexist ⩾25°C [b]	Fig [c]
13:0-PC	4Me-16:0-PC	– 0.7 [d]	Yes	26a
16:0-PC	20:1-PC	– 3.5	Yes	26a
16:0-PC	22:1-PC	– 7.4	Yes[e]	26a
12:0-PC	4Me-16:0-PC	– 2.8	No	26b
14:0-PC	20:1-PC	– 5.8	No	26b
17:0-PC	22:1-PC	– 5.8[d]	No	26c
16:0-PC	24:1-PC	– 13.2	No	26c
18:0-PC	24:1-PC	– 10.0	No	26c

[a]Difference in membrane thickness between single component membranes comprised of the high-T_{melt} (d_{high}) and low- T_{melt} (d_{low}) lipids (5,69). [b]Whether or not the ternary system (with cholesterol) exhibits coexisting liquid phases above 25°C. [c]Location of phase diagrams in Figure 26. [d]Data estimated as an average of thicknesses of membranes comprised of lipids with tails containing one more and one less carbon. [e]Requires exposure to light to phase separate.

show the difficulty of breaking the correlation between lipid tail order, T_{melt}, and thickness in systems containing coexisting liquid phases.

3.2 Materials and Methods

Lipids: All phosphocholine-lipids (Avanti Polar Lipids, Alabaster, AL), Texas Red dihexadecanoyl-PE (DHPE; Life Technologies, Grand Island, NY), and cholesterol (chol; Sigma, St. Louis, MO) were purchased and used without further purification. The PC-lipids and their single-component membrane T_{melt} values were as follows: dilauroyl-PC (12:0-PC, –2 ˚C), ditridecanoyl-PC (13:0-PC, 14 ˚C), dimyristoyl-PC (14:0-PC, 24˚C), dipalmitoyl-PC (16:0-PC, 41 ˚C), diheptadecanoyl-PC (17:0-PC, 50 ˚C), distearoyl-PC (18:0-PC, 55 ˚C), dioleoyl-PC (18:1-PC, –17 ˚C), dieicosenoyl-PC (20:1-PC, –4 ˚C), dierucoyl-PC (22:1-PC, 13 ˚C), dinervonoyl-PC (24:1-PC, 27 ˚C), and diphytanoyl-PC (4Me-16:0-PC, < –120 ˚C) (5, 75-76)(4)(74)(75). Properties of the lipids are summarized in Table 4 and in Table 7 in the Chapter 5 of this thesis.

Preparation of GUVs: Spherical GUVs were produced by electroformation (24, 32) at 60 ˚C for 1 hr. with the application of 1.5 V at 10 Hz. Vesicles to be assessed by AFM were made in 200 mM sucrose; the freshly-made vesicle solution was cooled to room temperature and diluted in 3 mL of 200 mM sucrose. Vesicles to be assessed by fluorescence microscopy alone were made in 18 MΩ-cm water, and further diluted before viewing. Electroformation in sucrose did not significantly shift T_{mix} for vesicles containing zwitterionic lipids (as opposed to lipids with a net charge) (76). Vesicles for fluorescence microscopy were labeled with 0.8 mol% Texas Red DHPE and used within 4 hours of electroformation.

Determination of T_{mix} in GUVs: Vesicles were imaged by fluorescence microscopy and T_{mix} values were determined as described previously (73). Briefly, the vesicle solution was placed between two coverslips, sealed with vacuum grease, and thermally coupled to a temperature-controlled stage on a fluorescence microscope. As temperature decreased, the percentage of vesicles exhibiting micron-scale liquid-liquid phase separation was recorded, and the resulting data was fit with a sigmoidal curve to determine T_{mix}, the temperature at which 50% of vesicles are phase separated. Variation in T_{mix} arises from small vesicle-to-vesicle compositional differences (24). In taut vesicles, gel domains were visually identified by their lack of coalescence and rigid, noncircular shapes; liquid domains are circular and coalesce (77).

Rupture of GUVs into spatially separated SLBs: The top layers of a mica disk (Highest Grade V1, Ted Pella, Redding, CA) were cleaved with Scotch tape (3M, St. Paul, MN) to reveal a clean surface. Then 500 µL of 200 mM glucose/5mM $CaCl_2$ was pipetted onto the mica, followed by 50 µL of GUV-rich sucrose solution. After 15 min., the bilayer was rinsed with 1 mL aliquots of water 20 times, taking care that the surface was never exposed to air. This process resulted in a mica surface densely covered with individual SLBs separated by areas of bare mica (Figure 1b). This surface remained submerged under water for the remainder of the experiment.

Conservation of area fraction upon GUV rupture: In Figure 25b, the total surface area of the free-floating vesicle was the same ($2.57 \pm 0.40 \times 10^3$ µm^2) as the SLB it became ($2.50 \pm 0.08 \times 10^3$ µm^2). The area fraction of the Ld phase was the same before (75 ± 4%) and after rupture (77 ± 2%). Equivalent area fractions in free-floating vesicles and SLBs are consistent with an absence of a major shift in miscibility tie-line endpoints upon rupture.

Measuring Lo/Ld area fractions: Free-floating, fluorescently labeled GUVs were imaged on a Nikon YFL microscope (Nikon, Melville, NY) to determine the Lo:Ld area ratio. The GUVs ruptured onto a mica disk to form SLBs as described above, and the area ratio was measured again by fluorescence microscopy (40). Fluorescence images were captured on a Coolsnap HQ charge-coupled device camera (Photometrics, Tuscon, AZ).

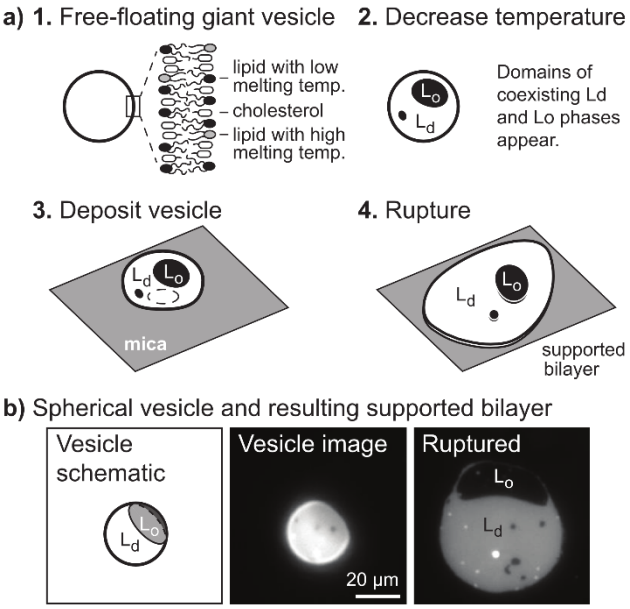

Figure 25 (a) Schematic of rupturing phase separated GUVs (b) Deposition and rupture of a phase separated GUV comprised of 18:1-PC/16:0-PC/chol/Texas Red DHPE (40/40/20/0.8 mol/mol) on mica via flourescence microscopy.

AFM not coupled with fluorescence microscopy: GUVs were ruptured onto a mica disk to form SLBs. The disk was adhered with Vaseline (Unilever, Englewood Cliffs, NJ) to the bottom of a perfusion cell (Bruker, Santa Barbara, CA). Images were acquired on a Dimension Icon Atomic Force Microscope (Bruker, Santa Barbara, CA) in quantitative nanomechanical mapping mode using SCANASYST-AIR cantilevers (k = 0.4 N/m, Bruker). We determined the thick:thin

area ratio of an individual SLB by imaging its entire surface. We compared the Lo:Ld area ratio to the thick:thin area ratio in order to associate the phases measured by AFM with the phases measured by fluorescence.

AFM coupled with fluorescence microscopy: Fluorescently labeled vesicles of 20/55/25 22:1-PC/16:0-PC/chol were introduced to a solution of 200 mM glucose/5mM $CaCl_2$ above the mica substrate and imaged with a fluorescence Hg light source filtered through a Texas Red HYQ filter block (Nikon) for approximately 5 minutes. Vesicles that remained unexposed to the light source did not phase separate. Bilayers were imaged with an MFP-3D-BIO Atomic Force Microscope (Asylum Research) seated on a Nikon Eclipse Ti microscope (78). Fluorescence images were captured on a Spot FX1520 CCD Camera (Spot Imaging Solutions, Sterling Heights, MI). Scans were performed in contact mode using DNP-10 tips (0.12 N/m, Bruker) at a constant scanning force from 0.2 - 0.4 nN (41).

AFM image processing: AFM images are flattened in Gwyddion as described in Chapter 5 (62). Height histograms are exported to MATLAB (MathWorks, Natick, MA) and fit with two Gaussian peaks corresponding to the thick and thin phases (ipf.m by TomO'Haver,http://terpconnect.umd.edu/~toh/spectrum/InteractivePeakFitter.htm#Keypress_operated_version:_ipf.m, February **2015**) as described in the supplementary methods. Reported membrane thicknesses are differences between the centers of these peaks and are summarized in Tables 9-13 in Chapter 5.

3.3 Results

We used fluorescence microscopy to determine giant unilamellar vesicles (GUVs) made from the ternary mixtures of the lipids listed in the rows of Table 4 (plus cholesterol) are capable of liquid-liquid phase separation in the temperature range of 10-50 ˚C. We plot our results on Gibbs phase triangles (Figure 26). Systems consisting of 4Me-16:0-PC/13:0-PC/chol or 20:1-PC/16:0-PC/chol (Figure 26a) demix into coexisting liquid phases above 25 ˚C. Systems consisting of 4Me-16:0-PC/12:0-PC/chol or 20:1-PC/14:0-PC/chol (Figure 26b) exhibit coexisting liquid phases below 25 ˚C. Systems consisting of 22:1-PC/17:0-PC/chol, 24:1-PC/18:0-PC/chol or 24:1-PC/16:0-PC/chol (Figure 26c) do not separate into coexisting liquid phases, but instead exhibit gel-liquid coexistence. Probing only a few compositions is sufficient to determine that no liquid-liquid phase coexistence occurs because any such coexistence in these systems would appear at the upper boundary of the gel-liquid region (31, 79-82). Systems consisting of 22:1-PC/16:0-PC/chol (Figure 26d) also do not exhibit liquid-liquid coexistence except in the case of intentional photo-oxidation, which is explicitly avoided elsewhere in our experiments. Photo-oxidation, which typically raises T_{mix} (72, 83), produces coexisting liquid phases at the composition marked with the colored circle (Fig. 26d). All colored regions or circles in the phase diagrams correspond to the determined value of T_{mix}.

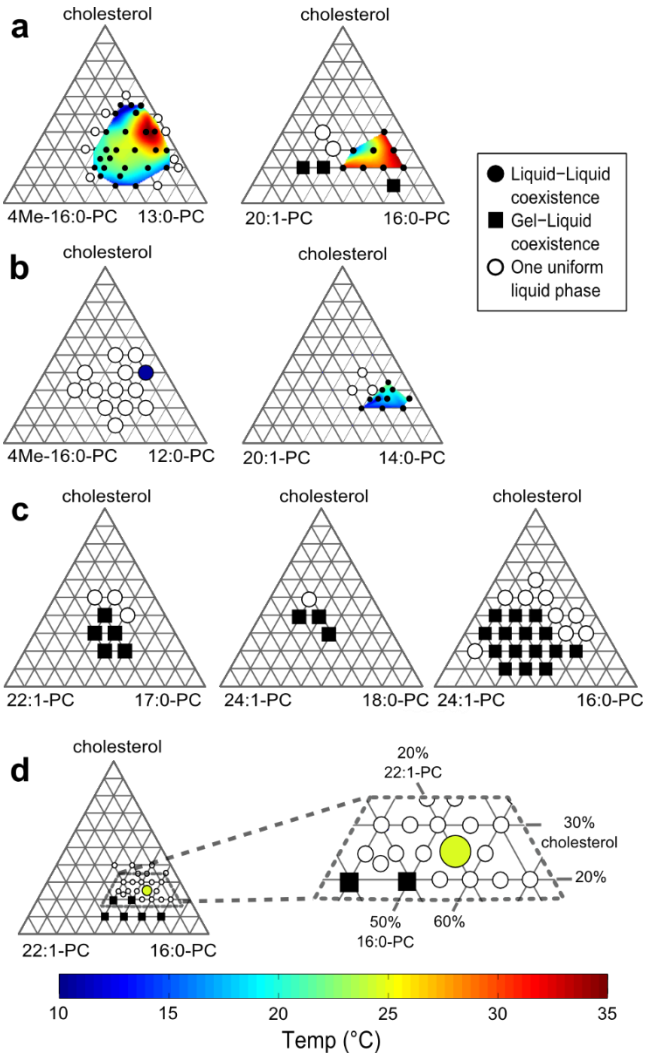

Figure 26 Gibbs phase triangles of ternary giant unilamellar vesicles (GUVs) as determined by fluorescence microscopy. Phase diagrams exhibit (a) coexisting liquid phases above 25 ˚C, (b) coexisting liquid phases only below 25 ˚C, (c) no coexisting liquid phases, or (d) coexisting liquid phases only after photo-oxidation.

To quantitatively assess whether T_{mix} of our ternary systems correlates with the physical properties of single-component membranes comprised of the composite lipids, we graphed the highest T_{mix} versus the difference in the number of carbons in the acyl chains of the two PC-lipids (Figure 27a), the highest phospholipid T_{melt} in the system (Figure 27b), the difference in

thicknesses of single-component membranes of PC-lipids (Figure 27c), or the difference in T_{melt} of single-component membranes of PC-lipids (Figure 27d). We find that there is no monotonic relationship between the highest T_{mix} of the ternary system and any of these single-component system parameters. This lack of a clear correlation demonstrates the difficulty of predicting T_{mix} of ternary mixtures from the composition alone.

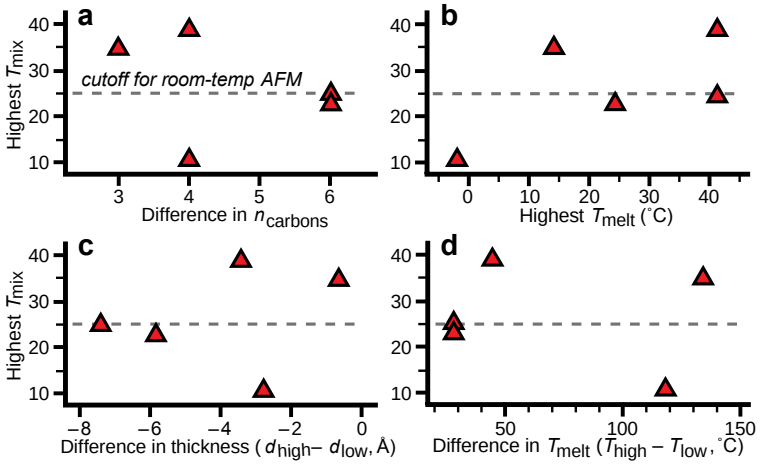

Figure 27 Comparison of properties of ternary membranes to physical parameters of the underlying single-component systems. Plotted are the highest liquid-liquid demixing temperature (T_{mix}) of the ternary systems versus (a) the difference in the number of carbons in the two PC-lipid tails, (b) the highest lipid gel-to-liquid melting temperature (T_{melt}), (c) the difference in thicknesses of the single-component membranes (d_{high} - d_{low}), or (d) the difference in T_{melt} of the single-component membranes. Numerical values are tabulated in Table 7 in the supplement of this thesis.

Our second goal was to determine if the Ld phase is thicker than the Lo phase in any of our membranes that exhibit liquid-liquid phase coexistence. Because we assessed thicknesses with room-temperature AFM, we limited our sample set to membranes that demix above 25 ˚C: 4Me-16:0-PC/13:0-PC/chol, 20:1-PC/16:0-PC/chol, and 22:1PC/16:0-PC/chol.

Table 5 lists the Lo:Ld area ratios and thickness measurements for all phase separated systems scanned in AFM at room temperature. For the 20:1-PC/16:0-PC/chol and 4Me-16:0-PC/13:0-PC/chol ternary mixtures, we performed flourescence and AFM on separate populations of GUVs for two different molar ratios: one rich in the Lo phase and the other rich in the Ld phase, making four systems in total. To verify that the rupturing process does not change phase behavior, we measured the area ratios of free floating GUVs and the resulting supported lipid bilayers and found no appreciable change in area ratio. We then scanned individual supported lipid bilayers by AFM and measured the thickness difference between the two phases and the thick:thin membrane area ratio. By comparing area ratios, we determined that all four of these systems have thicker Lo phases than Ld phases. Figure 28 shows fluorescence micrographs (Figure 28 a,b) and AFM scans (Figure 28 c,d) of GUVs composed of 20/40/40 mol% 4Me-16:0-PC/13:0-PC/chol. All AFM scans and height values are summarized in Tables 9-13 in the supplement of this thesis.

We found that GUVs comprised of 20/55/25% 22:1-PC/16:0-PC/chol require exposure to light to exhibit phase separation. Our original AFM setup was not coupled to a fluorescence light source. For measuring 20/55/25% 22:1-PC/16:0-PC/chol we moved to an AFM coupled with a fluorescence microscope. Besides providing a light source, the coupled fluorescence microscope-AFM had the added advantage of allowing us to directly compare the Lo and Ld phases in fluorescence microscopy with the thicker and thinner phases in AFM scans (Fig. 28d,e). We found that the Ld phase was thicker than the Lo phase in this photo-oxidized system (Table 5).

Table 5 Experimentally determined Lo and Ld area ratios and thickness mismatches at room temperature.

System	Lo:Ld GUVs [a]	Lo:Ld SLBs [b]	Thick:Thin AFM [c]	Thickness Mismatch (Lo – Ld, Å) [d]
20/60/20% [f] 20:1-PC/16:0-PC/chol	67:33 ± 2 [g] (N = 23) [h]	78:22 ± 3 (N = 8)	73:27 ± 2 (N = 3)	9.6 ± 0.1 (N = 3)
50/30/20% 20:1-PC/16:0-PC/chol	24:76 ± 2 (N = 25)	25:75 ± 3 (N = 7)	32:68 ± 9 (N = 4)	8.3 ± 0.1 (N = 4)
30/40/30% 4Me-16:0-PC/13:0-PC/chol	43:57 ± 2 (N = 23)	43:57 ± 1 (N = 10)	40:60 ± 8 (N = 3)	3.3 ± 1.2 (N = 3)
20/40/40% 4Me-16:0-PC/ 13:0-PC/chol	64:36 ± 3 (N = 13)	69:31 ± 1 (N = 46)	75:25 ± 7 (N = 4)	5.9 ± 1.0 (N = 4)
20/55/25% 22:1-PC/16:0-PC/chol	-- direct identification --			– 4.4 (N = 1)

[a]Ratio of areas of Lo and Ld phases within free floating GUVs imaged by fluorescence microscopy. [b]Ratio of areas of Lo and Ld phases within supported lipid bilayers (SLBs) made from individual, ruptured GUVs, imaged by fluorescence microscopy. [c]Ratio of areas of thick and thin membranes within SLBs imaged by AFM. [d]Measured thickness mismatch of Lo and Ld phases measured by AFM. [e]Location in Figure 26 where data are found. [f]Percent mole ratio of the three components. [g]Standard error of the mean. [h]Number of vesicles recorded.

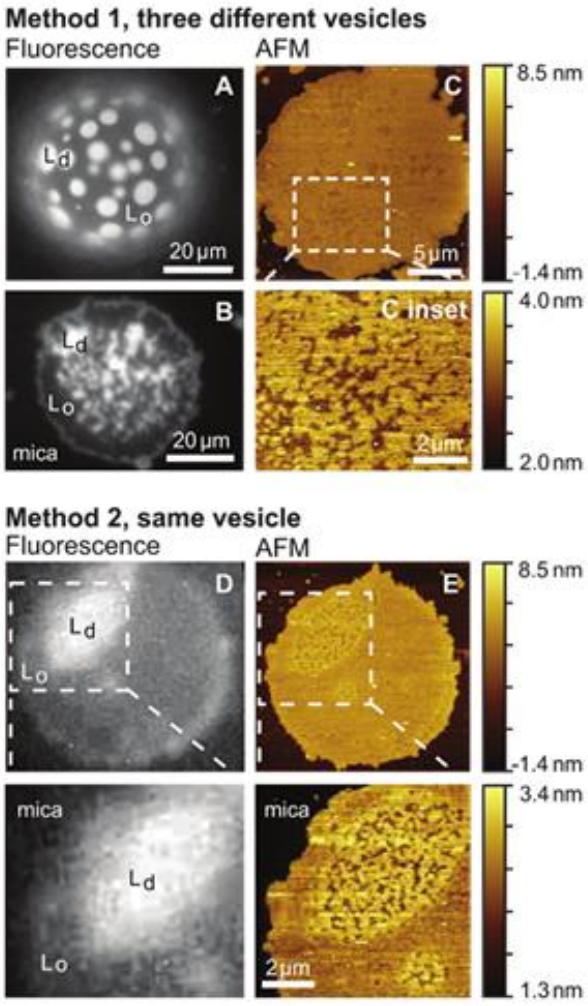

Figure 28 Room temperature fluorescence microscopy (left) and AFM topography (right) of membranes composed of 20/40/40 mole % 4Me-16:0-PC/13:0-PC/chol (top) and 20/55/25 mole % 22:0-PC/16:0-PC/chol (bottom). A-C: (A) Fluorescence microscopy image of a GUV and (B) an isolated supported bilayer formed by rupturing a GUV onto mica. (C) AFM topography of an isolated supported bilayer (D) fluorescence microscopy image and (E) AFM topography of the same supported bilayer

3.4 Discussion

Our finding that ternary membranes comprised of long-chain low-T_{melt} lipids, short chain high-T_{melt}, and cholesterol produce thicker Lo than Ld phases under standard experimental conditions is surprising. Given that low-T_{melt} lipids partition preferentially into the Ld phase (and high-T_{melt} lipids into Lo phases) and that single-component membranes made of the low-T_{melt} lipid are thicker than those made of the high-T_{melt} lipid, we expected to find some cases of thicker

Ld than Lo phases. We find none (Table 5) except for when vesicles are intentionally photo-oxidized.

Our work shows that it is challenging to translate thickness data collected for single-component membranes into quantitative predictions of thickness differences between the Lo and Ld phases in ternary systems. The Lo and Ld phases contain mixtures of the low-T_{melt} lipid, high-T_{melt} lipid and cholesterol (79). Cholesterol thickens membranes and is hypothesized to differentially thicken the Lo phase for two reasons. First, in PC-lipid membranes, the Lo phase contains marginally higher fractions of cholesterol than the Ld phase does (9, 27, 79-80, 84). Second, the Lo phase contains higher fractions of saturated lipids, and cholesterol thickens membranes of saturated lipids more than it thickens those comprised of unsaturated lipids (9, 85).

In theory, preferential thickening of the Lo phase by cholesterol could be overcome by shortening the high-T_{melt} lipid or lengthening the low-T_{melt} lipid. However, we find that doing this drives the liquid-liquid coexistence region to temperatures below 25 ˚C or eliminates it altogether. For systems that exhibit liquid-liquid phase separation, there is no monotonic relationship between the highest T_{mix} and any of several physical parameters of the lipid components, such as the difference in thicknesses or T_{melt} values of pure bilayers (Figure 3). This lack of a clear correlation implies that the properties of lipid mixtures depend on nuances of lipid structure that are not captured by the properties of single-component membranes.

To date, quantitative measurements of the thickness mismatches between Lo and Ld phases have been reported for only a few systems (6-7, 36, 41, 43, 45-48, 54, 86-90). Those published data, combined with our thickness difference measurements in Table 7 in the supplement

provides evidence about the alignment of bilayers on solid supports. In a supported bilayer, all phospholipid headgroups that face the substrate may lie in the same plane, such that any thickness mismatch is accommodated entirely in the monolayer furthest from the surface. Evidence in support of this scenario is found in some reported thickness differences between Lo and Ld phases in 40/40/20 18:1-PC/16:0-PC/chol supported lipid bilayers. Measurements by AFM, which are sensitive to the difference in height between the top leaflets of each phase, give values of 1.2 ± 0.1 (from our data in Table 8 in Chapter 5), 1.2 ± 0.2 (87) and 0.65 ± 0.02 nm (54). All of these values are larger than thickness differences measured by x-ray diffraction, which is sensitive to the thickness of both leaflets (0.56 ± 0.2 nm) for the same system (88). On the other hand, Nielsen and Simonsen make the opposite argument (36) and report a thickness difference by ellipsometry of supported bilayers, which, like X-ray diffraction, is sensitive to the total thickness difference. Their value of 1.69 nm is significantly larger than all step heights reported by AFM, from which they conclude that thickness differences in supported bilayers are accommodated on both faces of the membrane. The central results of our study depend only on the sign of the thickness difference between the Lo and Ld phase, not on the alignment of the bilayer on the substrate.

Within the limited set of reports of thickness mismatches between Lo and Ld phases, there are no direct observations of a thicker Ld phase (6-7, 36, 41, 43-48, 54, 86-90). Lin and London previously reported indirect results consistent with a thicker Ld phase and interpreted changes in fluorescence signals as evidence that mutants of perfringolysin O of different lengths partition into different phases of a model membrane (23). The membrane they used was a quaternary mixture that does not produce micron-scale liquid domains.

Here, we report a direct measurement of a thicker Ld phase, with the major caveat that it occurs for a single lipid composition and requires photo-oxidation, which perturbs the membrane's lipid composition (72). A less important caveat is that the origin and significance of the small-scale structure in Figure 28E is unclear; it may not exist in a corresponding membrane of a free-floating vesicle. For instance, submicron inhomogeneity may arise due to an offset between the temperature of the AFM and the temperature at which vesicles are ruptured, or due to a shift in miscibility transition temperature between a vesicle and a supported bilayer. Indeed, shifts in T_{mix} can result from membrane adhesion to surfaces (76, 91-93). As a result of temperature shifts, the membrane may approach a critical point (31, 73), or new solid or liquid domains may nucleate but be hydrodynamically hindered from coarsening (37, 77, 94). Temperature shifts that result in three-phase (Lo-Ld-gel) membranes provide a particularly compelling explanation of the appearance of noncircular, small domains in supported membranes made from ruptured GUVs (31, 40).

Review of the data amassed in Table 4 and Figure 27 suggests tactics to be employed in future direct searches of thicker Ld than Lo phases. A lack of temperature control in our AFM setup requires room-temperature phase-separation in membranes. Methods that assess membrane thickness below room temperature could be applied to 20:1-PC/14:0-PC/chol, which is a promising system both because of the large difference in acyl chain lengths and because of implications by Lin and London that a similar system (20:1-PC/16:0-PC/14:0-PC/chol) features thicker Ld than Lo phases. Another tactic would be to employ chemical synthesis to produce a low-T_{melt} lipid with longer methylated chains than 4Me-16:0-PC. Any tactic that involves replacing the low-T_{melt} lipid with a polyunsaturated lipid (e.g., 22:6-PC) should be undertaken

with caution because acyl chains of polyunsaturated lipids are readily photo-oxidized and because those chains are more likely than chains of singly unsaturated lipids to fold back on themselves such that their methyl carbons lie near lipid head groups, which negates the expected thickening from adding carbons to the tail (95).

3.5 Conclusion

In conclusion, here we combine fluorescence microscopy and room temperature AFM to measure transition temperatures and Lo-Ld thickness mismatch in model membranes. Despite using non-canonical ternary lipid mixtures where the pure membrane of the low-T_{melt} lipid is thicker than a pure membrane of the high-T_{melt} lipid, we found that none of the non-canonical compositions in Table 5 produced thicker Ld than Lo phases under standard experimental conditions (i.e. without photo-oxidation of the membrane). Moreover, we find no simple monotonic relationship between the highest possible miscibility transition temperature in these ternary membranes and the relative properties of pure membranes of the low-T_{melt} and high-T_{melt} lipids. It is a common (96-97) and even textbook assertion (98-99) that rafts within cell membranes contain lipids with more ordered acyl chains and are thicker than the surrounding cell membrane. Even when we employ the non-canonical lipid mixtures in Table 4, we find no physical reason to challenge this assertion. Future direct searches for thicker Ld regions may find it productive to employ low-temperature methods or to incorporate lipids with longer methylated chains in the membranes.

Chapter 4

THICKNESS DIFFERENCES BETWEEN LO AND LD BILAYERS DO NOT UNIQUELY DETERMINE MIXING TEMPERATURES

4.0 Contributions

This chapter is slightly modified from a manuscript of the same title by Joan V. Bleecker, Phillip A. Cox, and Sarah L. Keller, in preparation for submission to the Biophysical Journal.

4.1 Introduction

Model lipid membranes composed of a high-melting temperature (T_{melt}) lipid, a low-T_{melt} lipid, and a sterol can phase separate into liquid ordered (Lo) and liquid disordered (Ld) phases (100). Phase separation is a proposed mechanism for the formation of rafts in cell membranes. Typically the Lo phase is thicker than the Ld phase (48, 101-102) and is sometimes referred to as the "raft-like" or "raft" phase by researchers seeking to connect membrane phases to the raft hypothesis (103).

Two important parameters of phase separation are the mixing temperature, T_{mix}, below which the Lo and Ld phases appear, and the thickness difference between the Lo and Ld phases, Δh. Bilayer thickness affects protein function (10, 21) and Δh affects protein sorting (104). Here we address relationships between T_{mix} and Δh in ternary model membranes.

We frame how Δh and T_{mix} are related in a general way in Figure 29. Comparing various

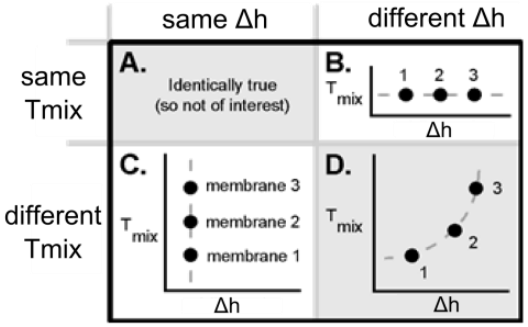

Figure 29 General trends between thickness mismatch, Δh and mixing temperatures, T_{mix} for ternary phase separated membranes. D was previously seen in (9). We present membranes with trends in B and C.

bilayer systems, Δh can be the same or not (Figure. 29, vertical labels) and T_{mix} be the same or not (Figure 29, horizontal labels). Previous work by Garcia-Sáez et al. found that T_{mix} increases with increasing Δh (Figure 29D) for systems of 40/40/20 mole % N-stearoyl-D-erythro-sphingosylphosphorylcholine/low-Tm lipid/cholesterol in which the low-Tm lipid phosphocholine (PC) lipid is systematically lengthened by two carbons from 14:1 (largest T_{mix} and Δh) to 22:1 (smallest T_{mix} and Δh) (48). These results have been interpreted to mean that hydrophobic thickness mismatch is a key parameter which "promotes" or "drives" phase separation, possibly through increasing line tension (97, 104). Here we address whether the correlation seen in Garcia-Sáez et al. between Δh and T_{mix} is determinant: if two systems exhibit different values of Δh, do they necessarily exhibit different values of T_{mix}, and vice versa?

We measure T_{mix} of labeled giant unilamellar vesicles, GUVs, with fluorescence microscopy and measure Δh of supported lipid bilayers with atomic force microscopy, AFM. Our results show two cases in which changing either Δh or changing T_{mix} does not result in a change of the other parameter (Figure 29 B and C).

4.2 Materials and Methods

For the relationship in Figure 29B, we measure Δh of membranes with compositions along a 40-41°C T_{mix} isotherm. Each starting composition falls on a different tie-line. Shorter tie-lines result in Lo and Ld phases with more similar phase compositions (27, 41) and smaller Δh.

For the relationship in Figure 29C, we measure membranes with compositions on a 22°C tie line (27). Compositions along the tie line phase separate into Lo and Ld phases with the same phase compositions (Figure 30) (24). The change in T_{mix} along a tie line is related to the change

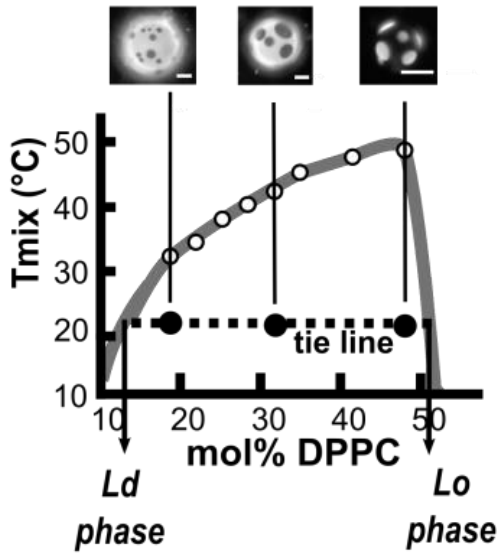

Figure 30 Phase separated compositions along a tie line. The thick gray line is to guide the eye. White circles are the experimentally determined T_{mix}. Black circles are the composition along the tie line (27). Fluorescence micrographs of DiPhyPC/DPPC/chol GUVs are at 22°C. Scale bars are 10 μm. Tie line compositions and T_{mix} are listed in Table 6.

in mole fraction Lo and Ld phases via the lever rule (24). We observe the expected trend that Lo area fraction increases with increasing mole % DPPC (Figure 30).

All phospholipids (Avanti Polar Lipids, Alabaster, AL) Texas Red DHPE (Life Technologies, Grand Island, NY), and cholesterol (chol; Sigma, St. Louis, MO) were used without further purification. Vesicles were composed of different ratios of dipalmitoyl-PC (DPPC), diphytanoyl-PC (DiPhyPC), and cholesterol. We used all saturated lipids to minimize photooxidation. Vesicles were fluorescently labeled with 0.8 mole % Texas Red dihexadecanoyl-PE (Texas Red DHPE), which partitions preferentially to the Ld phase. GUVs were electroformed and imaged as previously described (105). We define T_{mix} of GUVs as the temperature at which 50% of the vesicles are phase separated given a sigmoidal fit of % vesicles phase separated vs. T_{mix} as described by Gray et. al. (Figure 31) (106). Uncertainties in T_{mix} are reported as 95% confidence intervals of the fit (Figure 31A).

To form continous supported lipid bilayers for AFM measurements, sonicated small unilamellar vesicles were deposited on mica at 60°C in 5mM $CaCl_2$ (41). The resulting bilayer

was pipette rinsed with water and allowed to cool to room temperature (21-23°C). The bilayer was scanned underwater on an Asylum Cypher ES Environmental AFM system SLD-DD (Asylum Research, Santa Barbara, CA) in tapping mode with blueDrive™ Photothermal Excitation using an Arrow UHFAuD tip (6 N/m, NanoWorld, Neuchâtel, Switzerland). The sample chamber was kept at 22°C throughout scanning.

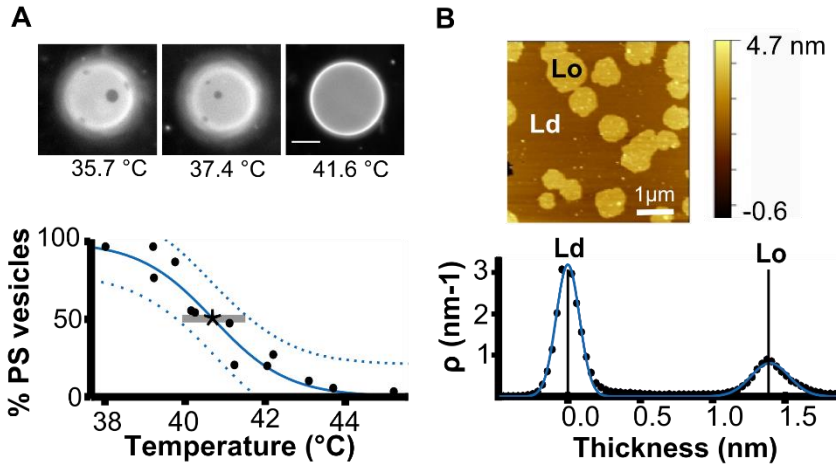

Figure 31 Experimental measurements of T_{mix} and Δh for 48/32/20 DiPhyPC/DPPC/chol bilayers. (A) GUV micrographs (top) and a graph of % GUVs phase separated vs. temperature (bottom). Black dots are data points. The blue line is the sigmoidal fit of the data. Dashed blue lines are the 95% confidence interval. The star is the reported T_{mix}, and the gray bar is the reported uncertainty of T_{mix} 40.7 ± 0.3°C (B) AFM scan of supported lipid bilayer at 22°C (top) and height histogram of the AFM scan (bottom). Black dots are the data. The blue line is the Gaussian peak fit of the data. Reported Δh is the distance between the two peak averages and reported uncertainty is the standard deviation of the bootstrap fit, 1.39 ± 0.02 nm. All T_{mix} and Δh are listed in Table 6.

AFM images were flattened in Gwyddion (62). Height histograms were exported to MATLAB (MathWorks, Natick, MA) and fit with Gaussian peaks representing the thicker Lo and thinner Ld layers (ipf.m by Tom O'Haver, http://terpconnect.umd.edu/~toh/spectrum /InteractivePeakFitter.htm#Keypress_operated_version:_ipf.m, February 2015). Fit uncertainties,

determined by a 100 trial bootstrap method, were much smaller than scan to scan variation (Figure 31 B). Reported uncertainties in Table 6 are the uncertainties of the mean of at least 3 separate scans per composition.

4.3 Results

Our results are graphed in Figure 30 and 32 and listed in Table 6. The two graphs in Figure 32 show how changing the composition, i.e. the mole % of of DiPhyPC/DPPC/chol, results in trends in which T_{mix} and Δh of the systems vary independently. Phase boundaries and tie lines of other low-T_{melt} lipid/high-T_{melt} lipid/cholesterol systems behave similarly to this system. Therefore our results apply to a broad range of Lo-Ld phase separated systems.

4.4 Discussion

We present systems in which membrane thickness differences do *not* uniquely predict mixing temperatures. Previously Garcia-Sáez et al. measured ternary membranes in which the low-T_{melt}

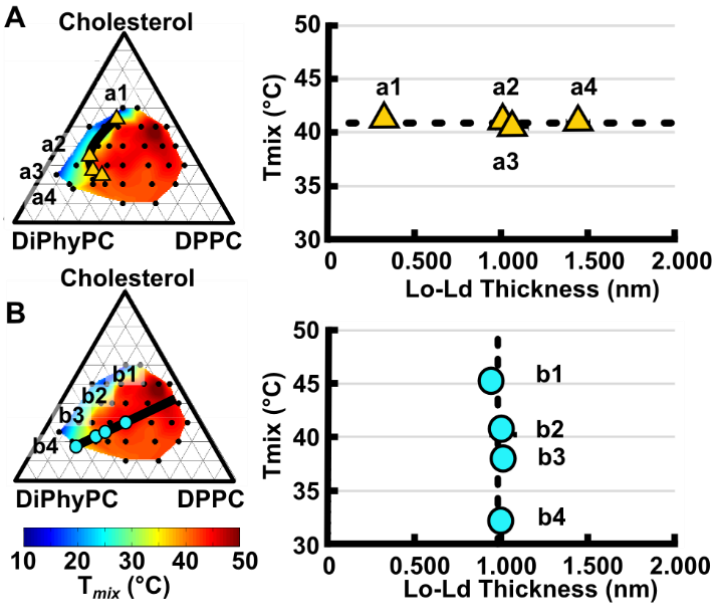

Figure 32 Experimental T_{mix} and Δh at 22°C of (A) compositions along a 40-41°C T_{mix} isotherm and (B) compositions along a previously determined 22°C tie-line. Error bars are covered by the symbols. Vertical and horizontal dashed lines on the graph are drawn for clarity.

Table 6 Miscibility temperatures and Lo/Ld thickness mismatch of phase separated supported lipid bilayers.

	mole % DiPhyPC/DPPC/chol	T_{mix} (°C)	Average Lo – Ld thickness (nm)
Tie-line Compositions			
a1	35 / 35 / 30	45.3 ± 0.5	0.94 ± 0.07
a2	46.5 / 28.5 / 25	40.2 ± 0.5	1.06 ± 0.09
a3	52.2 / 25.3 / 22.5	38.0 ± 1.1	1.03 ± 0.03
a4	63.7 / 18.8 / 17.5	32.2 ± 0.5	1.01 ± 0.03
Isothermal Compositions			
b1	27 / 23 / 50	41.0 ± 0.4	0.320 ± 0.003
b2	50 / 20 / 30	40.9 ± 1.2	1.003 ± 0.0003
b3	46.5 / 28.5 / 25	40.2 ± 0.5	1.06 ± 0.09
b4	48 / 32 / 20	40.7 ± 0.3	1.43 ± 0.07

T_{mix} uncertainties are from the 95% confidence intervals sigmoidal fit of % vesicles phase separated vs. temperature. Lo-Ld thickness uncertainties are the standard errors of the mean of Lo-Ld for at least three separate AFM scans per composition.

was systematically shortened from 22 to 14 carbons (Figure 29D) found an increase in both Δh and T_{mix}. To give a more complete picture of how changing the length of one of the lipid tails changes phase behavior, we map the difference in phase behavior for DiPhyPC/DPPC/chol vs. DiPhyPC/Di13:0 PC/chol (Figure 33). Di13:0 PC has three fewer carbons in each tail than DPPC. Wider phase boundaries translate to longer tie-lines and larger Δh. Like Garcia-Sáez et al., we would measure that a higher Δh results in a higher T_{mix} if we arbitrarily fixed the ratio of the three membrane components. However, it is not clear which ratio should be chosen given that the liquid-liquid coexistence region is not radially symmetric around a common lipid ratio. A different choice of this ratio will result in a different quantitative relationship between Δh and T_{mix}. Our results in Figure 32 show the challenges of establishing how Δh quantitatively relates to T_{mix}: increased height mismatch need not result in increased T_{mix} if the ratio of lipids is changed.

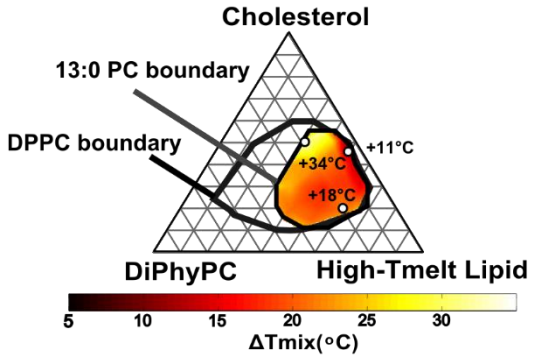

Figure 33 Change in T_{mix} (ΔT_{mix}) for GUVs of DiPhyPC/DPPC/chol versus DiPhyPC/13:0-PC/chol. DiPhyPC/DPPC/chol has higher T_{mix} for all ratios in the shared miscibility region and larger phase boundary.

As observed elsewhere, here we found that all domains of the same phase merged on the surface of taut GUVs until only one domain of each phase remained (77). Heberle et al. measured the number and size of domains on phase separated 60nm diameter vesicles using small angle neurtron scattering and found that systems with smaller Δh had a higher number of unmerged domains (from < 2 domains per vesicle for Δh = 0.97 nm to 23 domains per vesicle for Δh = 0.64 nm) (6). They compared their height measurements to previous AFM measurements (48). Our smallest Δh, 0.32 nm, did not exhibit mulitple stable domains; domains always merged in taut vesicles. Our results imply that a small value of Δh alone does not determine the number of stable domains for a phase separated system.

We present systems in which membrane thickness differences do *not* uniquely predict mixing temperatures. Our work is an experimental counterpoint to the previously reported trend that mixing temperatures depend strongly on the thickness mismatch of the two phases.

Chapter 5
SUPPLEMENT

5.1. Method: AFM image processing (flattening) in Gwyddion.

AFM images produce a false color topographic map. The default gray color is set to gold (Figure 23, AFM Methods). Mean plane subtraction is used to eliminate background tilt that obscures bilayer thicknesses. Next, scan lines are corrected by matching height medians, and the image is corrected for horizontal scars. The mica and the lipid membrane, which may contain both thick and thin regions, produce at least two distinct height populations. To avoid to non-physical flattening results due to these populations, we mask out each layer individually using the marks grains tool and by performing a median line scan correction on each layer separately. Last, we mask out of the lowest feature, which is either the mica or thin membrane, and perform a zeroth order background subtraction to set this feature to ~0 nm. An exact zero is not necessary for interpreting height differences because we can subtract differences when evaluating data. We then use Gywddion's 1D statistical functions to obtain the height histogram. We export height histogram values to excel, read the excel file into Matlab and fit the data with peaks using 100 bootstrap trial method as part of a peak fitting program (ipf.m by Tom O'Haver, http://terpconnect.umd.edu/~toh/spectrum/InteractivePeakFitter.htm#Keypress_operated_version:_ipf.m, February 2015).

5.2 Method: Fitting AFM height histogram peaks to determine thickness mismatch

The interactive Matlab peak-fitting program Ipf.m uses an unconstrained non-linear optimization algorithm to decompose separate and/or overlapping-peaks into component peaks.[17]

This process gives us differences in thickness between membrane regions, standard deviations in thickness, and areas of the peaks, which allows us to calculate the percent of the membrane area covered by thin and thick phases.

The default peak shape is a Gaussian, and other peak types are available. We find that changing peak type from Gaussian to other peak types, like Lorentzian, results in larger fit uncertainties and larger standard deviations from bootstrap methods. Running ipf.m produces a scatter plot of the height histogram data within an interactive graph. The user then selects the range of x-values (heights in nm) that encompasses all peaks of interest. The program requires first guesses for the peak positions, which is done automatically or by clicking on peaks. We used the clicking functionality because it is recommended for data like ours for which peaks are not evenly spaced.

We next performed a 100 trial bootstrap fit. In each trial, the data set is divided into two sub-sets, each of which is fit, and then the process is repeated. The resulting standard deviation reflects the stability of the peak fit with respect to random noise in the data. Our reported values for thickness differences between thick and thin regions of membranes (Tables 9-20) are the differences in the bootstrap mean value of the fitted peaks from the bootstrap fit. The reported uncertainties in the values for each image are the propagated errors from standard deviations produced by the bootstrap method. These uncertainties range from very small values (requiring three decimal places) to two unusually large values. The two examples of large uncertainties appear in Table 11 #2 and Table 12 #4, for which the bootstrap standard deviation is larger than the interquartile range, indicating that at least one trial fit is significantly different from the

average fit. For those cases, the standard deviation from the interquartile range is used instead of the bootstrap standard deviation, because the interquartile range is less susceptible to outliers.

Only two images (Table 11 #1 and #3) presented cases in which the bootstrap calculation failed to produce a physically plausible, stable fit. This is unsurprising because the two bilayer peaks significantly overlap for these two images. For these two images, we surveyed the trial fits until we found a fit that made physical sense. We then pinned the peak means to the means of these fits and performed a bootstrap fit to determine the areas of the two bilayer peaks. We did not report standard deviations for these fits. Inclusion of these images does not skew our data because we would obtain similar results from the image in Table 11 #2 alone.

5.2 Physical parameters of lipid pairs in Study 2 and AFM control

Table 7 Physical parameters of lipid pairs that exhibit liquid-liquid phase separation with cholesterol

high-T_{melt} lipid[a]	low-T_{melt} lipid[a]	high-T_{melt}[b] (°C)	low T_{melt}[b] (°C)	Δn_{carbon}[c]	ΔT_{melt}[d] (°C)	d_{high}-d_{low}[e] (Å)	Max T_{mix}[f] (°C)
12:0 PC	4Me-16:0 PC	-2	-120	4	118	-2.8	11
13:0 PC	4Me-16:0 PC	14	-120	3	134	-0.7[g]	35
14:0 PC	20:1 PC	24	-4	6	28	-5.8	23
16:0 PC	20:1 PC	41	-4	4	45	-3.5	39
16:0 PC	22:1 PC	41	13	6	28	-7.4	25[h]

[a]High and low melting temperature (T_{melt}) lipid pairs. Numbers indicate acyl chain length:degree of unsaturation of the two lipid tails. 4Me indicates four methyl groups along the acyl tail. [b]Melting temperatures of pure lipid bilayers. [c]Difference in the number of carbons on the acyl chain. [d]Difference in melting temperatures of the two lipids [e]Difference in pure membrane thicknesses from (54, 69)(54)(69). [f]Maximum observed transition temperature for low-T_{melt}/high-T_{melt}/cholesterol [g]13:0 PC thickness not measured, estimated as an average of lipids with 1-greater and 1-fewer carbon tail. [h]Vesicles require exposure to light to phase separate.

Table 8 Control system for AFM

Method 2 Control	T_{mix}[a] (°C)	Lo – Ld[b] AFM (nm)	Literature Ld - Lo AFM (nm)
40% 18:1 PC	34 ±1	1.240±0.018[c]	1.2±0.2[d]
40% 16:0 PC		1.182±0.019	0.65±0.02[e]
20% chol		0.958±0.011	
		1.381±0.004	

[a]Transition temperature previously determined by (105). [b]Bootstrap peak fit thickness mismatch of AFM scans ± bootstrap standard deviation. The average thickness mismatch of the four images is 1.190 ± 0.101 nm. [d] (54) [e] (87)

5.3 Tables of AFM scans for Chapter 3

Table 9 AFM images, peak fits, and resulting data for 20/60/20 mole % 20:1-PC/16:0-PC/chol supported lipid bilayer

#	AFM image[a]	(Top) Height histogram[b] (Bottom) Peak fit[c]	Difference in thickness between thin and thick membrane regions (nm) [d]	Ratio of areas of thick:thin regions [e]	Avg. thickness mismatch (nm) and ratio of areas of thick:thin regions [f]
1	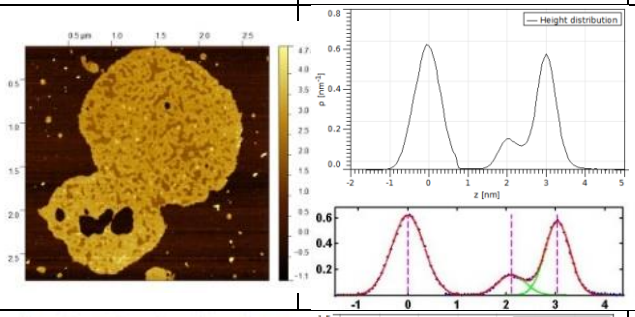		0.938 ± 0.391	77:23	0.95 ± 0.06 73:27 ± 2
2	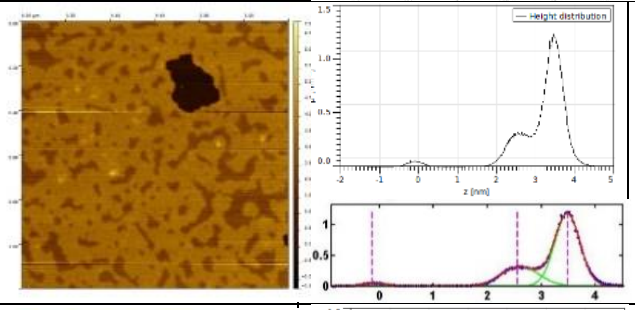		0.872 ± 0.004	72:28	
3	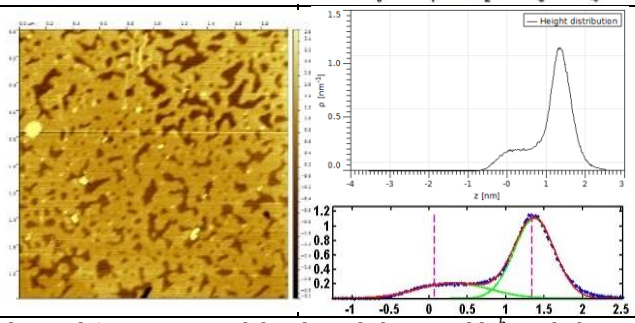		1.037 ± 0.066	74:26	

[a]Flattened AFM image with height scale bar in gold. [b]Height histogram in Gwyddion. [c]Typical peak fit trial of the height histogram in a 100-trial bootstrap fit. Blue dots fit by the dark red line is the total peak fit, light green lines are the component peaks, and magenta dashed lines show the first guess at peak position from the previous trial. [d]Difference between thickness of the thin and thick regions of the membrane reported as the mean difference in the location of the peaks determined by the bootstrap method. The reported uncertainty is the propagated standard deviation from the bootstrap fit of the two bilayer peaks. [e]Ratio of areas of thick and thin membrane regions from the bootstrap average areas of the two bilayer peaks. [f]Average thickness difference from column 4. The reported uncertainty is the standard error of the three values. [g]The image in row 2 is a higher-magnification region of the vesicle in row 1.

Table 10 AFM images, peak fits, and resulting data for 50/30/20 mole % 20:1-PC/16:0-PC/chol supported lipid bilayer.

#	AFM image[a]	(Top) height histogram[b] (Bottom) peak fit[c]	Difference in thickness between thin and thick membrane regions(nm) [d]	Ratio of areas of thick:thin regions [e]	Avg thickness mismatch (nm) and ratio of areas of thick:thin regions [f]
1	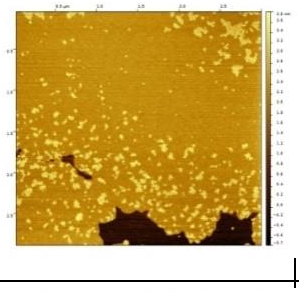	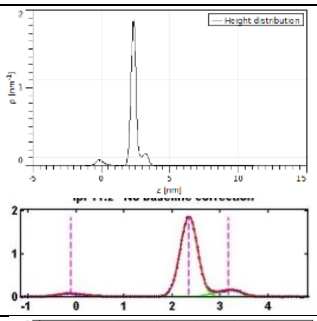	0.824 ± 0.003	12:88	0.83 ± 0.08 32:68 ± 9
2	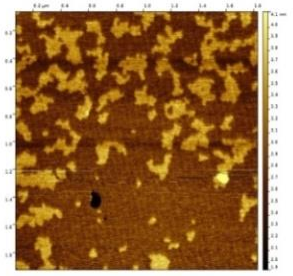	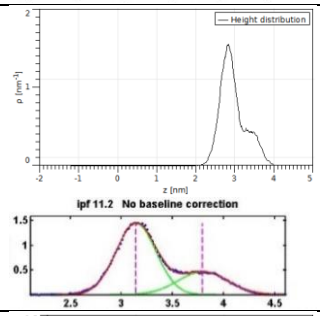	0.652 ± 0.002	29:71	
3	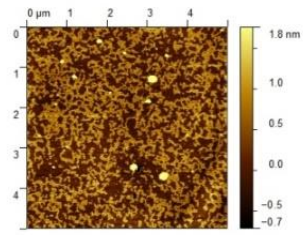	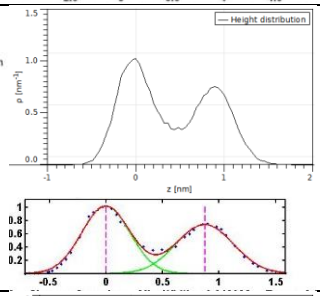	0.874 ± 0.002	46:54	
4	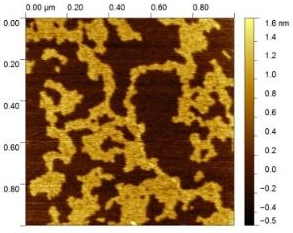	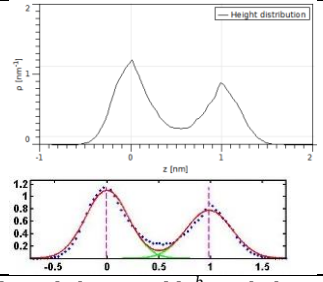	0.985 ± 0.002	43:57	

[a]Flattened AFM image with height scale bar in gold. [b]Height histogram in Gwyddion. [c]Typical peak fit trial of the height histogram in a 100-trial bootstrap fit. Blue dots fit by the dark red line is the total peak fit, light green lines are the component peaks, and magenta dashed lines show the first guess at peak position from the previous trial. [d]Difference between thickness of the thin and thick regions of the membrane reported as the mean difference in the location of the peaks determined by the bootstrap method. The reported uncertainty is the propagated standard deviation from the bootstrap fit of the two bilayer peaks. [e]Ratio of areas of thick and thin membrane regions from the bootstrap average areas of the two bilayer peaks. [f]Average thickness difference from column 4. The reported uncertainty is the standard error of the three values.

Table 11 AFM images, peak fits, and resulting data for 30/40/30 mole % 4Me-16:0-PC/13:0-PC/chol supported lipid bilaye-

#	AFM image[a]	(Top) height histogram[b] (Bottom) peak fit[c]	Difference in thickness between thin and thick membrane regions(nm) [d]	Ratio of areas of thick:thin regions [e]	Avg thickness mismatch (nm) and ratio of areas of thick:thin regions [f]
1	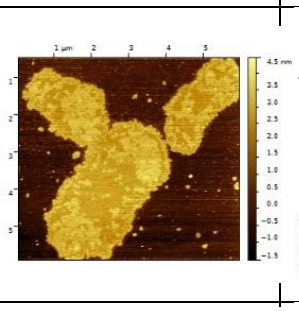	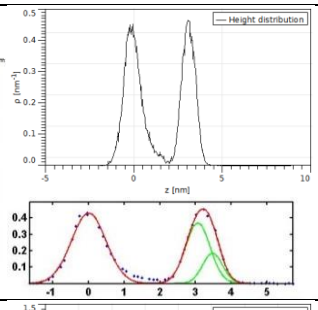	0.413[g]	29:71	0.37 ± 0.07 40:60 ± 8
2[h]	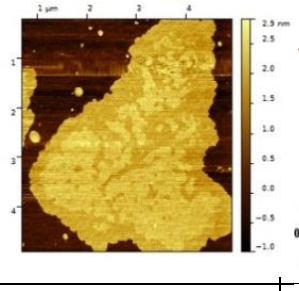	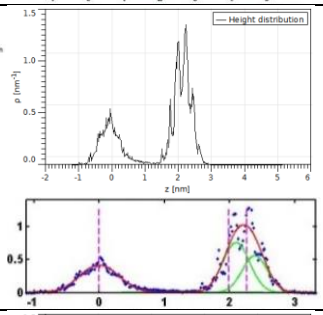	0.392 ± 0.217[i]	41:59	
3[h]	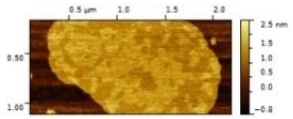	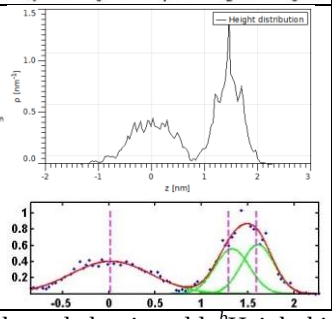	0.296[g]	51:49	

[a]Flattened AFM image with height scale bar in gold. [b]Height histogram in Gwyddion. [c]Typical peak fit trial of the height histogram in a 100-trial bootstrap fit. Blue dots fit by the dark red line is the total peak fit, light green lines are the component peaks, and magenta dashed lines show the first guess at peak position from the previous trial. [d]Difference between thickness of the thin and thick regions of the membrane reported as the mean difference in the location of the peaks determined by the bootstrap method. The reported uncertainty is the propagated standard deviation from the bootstrap fit of the two bilayer peaks. [e]Ratio of areas of thick and thin membrane regions from the bootstrap average areas of the two bilayer peaks. [f]Average thickness difference from column 4. The reported uncertainty is the standard error of the three values. [g]The bootstrap calculation failed to produce a physically-plausible, stable fit. For these two images, we surveyed the trial fits until we found a fit that made physical sense. We then pinned the peak means to the means of these fits and performed a bootstrap fit to determine the areas of the two bilayer peaks. We did not report standard deviations for these fits. [h]The experiment in row 1 was conducted on a different day than the experiments in rows 2 and 3. [i]For this system the bootstrap standard deviation is much larger than the bootstrap interquartile range (IQR), indicating that at least one trial had a significantly different fit. IQR is more robust to outliers. In this case, a better indicator of experimental uncertainty is the standard deviation given by IQR/1.34896 (107).

Table 12 AFM images, peak fits, and resulting data for 20/40/40 mole % 4Me-16:0-PC/13:0-PC/chol supported lipid bilayer

#	AFM image[a]	(Top) height histogram[b] (Bottom) peak fit[c]	Difference in thickness between thin and thick membrane regions(nm) [d]	Ratio of areas of thick:thin regions [e]	Avg thickness mismatch (nm) and ratio of areas of thick:thin regions [f]
1[g]	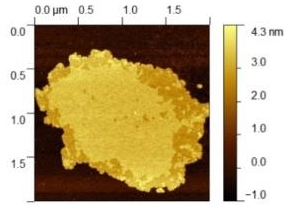	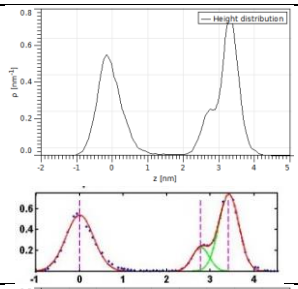	0.642 ± 0.005	79:21	0.59 ± 0.10 75:25 ± 7
2[g]	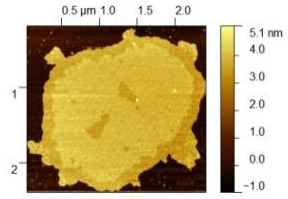	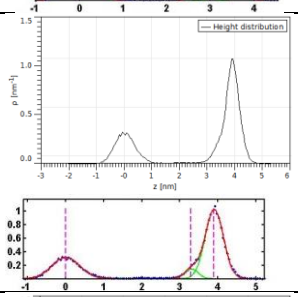	0.592 ± 0.067	90:10	
3[h]	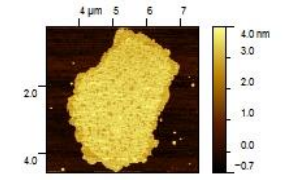	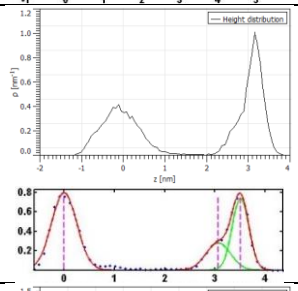	0.450 ± 0.046	66:34	
4[h]	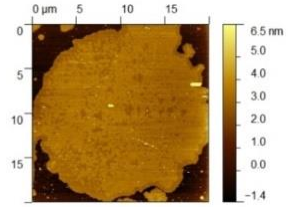	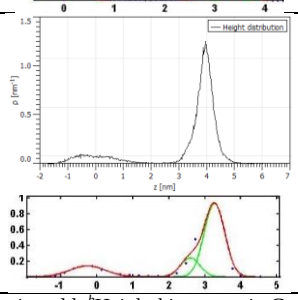	0.676 ± 0.406[i]	65:35	

[a]Flattened AFM image with height scale bar in gold. [b]Height histogram in Gwyddion. [c]Typical peak fit trial of the height histogram in a 100-trial bootstrap fit. Blue dots fit by the dark red line is the total peak fit, light green lines are the component peaks, and magenta dashed lines show the first guess at peak position from the previous trial. [d]Difference between thickness of the thin and thick regions of the membrane reported as the mean difference in the location of the peaks determined by the bootstrap method. The reported uncertainty is the propagated standard deviation from the bootstrap fit of the two bilayer peaks. [e]Ratio of areas of thick and thin membrane regions from the bootstrap average areas of the two bilayer peaks. [f]Average thickness difference from column 4. The reported uncertainty is the standard error of the three values. [g]Vesicles were made without dye. [h]Experiments #3 and #4 were conducted on a different day than #1 and #2. [i]For this system, the bootstrap standard deviation is much larger than the bootstrap interquartile range (IQR), indicating that at least one trial had a significantly different fit. IQR is more robust to outliers. In this case, a better indicator of experimental uncertainty is the standard deviation given by IQR/1.34896 (107).

Table 13 AFM image, peak fits, and resulting data for 55/20/25 mole % 22:1-PC/16:0-PC/chol supported lipid bilayer

AFM image[a]	(Top) height histogram[b] (Bottom) peak fit[c]	Lo-Ld thickness mismatch[d] (nm) and ratio of areas of thick:thin membrane regions[e]
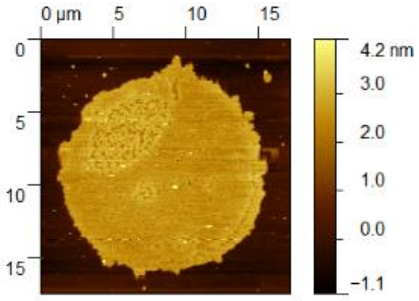	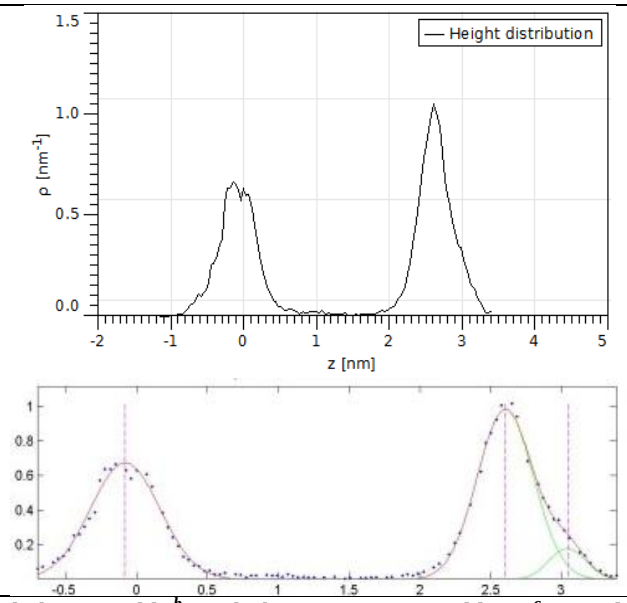	– 0.44 ± 0.01 89:11

[a]Flattened AFM image with height scale bar in gold. [b]Height histogram in Gwyddion. [c]Typical peak fit trial of the height histogram in a 100-trial bootstrap fit. Blue dots fit by the dark red line is the total peak fit, light green lines are the component peaks, and magenta dashed lines show the first guess at peak position from the previous trial. [d]Difference between thickness of the thin and thick regions of the membrane reported as the mean difference in the location of the peaks determined by the bootstrap method. The reported uncertainty is the propagated standard deviation from the bootstrap fit of the two bilayer peaks. [e]Ratio of areas of thick and thin membrane regions from the bootstrap average areas of the two bilayer peaks.

5.4 Table of AFM scans for Chapter 4

Table 14 AFM image, peak fits, and resulting data for 35/35/30 mole % DiPhyPC/DPPC/chol supported lipid bilayer

#	AFM image[a]	(Top) height histogram[b] (Bottom) peak fit[c]	Difference in thickness between thin and thick membrane regions(nm) [d]	Ratio of areas of thick:thin regions [e]	Avg. thickness mismatch (nm) [f] and area ratio of thick:thin regions [f]
1	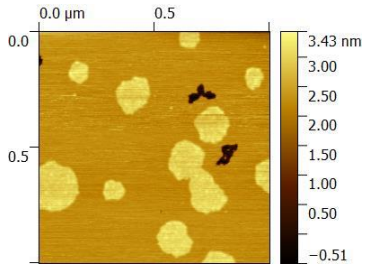	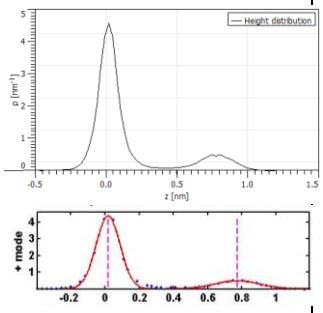	0.757 ± 0.002	17:83	0.94 ± 0.07 40:60 ± 15
2[g]	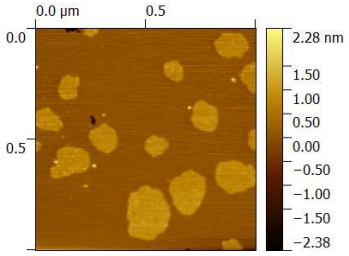	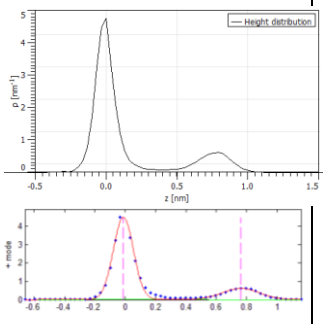	0.773 ± 0.002	20:80	
3	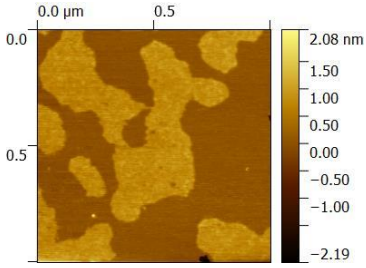	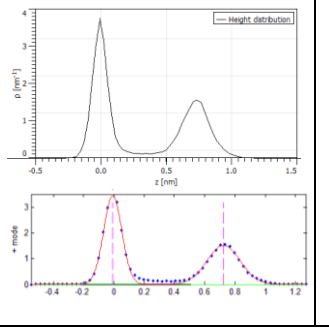	0.732 ± 0.006	45:55	

4	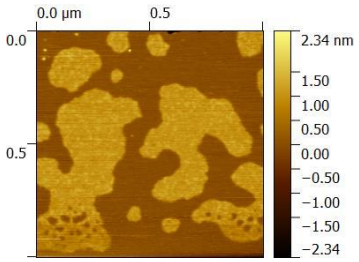	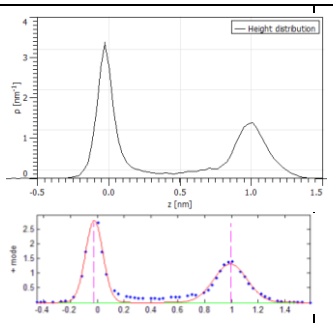	1.018 ± 0.002	47:53	
5	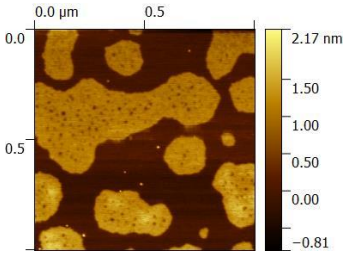	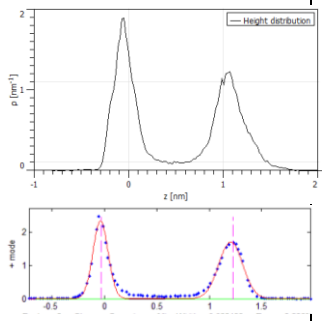	1.243 ± 0.001	53:47	
6	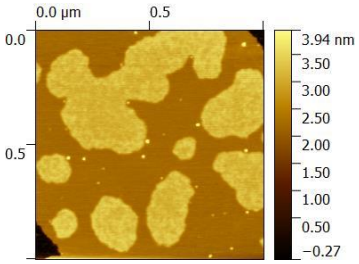	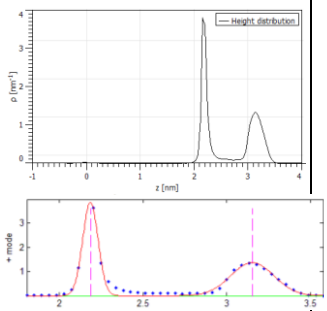	0.962 ± 0.008	50:50	
7	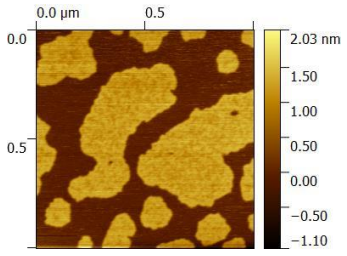	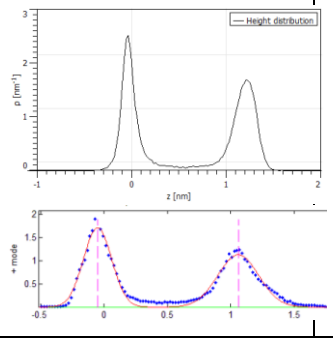	1.111 ± 0.002	49:51	

[a]Flattened AFM image with height scale bar in gold. [b]Height histogram in Gwyddion. [c]Typical peak fit trial of the height histogram in a 100-trial bootstrap fit. Blue dots fit by the dark red line is the total peak fit, light green lines are the component peaks, and magenta dashed lines show the first guess at peak position from the previous trial. [d]Difference between thickness of the thin and thick regions of the membrane reported as the mean difference in the location of the peaks determined by the bootstrap method. The reported uncertainty is the propagated standard deviation from the bootstrap fit of the two bilayer peaks. [e]Ratio of areas of thick and thin membrane regions from the bootstrap average areas of the two bilayer peaks. [f]Average thickness difference from column 4. The reported uncertainty is the standard error of the three values. [g]Tall features were (top 12%) were masked out to exclude from the height histogram.

Table 15 AFM image, peak fits, and resulting data for 46.5/28.5/25 mole % DiPhyPC/DPPC/chol supported lipid bilayer

#	AFM image[a]	(Top) height histogram[b] (Bottom) peak fit[c]	Difference in thickness between thin and thick membrane regions(nm) [d]	Ratio of areas of thick:thin regions [e]	Avg. thickness mismatch (nm) [f] and area ratio of thick:thin regions [f]
1[g]	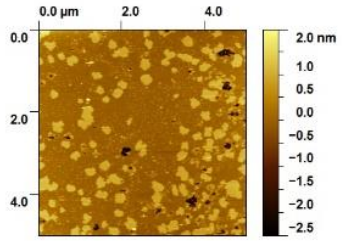	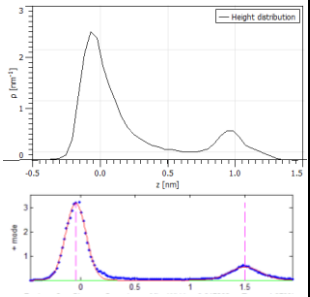	0.952 ± 0.069	24:76	
2	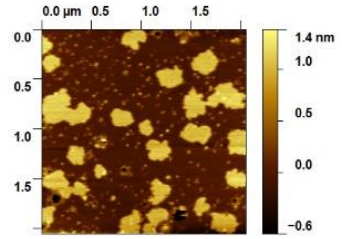	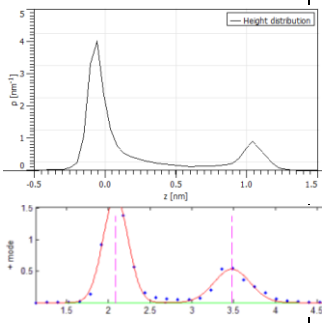	1.093 ± 0.014	24:76	1.06 ± 0.09 24:76 ± 1
3[g]	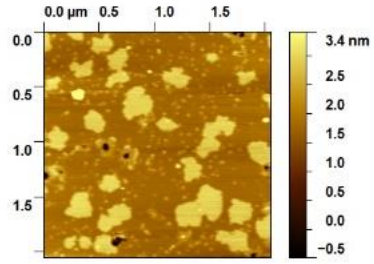	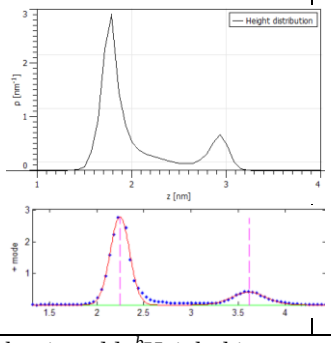	1.129 ± 0.016	22:78	

[a]Flattened AFM image with height scale bar in gold. [b]Height histogram in Gwyddion. [c]Typical peak fit trial of the height histogram in a 100-trial bootstrap fit. Blue dots fit by the dark red line is the total peak fit, light green lines are the component peaks, and magenta dashed lines show the first guess at peak position from the previous trial. [d]Difference between thickness of the thin and thick regions of the membrane reported as the mean difference in the location of the peaks determined by the bootstrap method. The reported uncertainty is the propagated standard deviation from the bootstrap fit of the two bilayer peaks. [e]Ratio of areas of thick and thin membrane regions from the bootstrap average areas of the two bilayer peaks. [f]Average thickness difference from column 4. The reported uncertainty is the standard error of the three values. [g]Tall features were (top 12%) were masked out to exclude from the height histogram.

Table 16 AFM image, peak fits, and resulting data for 52.2/25.3/22.5 mole % DiPhyPC/DPPC/chol supported lipid bilayer

#	AFM image[a]	(Top) height histogram[b] (Bottom) peak fit[c]	Difference in thickness between thin and thick membrane regions(nm) [d]	Ratio of areas of thick:thin regions [e]	Avg. thickness mismatch (nm) [f] and area ratio of thick:thin regions [f]
1	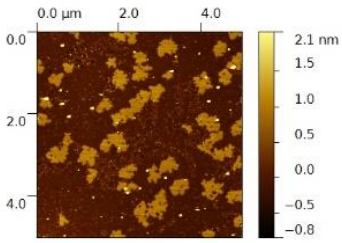	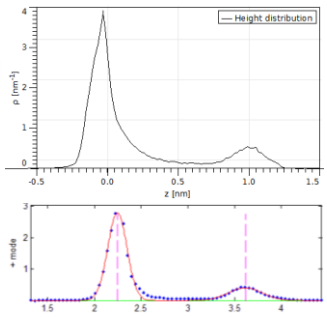	0.952 ± 0.069	20:80	
2[g]	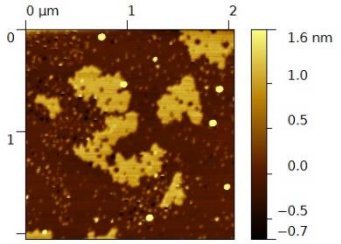	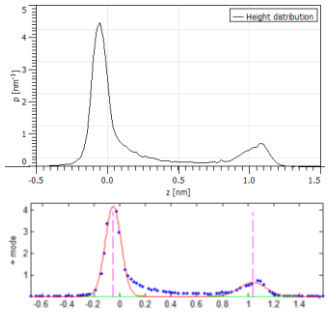	1.088 ± 0.003	21:79	1.03 ± 0.03 26:74 ± 4
3[h]	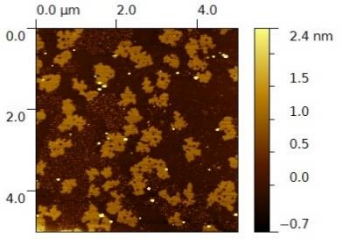	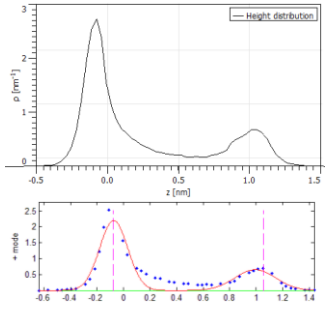	1.1067 ± 0.006	30:70	

4[g]	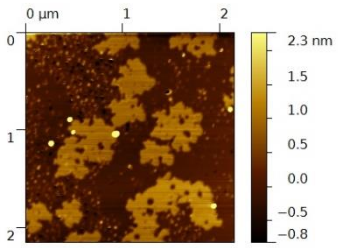	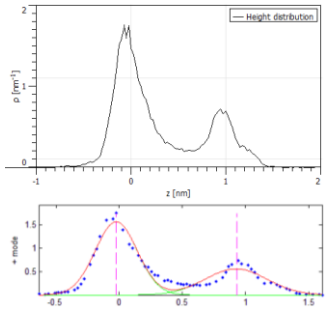	0.956 ± 0.006	34:66	

[a]Flattened AFM image with height scale bar in gold. [b]Height histogram in Gwyddion. [c]Typical peak fit trial of the height histogram in a 100-trial bootstrap fit. Blue dots fit by the dark red line is the total peak fit, light green lines are the component peaks, and magenta dashed lines show the first guess at peak position from the previous trial. [d]Difference between thickness of the thin and thick regions of the membrane reported as the mean difference in the location of the peaks determined by the bootstrap method. The reported uncertainty is the propagated standard deviation from the bootstrap fit of the two bilayer peaks. [e]Ratio of areas of thick and thin membrane regions from the bootstrap average areas of the two bilayer peaks. [f]Average thickness difference from column 4. The reported uncertainty is the standard error of the three values. [g]Tall features were (top 20%) were masked out to exclude from the height histogram. [h]Tall features were (top 12%) were masked out to exclude from the height histogram.

Table 17 AFM image, peak fits, and resulting data for 63.7/18.8/17.5 mole % DiPhyPC/DPPC/chol supported lipid bilayer

#	AFM image[a]	(Top) height histogram[b] (Bottom) peak fit[c]	Difference in thickness between thin and thick membrane regions(nm) [d]	Ratio of areas of thick:thin regions [e]	Avg. thickness mismatch (nm) [f] and area ratio of thick:thin regions [f]
1	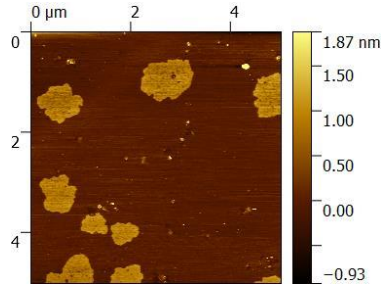	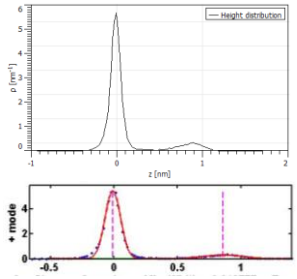	0.873 ± 0.002	13:87	
2	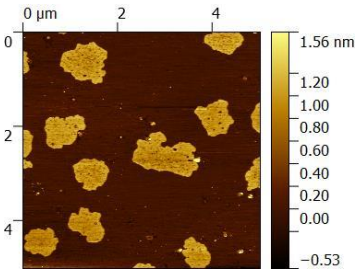	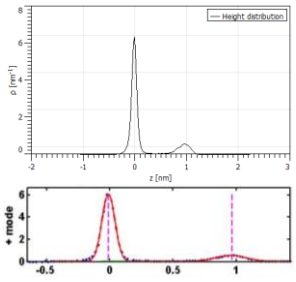	0.966 ± 0.001	18:82	1.01 ± 0.03 12:88 ± 5
3	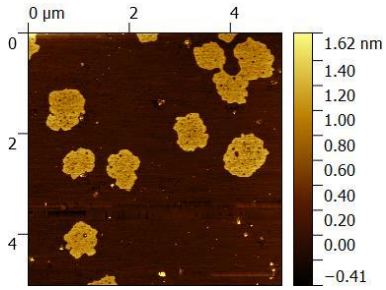	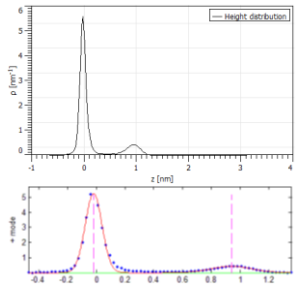	0.959 ± 0.002	16:84	

4	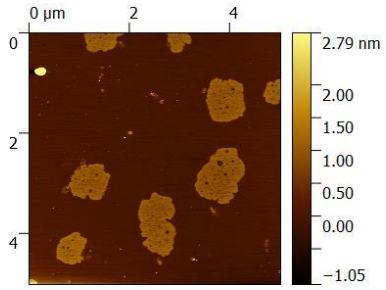	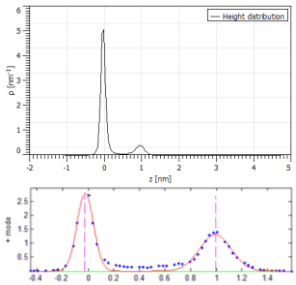	0.979 ± 0.003	14:86	
5	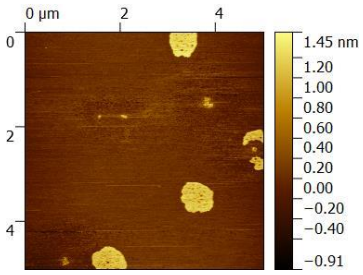	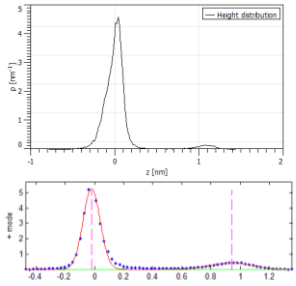	1.076 ± 0.003	4:96	
6	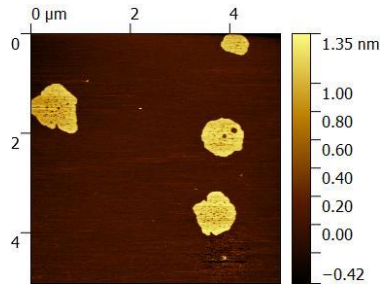	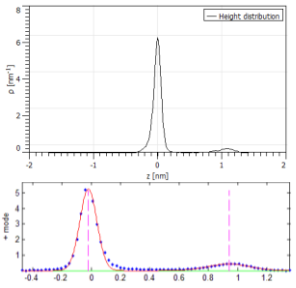	1.067 ± 0.003	8:92	
7	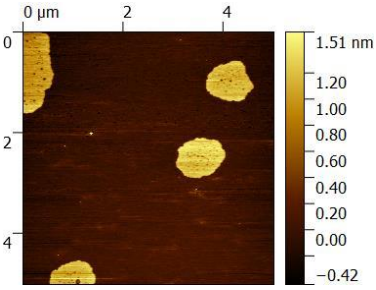	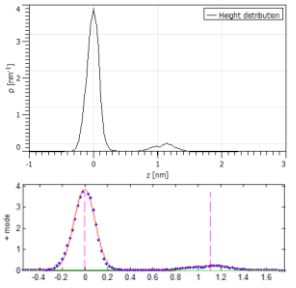	1.113 ± 0.003	9:91	

[a]Flattened AFM image with height scale bar in gold. [b]Height histogram in Gwyddion. [c]Typical peak fit trial of the height histogram in a 100-trial bootstrap fit. Blue dots fit by the dark red line is the total peak fit, light green lines are the component peaks, and magenta dashed lines show the first guess at peak position from the previous trial. [d]Difference between thickness of the thin and thick regions of the membrane reported as the mean difference in the location of the peaks determined by the bootstrap method. The reported uncertainty is the propagated standard deviation from the bootstrap fit of the two bilayer peaks. [e]Ratio of areas of thick and thin membrane regions from the bootstrap average areas of the two bilayer peaks. [f]Average thickness difference from column 4. The reported uncertainty is the standard error of the three values.

Table 18 AFM image, peak fits, and resulting data for 27/23/50 mole % DiPhyPC/DPPC/chol supported lipid bilayer

#	AFM image[a]	(Top) height histogram[b] (Bottom) peak fit[c]	Difference in thickness between thin and thick membrane regions(nm) [d]	Ratio of areas of thick:thin regions [e]	Avg. thickness mismatch (nm) [f] and area ratio of thick:thin regions [f]
1	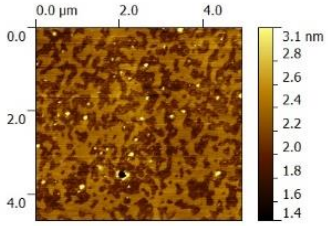	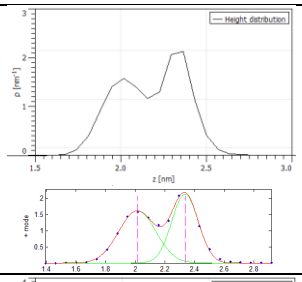	0.322 ± 0.010	49:51	
2	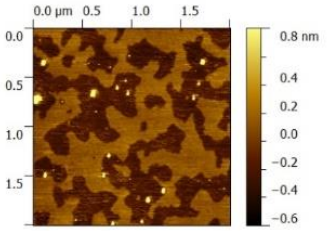	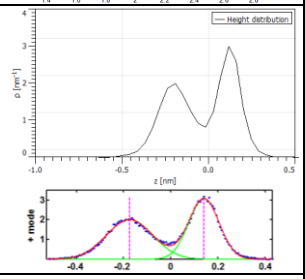	0.316 ± 0.001	50:50	0.320 ± 0.003 49:51 ± 1
3	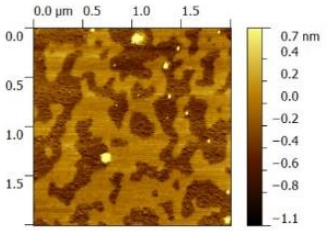	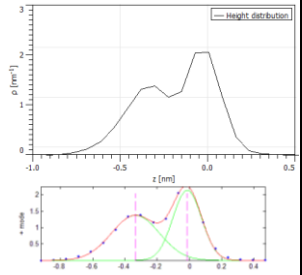	0.321 ± 0.012	48:52	

[a]Flattened AFM image with height scale bar in gold. [b]Height histogram in Gwyddion. [c]Typical peak fit trial of the height histogram in a 100-trial bootstrap fit. Blue dots fit by the dark red line is the total peak fit, light green lines are the component peaks, and magenta dashed lines show the first guess at peak position from the previous trial. [d]Difference between thickness of the thin and thick regions of the membrane reported as the mean difference in the location of the peaks determined by the bootstrap method. The reported uncertainty is the propagated standard deviation from the bootstrap fit of the two bilayer peaks. [e]Ratio of areas of thick and thin membrane regions from the bootstrap average areas of the two bilayer peaks. [f]Average thickness difference from column 4. The reported uncertainty is the standard error of the three values. [g]Tall features were (top 20%) were masked out to exclude from the height histogram. [h]Tall features were (top 12%) were masked out to exclude from the height histogram.

Table 19 AFM image, peak fits, and resulting data for 50/30/20 mole % DiPhyPC/DPPC/chol supported lipid bilayer

#	AFM image[a]	(Top) height histogram[b] (Bottom) peak fit[c]	Difference in thickness between thin and thick membrane regions(nm) [d]	Ratio of areas of thick:thin regions [e]	Avg. thickness mismatch (nm) [f] and area ratio of thick:thin regions [f]
1	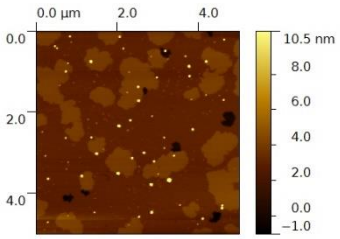	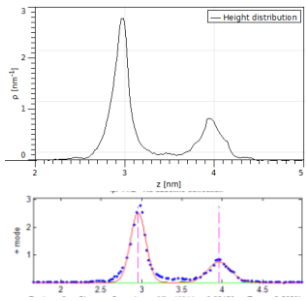	1.002 ± 0.003	30:70	
2[g]	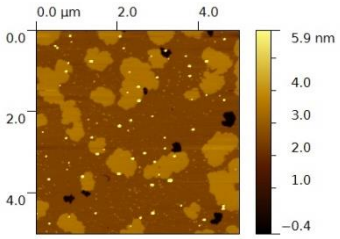	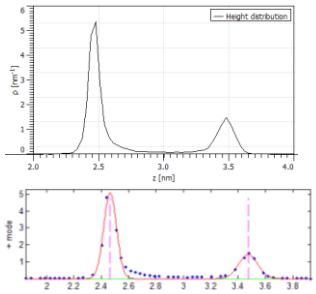	1.010 ± 0.004	29:71	1.003 ± 0.003 31:69 ± 7
3[g]	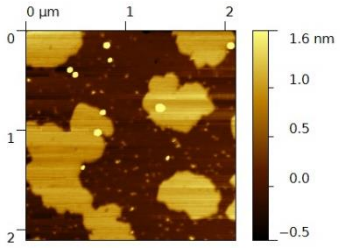	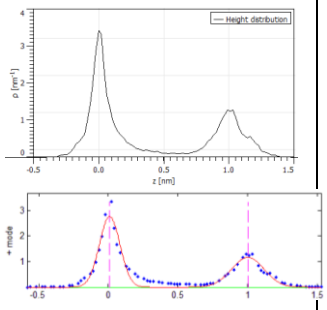	0.997 ± 0.003	41:59	

4[g]	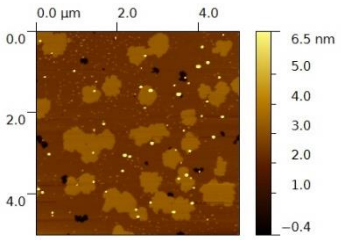	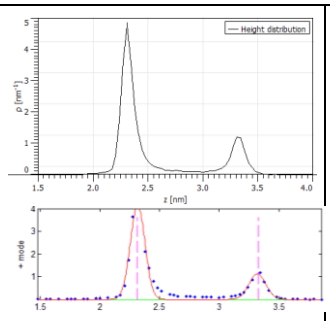	1.003 ± 0.005	24:76	

[a]Flattened AFM image with height scale bar in gold. [b]Height histogram in Gwyddion. [c]Typical peak fit trial of the height histogram in a 100-trial bootstrap fit. Blue dots fit by the dark red line is the total peak fit, light green lines are the component peaks, and magenta dashed lines show the first guess at peak position from the previous trial. [d]Difference between thickness of the thin and thick regions of the membrane reported as the mean difference in the location of the peaks determined by the bootstrap method. The reported uncertainty is the propagated standard deviation from the bootstrap fit of the two bilayer peaks. [e]Ratio of areas of thick and thin membrane regions from the bootstrap average areas of the two bilayer peaks. [g]Tall features were (top 12%) were masked out to exclude from the height histogram

Table 20 AFM image, peak fits, and resulting data for 48/32/20 mol % DiPhyPC/DPPC/chol supported lipid bilayer

#	AFM image[a]	(Top) height histogram[b] (Bottom) peak fit[c]	Difference in thickness between thin and thick membrane regions(nm) [d]	Ratio of areas of thick:thin regions [e]	Avg. thickness mismatch (nm) [f] and area ratio of thick:thin regions [f]
1	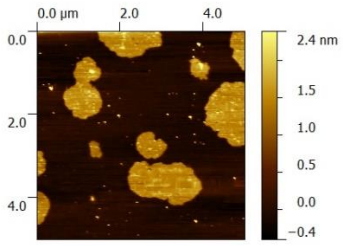	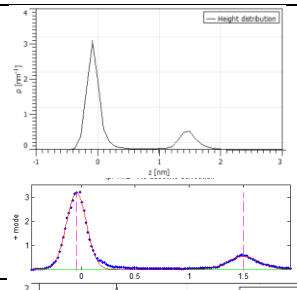	1.542 ± 0.001	21:79	
2	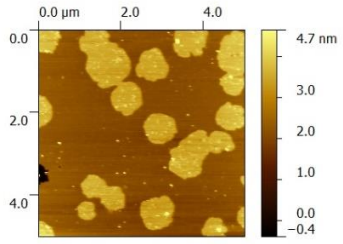	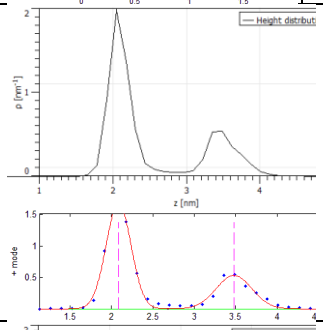	1.391 ± 0.022	31:69	1.43 ± 0.07 24:76 ± 6
3	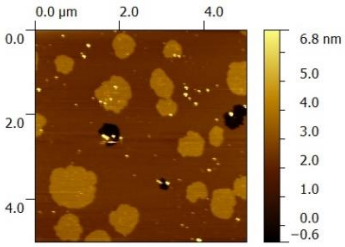	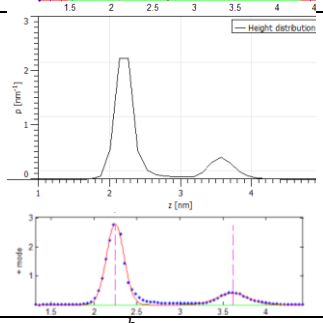	1.370 ± 0.004	20:80	

[a]Flattened AFM image with height scale bar in gold. [b]Height histogram in Gwyddion. [c]Typical peak fit trial of the height histogram in a 100-trial bootstrap fit. Blue dots fit by the dark red line is the total peak fit, light green lines are the component peaks, and magenta dashed lines show the first guess at peak position from the previous trial. [d]Difference between thickness of the thin and thick regions of the membrane reported as the mean difference in the location of the peaks determined by the bootstrap method. The reported uncertainty is the propagated standard deviation from the bootstrap fit of the two bilayer peaks. [e]Ratio of areas of thick and thin membrane regions from the bootstrap average areas of the two bilayer peaks. [f]Average thickness difference from column 4. The reported uncertainty is the standard error of the three values.

REFERENCES

1. **Mouritsen, O.G.** *Life-as a matter of fat: the emerging science of lipidomics.* Springer Science & Business Media, 2005.

2. *Membrane lipids: where they are and how they behave.* **van Meer, G., Voelker, D.R., and Feigenson, G.W.** 2, 2008, Nature Reviews Molecular Cell Biology, Vol. 9, pp. 112-124.

3. *Use of a fluorescent cholesterol derivative to measure lateral mobility of cholesterol in membranes.* **Alecio, M.R, Golan, D.E., Veatch, W.R., and Rando, R.R.** 29, 1982, Proceedings of the National Academy of Sciences, Vol. 31, pp. 5171-5174.

4. **Silvius, Dr. John R.** *Thermotropic Phase Transitions of Pure Lipids in Model Membranes and Their Modifications by Membrane Proteins.* New York : Wiley & Sons, Inc., 1982.

5. *Fluid phase lipid areas and bilayer thicknesses of commonly used phosphatidylcholines as a function of temperature.* **Kučerka, N., Nieh, M.P., and Katsaras, J.** 11, 2011, Biophysica Biochimica Acta, Vol. 1808, pp. 2761-2771.

6. *Bilayer Thickness Mismatch Controls Domain Size in Model.* **Heberle, F.A., Petruzielo, R.S., Pan, J., Drazba, P., Kucerka, N., Standaert, R.F., Feigenson, G.W., Katsaras, J.** 2013, Journal of the American Chemical Society, Vol. 135, pp. 6853-6859.

7. *Liquid-liquid domains in bilayers detected by wide angle x-ray scattering.* **Mills, T.T., Tristram-Nagle, S., Heberle, F.A., Morales, N.F., Zhao, J., Wu, J., Toombes, G.E.S., Nagle, J.F., and Feigenson, G.W.** 2, 2008, Biophysical Journal, Vol. 95, pp. 682-690.

8. *Lipid bilayer thickness varies linearly with acyl chain length in fluid phosphatidylcholine vesicles.* **Lewis, B.A. and Engelman, D.M.** 1983, Journal of Molecular Biology, pp. 211-217.

9. *Effect of cholesterol on structural and mechanical properties of membranes depends on lipid chain saturation.* **Pan, J., Tristram-Nagle, S. and Nagle J.F.** 2, 2009, Physical Review E, Statistical, nonlinear, and soft matter physics, Vol. 80, pp. 021931 - 12.

10. *Modulation of Na,K-ATPase and Na-ATPase Activity by Phospholipids and Cholesterol. I. Steady-State Kinetics.* **Cornelius, F.** 30, Biochemistry, 2001, Vol. 40, pp. 8842-8851.

11. *Functional rafts in cell membranes.* **Simons, K., and Ikonen, E.** 6633, 1997, Nature, Vol. 387, pp. 569-572.

12. *Do more complex organisms have a greater proportion of membrane proteins in their genomes?* **Stevens, T. J., and Arkin, I. T.** 4, 2000, Proteins: Structure, Function, and Bioinformatics, Vol. 39, pp. 417-420.

13. *The fluid mosaic model of the structure of cell membranes.* **Singer, S. J., and Nicolson, G. L.** 1972, Science, Vol. 175, pp. 720-731.

14. *Lipidomics: coming to grips with lipid diversity.* **Shevchenko, A., and Simons, K.** 8, 2010, Nature Reviews Molecular Cell Biology, Vol. 11, pp. 593-598.

15. *Lipid rafts as a membrane-organizing principle.* **Lingwood, D., and Simons, K.** 5961, 2010, Science, Vol. 327, pp. 46-50.

16. *Rafts defined: a report on the Keystone Symposium on Lipid Rafts and Cell Function.* **Pike, L.J.** 7, 2006, Journal of Lipid Research, Vol. 47, pp. 1597-1598.

17. *Cholesterol, lipid rafts, and disease.* **Simons, K., and Ehehalt, R.** 110, 2002, Journal of Clinical Investigation, Vol. 110, pp. 597-603.

18. *Lipid rafts: elusive or illusive?* **Munro, S.** 4, 2003, Cell, Vol. 115, pp. 377-388.

19. *Direct chemical evidence for sphingolipid domains in the plasma membranes of fibroblasts.* **Frisz, J. F., Lou, K., Klitzing, H. A., Hanafin, W. P., Lizunov, V., Wilson, R. L., Carpenter, K.J., Kim, R., Hutcheon, I.D., Zimmerberg, J., Weber, P.K., and Kraft, M.L.** 8, 2013, Proceedings of the National Academy of Sciences of the United States of America, Vol. 110, pp. E613-E622.

20. *Sphingolipid domains in the plasma membranes of fibroblasts are not enriched with cholesterol.* **Frisz, J. F., Klitzing, H. A., Lou, K., Hutcheon, I. D., Weber, P. K., Zimmerberg, J., & Kraft, M. L.** 23, 2013, Journal of Biological Chemistry, Vol. 288, pp. 16855-16861.

21. *Effects of Membrane Thickness on the Molecular Dynamics and Enzymatic Activity of Reconstituted Ca-ATPase.* **Cornea, R.L. and Thomas, D.D.** Biochemistry, 1994, Vol. 33, pp. 2912-2920.

22. *Bilayer Thickness and Membrane Protein Function: An Energetic Perspective.* **Anderson, O.S., and Koeppe II, R.E.** 2007, Annual Review of Biophysics and Biomolecular Structure, Vol. 36, pp. 107-130.

23. *Altering Hydrophobic Sequence Lengths Shows That Hydrophobic Mismatch Controls Affinity for Ordered Lipid Domains (Rafts) in the Multitransmembrane Strand Protein Perfringolysin O*.* **Lin, Q., London, E.** 2, 2012, The Journal of Biological Chemistry, Vol. 288, pp. 1340-1352.

24. *Seeing spots: complex phase behavior in simple membranes.* **Veatch, S. L., and Keller, S. L.** 3, 2005, Biochimica et Biophysica Acta, Vol. 1746, pp. 172-185.

25. *Line tension and interaction energies of membrane rafts calculated from lipid splay and tilt.* **Kuzmin, P. I., Akimov, S. A., Chizmadzhev, Y. A., Zimmerberg, J., and Cohen, F. S.** 2, 2005, Biophysical Journal, Vol. 88, pp. 1120-1133.

26. *Maximum area with Minkowski measures of perimeter.* **Strang, G.** 01, 2008, Proceedings of the Royal Society of Edinburgh: Section A Mathematics, Vol. 138, pp. 189-199.

27. *Closed-Loop Miscibility Gap and Quantitative Tie-Lines in Ternary Membranes Containing Diphytanoyl PC.* **Veatch, S.L. Gawrisch, K. and Keller, S.L.** 2006, Biophysical Journal, Vol. 90, pp. 4428-4436.

28. *Elucidating membrane structure and protein behavior using giant plasma membrane vesicles.* **Sezgin, E., Hermann-Josef, K., Baumgart, T., Schwille, P., Simons, K., and Levental, I.** 6, 2012, Nature Protocols, Vol. 7, pp. 1042-1051.

29. *Critical Fluctuations in Plasma Membrane Vesicles.* **Veatch, S.L., Cicuta, P., Sengupta, P., Honerkamp-Smith, A., Holowka, D., and Baird, B.** 5, 2008, ACS Chemical Biology, Vol. 3, pp. 287-293.

30. *Direct imaging reveals stable, micrometer-scale lipid domains that segregate proteins in live cells.* **Toulmay, A., and Prinz, W. A.** 1, 2013, The Journal of Cell Biology, Vol. 202, pp. 35-44.

31. **Veatch, S.L.** Electro-formation and fluorescence microscopy of giant vesicles with coexisting liquid phases. [book auth.] T. J. McIntosh. *Lipid Rafts.* Totowa : Humana Press, 2007, pp. 59-72.

32. *Preparation of giant vesicles by external AC electric fields. Kinetics and applications.* **Angelova, M. I., Soleu, S., Meleand P, Faucon and J.F., Bothorel.** 1992, Progress in Colloid and Polymer Science, Vol. 89, pp. 127-131.

33. *Liquid general anesthetics lower critical temperatures in plasma membrane vesicles.* **Gray, E., Karslake, J., Machta, B.B. and Veatch, S.L.** 12, 2013, Biophysical Journal, Vol. 105, pp. 2751-2759.

34. *Review: Advances in the characterization of supported lipid films with atomic force microscope.* **Yves F. Dufrene, Gil U Lee.** 2000, Biophysica Biochimica Acta, Vol. 509, pp. 14-41.

35. *Liposome adhesion on mica surface studied by atomic force microscopy.* **Egawa, Hiromi, and Kunio Furusawa.** 5, 1999, Langmuir, Vol. 15, pp. 1660-1666.

36. *Imaging ellipsometry of spin-coated membranes: mapping of multilamellar films, hydrated membranes, and fluid domains.* **Nielsen, M. M. B., and Simonsen, A. C.** 5, 2013, Langmuir, Vol. 29, pp. 1525-1532.

37. *Nonequilibrium Behavior in Supported Lipid Membranes Containing Cholesterol.* **Stottrup, B.L., Veatch, S.L. and Keller, S.L.** 5, 2004, Biophysical Journal, Vol. 86, pp. 2942-2950.

38. *Obstructed diffusion in phase-separated supported lipid bilayers: a combined atomic force microscopy and fluorescence recovery after photobleaching approach.* **Ratto, T. V., & Longo, M. L.** 6, 2002, Biophysical Journal, Vol. 83, pp. 3380-3392.

39. *Morphology of native and reconstituted biological membranes and their components analysed with atomic force microscopy.* **Kolb, H-A., O. Enders, and R. Schauer.** 2, 1999, Applied Physics A: Materials Science & Processing, Vol. 68, pp. 247-254.

40. *Fluid domain patterns in free-standing membranes captured on a solid support.* **Bhatia, T., Husen, P., Ipsen, J.H., Bagatolli, L.A., Simonsen, A.C.** 10, 2014, Biophysical et Biochimica Acta , Vol. 1838, pp. 2503-2510.

41. *Critical point fluctuations in supported lipid membranes.* **Connell, S.D., Heath G., Olmsted, P.D., and Kisil, A.** 2012, Farday Discussions Paper 161/6, pp. 1-21.

42. *Atomic force microscopy of biological membranes.* **Frederix, P. L., Bosshart, P. D., & Engel, A.** 2, 2009, Biophysical Journal, Vol. 96, pp. 329-338.

43. *AFM for structure and dynamics of biomembranes.* **Goksu, E.I., Vanegas, J.M., Blanchette, C.D., Lin, W.C., Longo, M.L.** 1, 2009, Biochimica et Biophysica Acta , Vol. 1788, pp. 254-266.

44. *Visualization of highly ordered striated domains induced by transmembrane peptides in supported phosphatidylcholine bilayers.* **Rinia, H.A., Kik, R.A., Demel, R.A., Snel, M.M.E., Killian, J.A., van der Eerden, J.P.J.M., and de Kruijff, B.** 19, 2000, Biochemistry, Vol. 39, pp. 5852-5858.

45. *Visualizing detergent resistet domains in model membranes with atomic force microscopy.* **Rinia, H.A., Snel, M.M., van der Eerden, J.P.J.M., and de Kruijff, B.** 1, 2001, FEBS Letter, Vol. 501, pp. 92-96.

46. *Phase Topology and Growth of Single Domans in Lipid Bilayers.* **Giocondi, M.C., Vié, V., Lesniewska, E., Milhiet, P.E., Zinke-Allmang, M., Le Grimmellec, C.L.** Langmuir, 2000, Vol. 17, pp. 1653-1659.

47. *Local Mobility in Lipid Domains of Supported Bilayers Characterized by Atomic Force Microscopy and Fluorescence Correlation Spectroscopy.* **Burns, A.R., Frankel, D.J., Buranda, T.** 2, Biophys J, 2005, Vol. 89, pp. 1081-1093.

48. *Effect of Line Tension on the Lateral Organization of Lipid Membranes.* **García-Sáez, A.J., Chiantia, S. and Schwille, P.** 2007, The Journal of Biological Chemistry, Vol. 282, pp. 33537-33544.

49. *Nano-scale mechanical probing of supported lipid bilayers with atomic force microscopy.* **Das, C., Sheikh, K.H., Olmsted, P.D., and Connell, S.D.** 4, 2010, Physical Review E, Vol. 82, p. 041920.

50. *Direct evidence of lipid rafts by in situ atomic force microscopy.* **Mingjun, Cai, Zhao, Weidong, Shang, Xin, Jiang, Juanguang, Ji, Hongbin, Tang, Zhiyong, and Wang, Hongda.** 8, 2012, Small, Vol. 8, pp. 1243-1250.

51. *Review: Advances in the characterization of supported lipid films with atomic force microscope.* **Dufrêne, , Y.F. and Lee G.U.** 2000, Biophysica Biochimica Acta, Vol. 509, pp. 14-41.

52. **Howland, R., and Benatar, L.** *A Practical Guide: To Scanning Probe Microscopy.* Park scientific instruments, 1996.

53. *Photothermal excitation for improved cantilever drive performance in tapping mode atomic force microscopy.* **Labuda, A., Cleveland, J., Geisse, N.A., Kocun, M., Ohler, B., Proksch, R., Viani, M.B. and Walters, D.** 3, 2014, Microscopy and Analysis, Vol. 28, pp. S21-S25.

54. *Ethanol effects on binary and ternary supported lipid bilayers with gel/fluid domains and lipid rafts.* **Marquês, J. T., Viana, A. S., and De Almeida, R. F.** 1, 2011, Biochimica et Biophysica Acta, Vol. 1808, pp. 405-414.

55. **Pittenger, B., Erina, N., Su, C.** *Application Note #128 Quantitative Mechanical Property Mapping at the Nanoscale with PeakForce QNM.* Santa Barbara, CA : Bruker Corporation, 2012.

56. **Instruments, Asylum.** *blueDriveTM Photothermal Excitation.* Santa Barbara, CA : Oxford Instruments.

57. *Kinetics of degradation of dipalmitoylphosphatidylcholine (DPPC) bilayers as a result of vipoxin phospholipase A 2 activity: An atomic force microscopy (AFM) approach.* **Konstantin, B., Atanasov, V., Mitewa, M., Petrova, S. and Bjørnholm, T.** 1, 2011, Biochimica et Biophysica Acta, Vol. 1808, pp. 191-198.

58. *AFM study of interaction forces in supported planar DPPC bilayers in the presence of general anesthetic halothane.* **Leonenko, Z., Eric F., and Cramb, D.** 8, 2006, Biochimica et Biophysica Acta, Vol. 1758, pp. 487-492.

59. *The growth of bilayer defects and the induction of interdigitated domains in the lipid-loss process of supported phospholipid bilayers.* **Fang, Y., and Yang, J.** 2, 1997, Biochimica et Biophysica Acta, Vol. 1324, pp. 309-319.

60. *High-resolution AFM of membrane proteins directly incorporated at high density in planar lipid bilayer.* **Milhiet, P.E., Gubellini, F., Berquand, A., Dosset, P., Rigaud, J.L., Le Grimellec, C., and Lévy, D.** 9, 2006, Biophysical Journal, Vol. 91, pp. 3268-3275.

61. **Eaton, P. and West, P.** *Atomic force microscopy.* New York : Oxford University Press, 2010.

62. *Gwyddion: an open-source software for SPM data analysis.* **Nečas, D., Klapetek, P.** 1, Cent. Eur. J. Phys., 2012, Vol. 10, pp. 181-188.

63. *Emerging roles for lipids in shaping membrane-protein function.* **Phillips, R., Ursell, T., Wiggins, P., and Sens, P.** 7245, 2009, Nature, Vol. 459, pp. 379-385.

64. **Heimburg, T.** *Thermal biophysics of membranes.* Weinheim : John Wiley & Sons, 2008.

65. *Revitalizing membrane rafts: new tools and insights.* **Simons, K., and Gerl, M. J.** 10, 2010, Nature Reviews Molecular Cell Biology, Vol. 11, pp. 688-699.

66. *Area per lipid and acyl length distributions in fluid phosphatidylcholines determined by 2 H NMR spectroscopy.* **Petrache, H. I., Dodd, S. W., and Brown, M. F.** 6, 2000, Biophysical Journal, Vol. 79, pp. 3172-3192.

67. *Dependence of lipid membrane phase transition temperature on the mismatch of protein and lipid hydrophobic thickness.* **Sperotto, M. M., and Mouritsen, O. G.** 1, 1988, European Biophysics Journal, Vol. 16, pp. 1-10.

68. *An introduction to biological membranes: from bilayers to rafts.* **Stillwell, W.** London : Elsevier, 2013.

69. *Areas of monounsaturated diacylphosphatidylcholines.* **Kučerka, N., Gallová, J., Uhríková, D., Balgavý, P., Bulacu, M., Marrink, S. J., & Katsaras, J.** 7, 1926-1932, Biophysical Journal, Vol. 97.

70. *Effect of hydrophobic mismatch on phase behavior of lipid membranes.* **Wallace, E. J., Hooper, N. M., and Olmsted, P. D.** 11, 2006, Biophysical Journal, Vol. 90, pp. 4104-4118.

71. *Registered and Antiregistered Phase Separation of Mixed Amphiphilic Bilayers.* **Williamson, J.J., and Olmsted, P.D.** 8, 2015, Biophysical Journal, Vol. 108, pp. 1963-1976.

72. *Lipid peroxides promote large rafts: effects of excitation of probes in fluorescence microscopy and electrochemical reactions during vesicle formation.* **Ayuyan, A. G., and Cohen, F. S.** 6, 2006, Biophysical Journal, Vol. 91, pp. 2172-2183.

73. *Experimental observations of dynamic critical phenomena in a lipid membrane.* **Honerkamp-Smith, A. R., Machta, B. B., & Keller, S. L.** 26, Physical Review Letters, Vol. 108, p. 265702.

74. *Physicochemical characterization of 1, 2-diphytanoyl-sn-glycero-3-phosphocholine in model membrane systems.* **Lindsey, H., Petersen, N. O., and Chan, S. I.** 1, 1979, Biochimica et Biophysica Acta , Vol. 555, pp. 147-167.

75. **Marsh, D.** *CRC Handbook of Lipid Bilayers.* Boca Raton, FL : CRC Press, 1990.

76. *Minimal effect of lipid charge on membrane miscibility phase behavior in three ternary systems.* **Blosser, M. C., Starr, J. B., Turtle, C. W., Ashcraft, J., and Keller, S. L.** 12, 2013, Biophysical Journal, Vol. 104, pp. 2629-2638.

77. *Coarsening dynamics of domains in lipid membranes.* **Stanich, C.A., Honerkamp-Smith, A.R., Putzel, G.G., Warth, C.S., Lamprecht, A.K., Mandal, P., Mann, E., Hua, T.D. and Keller, S.L.** 2, 2013, Biophysical Journal, Vol. 105, pp. 444-454.

78. *Mapping Nanoscale Variations in Photochemical Damage of Polymer/Fullerene Solar Cells with Dissipation Imaging.* **Cox, P. A., Waldow, D. A., Dupper, T. J., Jesse, S., and Ginger, D. S.** 11, 2013, ACS Nano, Vol. 7, pp. 10405-10413.

79. *Liquid domains in vesicles investigated by NMR and fluorescence microscopy.* **Veatch, S. L., Polozov, I. V., Gawrisch, K., and Keller, S. L.** 5, 2004, Biophysical Journal, Vol. 86, pp. 2910-2922.

80. *Comparison of three ternary lipid bilayer mixtures: FRET and ESR reveal nanodomains.* **Heberle, F.A., Wu, J. Goh, S.L., Petruzielo, R.S., and Feigenson, G.W.** 10, 2010, Biophysical Journal, Vol. 99, pp. 3309-3318.

81. *Phase diagram and tie-line determination for the ternary mixture DOPC/eSM/cholesterol.* **Bezlyepkina, N., Gracià, R. S., Shchelokovskyy, P., Lipowsky, R., and Dimova, R.** 7, 2013, Biophysical Journal, Vol. 104, pp. 1456-1464.

82. *Phase diagram of ternary cholesterol/palmitoylsphingomyelin/palmitoyloleoyl-phosphatidylcholine mixtures: spin-label EPR study of lipid-raft formation.* **Ionova, I. V., Livshits, V. A., and Marsh, D.** 8, 2012, Biophysical Journal, Vol. 102, pp. 1856-1865.

83. *Role of curvature and phase transition in lipid sorting and fission of membrane tubules.* **Roux, A., Cuvelier, D., Nassoy, P., Prost, J., Bassereau, P., and Goud, B.** 8, 2005, The EMBO Journal, Vol. 24, pp. 1537-1545.

84. *Phase equilibria in DOPC/DPPC-d 62/cholesterol mixtures.* **Davis, J. H., Clair, J. J., and Juhasz, J.** 2, 2009, Biophysical Journal, Vol. 96, pp. 521-539.

85. *The condensing effect of cholesterol in lipid bilayers.* **Hung, W. C., Lee, M. T., Chen, F. Y., and Huang, H. W.** 11, 2007, Biophysical Journal, Vol. 92, pp. 3960-3967.

86. *Real-time imaging of drug–membrane interactions by atomic force microscopy.* **Berquand, A., Mingeot-Leclercq, M. P., and Dufrene, Y. F.** 2, 2004, Biochimica et Biophysica Acta , Vol. 1664, pp. 198-205.

87. *Domain shapes, coarsening, and random patterns in ternary membranes.* **Jensen, M.H., Morris, E.J., and Simonsen, A.C.** 2007, Langmuir, Vol. 23, pp. 8135-8141.

88. *The partition of cholesterol between ordered and fluid bilayers of phosphatidylcholine: a synchrotron X-ray diffraction study.* **Chen, L., Yu, Z., and Quinn, P. J.** 11, 2007, Biochimica et Biophysica Acta, Vol. 1768, pp. 2873-2881.

89. *Influence of the lipidation motif on the partitioning and association of N-Ras in model membrane subdomains.* **Weise, K., Triola, G., Brunsveld, L., Waldmann, H., and Winter, R.** 4, 2009, Journal of the American Chemical Society, Vol. 131, pp. 1557-1564.

90. *Direct measurement of the mechanical properties of lipid phases in supported bilayers.* **Picas, L., Rico, F., and Scheuring, S.** 1, 2012, Biophysical Journal, Vol. 102, pp. L01-L03.

91. *Structure and dynamics of supported intermembrane junctions.* **Kaizuka, Y., and Groves, J. T.** 2, 2004, Biophysical Journal, Vol. 86, pp. 905-912.

92. *Adhesion promotes phase separation in mixed-lipid membranes.* **Gordon, V. D., Deserno, M., Andrew, C. M. J., Egelhaaf, S. U., and Poon, W. C.** 4, 2008, Europhysics Letters, Vol. 84, p. 48003.

93. *Adhesion stabilizes robust lipid heterogeneity in supercritical membranes at physiological temperature.* **Zhao, J., Wu, J., and Veatch, S. L.** 4, 2013, Biophysical Journal, Vol. 104, pp. 825-834.

94. *Hydrodynamics of particles embedded in a flat surfactant layer overlying a subphase of finite depth.* **Stone, H. A., and Ajdari, A.** 1998, Journal of Fluid Mechanics, Vol. 369, pp. 151-173.

95. *Acyl-chain methyl distributions of liquid-ordered and-disordered membranes.* **Mihailescu, M., Vaswani, R. G., Jardón-Valadez, E., Castro-Román, F., Freites, J. A., Worcester, D. L., ... and White, S. H.** 6, 2011, Biophysical Journal, Vol. 100, pp. 1455-1462.

96. *Membrane organization and lipid rafts.* **Simons, K., and Sampaio, J. L.** 10, 2011, Cold Spring Harbor Perspectives in Biology, Vol. 3, p. a004697.

97. *The challenge of lipid rafts.* **Pike, L.J.** 2008, Journal of Lipid Research.

98. **Lehninger, A., Nelson, D. L., and Cox, M. M.** *Lehninger's Principles of Biochemistry.* W.H. Freeman, 2005.

99. **Alberts, B., Johnson, A., Lewis, J., Raff, M., and Roberts, K.** *Molecular Biology of the Cell 4th Edition.* New York : Garland Science, 2002.

100. *Seeing spots: Complex phase behavior in simple membranes.* **Keller, Sarah L. Veatch and Sarah L.** 2005, Biophysica Biochimica Acta, Vol. 1746, pp. 172-185.

101. *Plasma membranes are poised for activation of raft phase coalescence at physiological temperature.* **Lingwood, Daniel, Jonas Ries, Petra Schwille, and Kai Simons.** 29 , 2008, Proceedings of the National Academy of Sciences, Vol. 105, pp. 10005-10010.

102. *Thickness mismatch of non-canonical Lo-Ld lipid membranes.* **Bleecker, J.V., Cox, P.A., Foster, R.N., Litz, J.P., Blosser, M.C., Castner, D.G., and Keller, S.L.** 2015, submitted.

103. *Lipid rafts as functional heterogeneity in cell membranes.* **Lingwood, D., Kaiser H.J., Levental, I., Simons, K.** Pt. 5, 2009, Biochem. Soc. Trans. , Vol. 37, pp. 955-960.

104. *Lipid rafts as a membrane-organizing principle.* **Lingwood D, Simons K.** 5961, 2010, Science, Vol. 327, pp. 46-50.

105. *Separation of Liquid Phases in Giant Vesicles of Ternary Mixtures of Phospholipids and Cholesterol.* **Veatch, S.L. and Keller, S.L.** 2003, Biophysical Journal, Vol. 85, pp. 3074-3083.

106. *Liquid general anesthetics lower critical temperatures in plasma membrane vesicles.* **Gray, Ellyn, Joshua Karslake, Benjamin B. Machta, and Sarah L. Veatch.** 12, 2013, Biophysical Journal, Vol. 105, pp. 2751-2759.

107. **O'Haver, T.** *Peak Fitter.* http://terpconnect.umd.edu/~toh/spectrum/InteractivePeakFitter.htm, 2015.

108.

109. *Lipids on the frontier: a century of cell-membrane bilayers.* **Edidin, M.** 5, 2003, Nature Reviews Molecular Cell Biology, Vol. 4, pp. 414-418.

110. **Honerkamp-Smith, A.** *Static and Dynamic Properties of Critical Fluctuations in Lipid Bilayers.* ProQuest Dissertations And Theses, 2010. AAT 3431603.

APPENDIX

Electroforming GUVs and Mapping Phase Diagrams

Materials:

All aqueous solutions are prepared using ultrapure water, 18Ω resistance water from an e-pure water purifier.

Lipids, sterols, dyes:

1. Lipids dissolved in chloroform (ex. 10mg/mL DPPC, Avanti Polar Lipids)
2. Sterol dissolved in chloroform (ex. 10mg/mL cholesterol, Sigma Aldrich)
3. Dye dissolved in chloroform (ex. 1mg/mL Texas Red- DHPE, Sigma Aldrich) **(Note 1)**
    a. *Note1: Texas Red – DHPE dye arrives as a solid in a plastic container. To store the dye, extract it from the container by dissolving the dye in clean ethanol. Transfer the ethanol + dye with a glass pipette into a 25mL glass vial, then dry the ethanol out with nitrogen. Place the vial with dye under vacuum for a few hours to ensure all the ethanol is evaporated. Add the correct amount of chloroform to the solid dye to the desired concentration (ex. 1mg/ml) and transfer to a glass storage vial.*

Storing Lipids and dyes:

Store lipids, sterols, and dyes in chloroform in 5mL clear glass v-bottomed vials (Wheaton USA). Seal with 15mm diameter red rubber septa lined with Teflon. **(Note 2 & 3)** To prevent chloroform evaporation, wrap Teflon thread seal tape then Parafilm twice around the cap. Store vials in a minus 20°C (-20°C) freezer for 6 months to a year.

- *Note 2: The Teflon side of the rubber septa is shiny and must face the chloroform, otherwise chloroform can dissolve the rubber and contaminate samples.*

- *Note 3: Lipids can be stored under dry nitrogen or argon to prevent oxidation.*

Plating lipids on ITO slides:

1. Chloroform.
2. Glass container to hold the chloroform. (ex. 25 ml screwtap vials)
3. Disposable culture tubes. (ex. 10x75mm glass culture tubes.)
4. 5 ¾" glass Pasteur pipettes with rubber bulbs
5. 10µL or 25µL glass syringe with 0.1µL tick marks (Hamilton)
6. ITO coated glass slides: unpolished float glass 25x75x1.1mm SiO_2 passivated Indium Tin Oxide coated surface. Rs 100-700Ω (Delta Technologies Limited) CG-90IN-S115.
7. Glass cutter (ex. diamond tip pen glass cutter)
8. Digital multimeter/voltmeter
9. Ethanol, 200 proof anhydrous
10. Lint-free wipes. (ex. nonwoven cellulose paper from Berkshire)
11. Small black binder clips.
12. 0.5mm thick Teflon spacers, 0.5cm wide and 2.5cm tall.**(Note 4)**
    - *Note 4: We make our own Teflon spacers cutting thin Teflon sheets with scissors. We've had successful electroformation with spacers anywhere from 0.3 to 1.5mm thick.*
13. Vacuum grease
14. Tweezers
15. Sharpie

16. Bus bars - thin aluminum sheets. Dimensions 40cm x 1cm x 1mm thick. **(Note 5)**

    - *Note 5: Dimensions of bus bars can vary, but they must thin enough for binder clips to fit over them, and small enough to fit in a lab oven.*

17. Oven-safe glass or plastic container (ex. Pyrex baking dish)
18. Plastic 1mL syringe with #22G ½ needle
19. Glass coverslips for viewing GUV's. (ex. size 25x25-1)
20. High thermal conductivity paste (Omega Engineering Inc.)

Instruments

1. Heating block that can reach 55°C with test tube holder.
2. Desiccator with vacuum pump
3. Oven at 60°C
4. AC function generator. (ex. FG-8002 from EZ Digital) and BNC cable with alligator clips
5. Fluorescence microscope with light source, appropriate filter cube and a CCD camera (ex. Nikon Y-FL microscope with 10x and 40x air objectives, mercury arc lamp, Texas Red HYQ filter cube for Texas Red dye, CoolSnap CCD camera)
6. Software for imaging (ex. MicroManager - open source)
7. Translational stage under the microscope (Parker)
8. Temperature control stage **(See Note 6)**

    - *Note 6: We use a home-built temperature control stage with an Alpha-Omega temperature controller. The stage consists of a Peltier thermoelectric device and*

a thermistor temperature probe (0.2°C accuracy – Sensor Scientific), which is thermally glued to a heat sink beside the sample. (108)

Methods

Mixing Lipids

1. Determine the volume of lipids/dye at desired mol % such that the total mass of lipids is 0.25mg (see Note 7&8**)**
    - *Note 7: Total Moles = 0.00025g/(MW_{Lipid1}* mole %$_{Lipid1}$ + MW_{Lipid2}* mole %$_{Lipid2}$+MW_{chol}* mole %$_{chol}$ +MW_{dye}* mole %$_{dye}$), Volume to add of Lipid1 (in μL) = 100,000* MW_{Lipid1}* mole %*(Total Moles)/(concentration of lipid - ex. 10mg/ml) etc… (Symbols: MW = molecular weight (g/mol), mole % = mole percent ex. 50% =0.5)*
    - *Note 8: We add 0.8 mole % Texas Red DHPE fluorescent dye (Ld-labeled) for a total mole% of 100.8%. Less dye can be used. Other commonly used dyes are Rhodamine DPPE (Ld – labeled) and 16:0 NBD PE (Lo – labeled, but the partitioning is weaker). (Avanti Polar Lipids)*
3. Take lipids, sterols and dyes out of the -20°C freezer and bring vials to room temperature.
4. Rinse out disposable culture tubes (1 per sample) with about ½ mL chloroform using the Pasteur pipette. Dispose of the chloroform in its own waste tube.
5. Rinse the needle end of the 10μL glass syringe with chloroform into the waste tube, then intake clean chloroform in the syringe and expel into the waste. Do this 10 times.

6. Rinse the syringe twice with the desired lipid, cholesterol, or dye and add the designated volume to the culture tube. Wash the syringe 10x with chloroform as before when switching to a new lipid.
7. After adding all the components, add about 4 drops of chloroform to the lipids in culture tube and mix by swirling or with a vortexor. (The volume need not be exact.)
8. Put the culture tubes with lipid solutions in culture tube holdings on the hot plate (55°C) while you prepare your ITO slides. **(Note 9)**
    - *Note 9: if chloroform evaporates while the lipids are on the hot plate add more chloroform and mix with a vortexer again.*

Plating lipids

1. While your lipids are on the hot plate, take ITO slides and break them in half length-wise to make two shorter plates. **(Note 10)**
    - *Note 10: To break the slides, sandwich half of slide between two plexiglass plates (mark the halfway point ahead of time). With a diamond tip pen, scratch the edge of the exposed plate. Apply gentle downward pressure to the exposed half until it pops off.*
2. To determine which side of the plate is conductive, measure the resistance across the surface with the digital multimeter/voltmeter. Place the leads at two different points on the slide and set the voltmeter to measure resistance (Ω symbol). The glass side will give an infinite resistance reading (O.L). The conductive side will register around 100 Ohm for every centimeter in spacing between your leads.

3. Label the non-conductive side using a permanent marker. Flip the plate over and clean the conductive with lint free wipes soaked in 200-proof ethanol. Place the plates on the hot plate next to the lipid samples, conductive side up, and let them warm to 55°C.
4. Meanwhile prepare glass Pasteur pipettes for the plating. Rinse the insides with chloroform and expel into the waste. You will need one clean pipette for each sample.
5. Take one of the ITO slides from the hot plate by pinching the sides at one end (preferably the rough - cut end). Never touch the center of the plate (that's where the lipids are going). Hold the plate steady and parallel to the bench for the next step. (If the plate is tilted you could lose sample.)
6. With a clean glass Pasteur pipette, suck up the lipid/chloroform solution from the test tube and deposit it in the bottom/center of the ITO slide (Figure 3).
7. QUICKLY use the flat exterior of the pipette tip to spread the lipid solution in an even layer along the ITO slide until the chloroform has completely evaporated. Make sure to leave some space at the far end of the slide (the end that you're holding). Do not spread the lipids too close the edges (See Figure 3). If plating has gone well there should be very little opacity and the lipid film should be iridescent (change colors with a change in angle of light). This is the trickiest step and requires some practice. Please refer to the notes for troubleshooting. You can either plate both slides with half of the lipid mixture, or all of the lipid solution on one plate.**(Notes 11)**
    - *Note 11: Common mistakes when plating lipids are: 1.) Not holding the plate flat such that the sample falls off. 2.) Waiting too long between depositing the lipid solution and spreading. This leaves a lipid clump in the center. 3.) Pushing the lipids*

off the plate when spreading. 4.) Not spreading for long enough, (i.e. before all the chloroform has evaporated) such that the lipids pool up. 5.) Not holding the pipette tip parallel to the surface (See Figure 3)

Making sandwiches

1. After plating, use a Pasteur pipette tip dipped in vacuum grease to put a small line of vacuum grease along the edges of the plates from the bottom to where lipid plating ends (See Figure 4). Do this by holding the greased pipette tip perpendicular to the edge of the ITO slide and move the tip diagonally across and down the side.
2. Take two, ~0.5mm thick, 0.5 x 2.5cm Teflon spacers and gently place them on one of the plates over the grease. Align the bottom of the spacer with the bottom edge of the glass and outside edge of the spacer with the outside of the plate (See Figure 4). Be careful not to touch the center of the plate. You can use tweezers for this step. **(Note 12)**
    - *Note 12: Teflon spacers are reuseable. After running samples, wipe the spacers thoroughly with ethanol soaked Kim wipes and transfer the strips to a storage vial filled with ethanol.*
3. Take the other greased ITO slide (without spacers). Flip it over so the conductive side is facing down. Align it so the top of the plate lines up with the end of the Teflon spacers. It should form an offset sandwich with the conductive faces of the ITO going into the sandwich (See Figure 4).
4. Take the binder clips and clip in the center of the offset sandwiches, just beyond Teflon edge to keep the sandwich sealed (See Figure 4).

5. Place the sandwiches into the desiccator and turn the vacuum pump on. At the end of five minutes, seal the desiccator to the outside and keep the sandwiches under vacuum for at least 30 minutes. This step is to evaporate any excess chloroform. **(Note 13)**
    - *Note 13: When the lipid sandwiches are in the vacuum, this is a good place to stop for the day. Sandwiches can be kept under vacuum overnight (provided the vacuum has a tight seal).*

Filling chamber

1. With a pipette tip, place grease in the opening between the two ITO slides on one side of the sandwich.
2. Fill the other side of the chamber with warm water (~60°C oven temperature). Water can be kept in the oven. Try not to get bubbles into the chamber and leave a little space at the top. **(Note 14&15)**
    - *Note 14: Bubbles make batches with much fewer vesicles. If bubbles form when filling the chamber, gently tap the sides of the plate until the bubbles rise to the top and pop.*
    - *Note 15: If you don't notice bubbles before after running electroformation, but see them after, try de-gasing the water.*
3. After the chamber has been filled with water, seal the open side with grease, trying not to leave any bubbles in the chamber.**(Note 16)**
    - *Note 16: To prevent bubbles in the chamber when sealing it, put the grease in the chamber starting from one side, working over to the other side. If bubbles form,*

tap them out of the unsealed portion. Once the plate is sealed there's no easy way to get rid of bubbles.

4. Clean off the excess grease around the chamber. Wipe first with a dry Kim wipe and then a Kim wipe soaked in ethanol. The conductive portion of the ITO slide next the chamber must be clean for the next steps.

Electroformation

1. Clean your aluminum bus bars with a Kim wipe soaked in ethanol
2. Attach the conductive sides of the sandwich (the inside next the grease filled chambers) to the bus bars using small, TIGHT binder clips. You want a little of the conductive side exposed to test conductivity**. (**Figure 5a and b) Don't put more than 4 sandwiches on a pair of bus bars. **(Note 17)**
    - *Note 17: Connectivity between the ITO slides and bus bars are much better if the binder clips are tight*
3. Using the voltmeter, check the resistance between the conductive side of the ITO slide and the bus bar. It should be less than 150 Ohms. If it is higher see notes **(Note 18)**
    - *Note 18:When testing the connection between the ITO plates and the aluminum bus bars, it's important to ensure the resistance is not too high (>150Ω), or vesicles may not form. The resistance reading may be too high because: 1.) The binder clips are not tight enough. Use tighter binders. 2.) There is a grease layer between the slide and the voltmeter. Clean the slides with Kim wipes soaked in ethanol. 3.) There is not enough surface of ITO slide under the binder clip.*

Position the chambers to get more contact between busbars and conductive ITO slide 4.) The bus bars may be dirty. Clean them with Kim wipes soaked in ethanol.

4. Place the bus bars with the filled chambers in an oven safe container and put the system in a 60° oven (above the melting temperature of your high-T_m lipid). **(Note 19)**
    - *Note 19: If you're making GUV's composed of only low-Tm lipids or low-Tm and cholesterol, electroformation can be run at room temperature.*
5. Turn on the generator function, which should be near the oven. With the voltmeter, check that it is set between 0.5 and 1.5V and 10Hz. Connect the each of two alligator clips from the BNC cable to the two bus bars, and make sure they are securely attached. Run the AC field across the bars for 45 minutes to 1 hour. You may have to carefully place the generator cables in a corner of the oven to close the oven door **(Notes 20 & 21)**.
    - *Note 20: Voltmeters don't detect field offsets, but such offsets can affect vesicle growth. Don't touch the offset settings on the generator. If you need to check for offsets, use an oscilloscope.*
    - *Note 21: Shorter run times can make small vesicles. Longer run times (over 90 minutes) commonly produce worse batches – fewer unilamellar vesicles.*

Transferring Vesicles

1. After the vesicles have grown, remove the generator alligator clips from the busbar, and unclip the sandwiches. Keep the samples in the oven.
2. Use a plastic syringe with a #22G ½ needle, extract vesicle solution from the sandwich. You may have to physically peel apart the slide from the spacer to fit the needle. Try to

avoid plugging the needle with grease while extracting the lipids. You don't need to get all of the liquid; the vesicle yields are quite high. Take the lipids up into the syringe slowly.

3. Put lipid contents into warmed test tubes in the oven and dilute 3:1 with warm water. **(Note 22&23)**
    - *Note 22: Dilute the vesicles in whatever solution you ran the vesicles in, unless you want a difference in osmotic pressure. If the vesicles are not taut and spherical, add a little sucrose (ex. 1-10mM) on the inside of vesicles and dilute vesicles in water.*
    - *Note 23: This is one of two dilution steps. If you suspect a low yield, skip this dilution or change dilution factor.*

Viewing Vesicles

1. Put a thin layer of grease on the four edges of a 25x25 glass coverslip. This will be the bottom half of the viewing sandwich. (Make several of these and store in the oven.)
2. Turn on microscope, CCD camera, fluorescent light source, and open imaging software.
3. Turn on the temperature stage and set it to 50-60°C (around oven temperature).
4. Using the syringe, place one drop of diluted lipid mixture in the center of this coverslip and add 9 drops of water. Then top it with another coverslip (no grease on this one) and squeeze the sides of the slips to seal it. **(Note 24)**
    a. *Note 24: Do not push down on the sandwich. The lipid solution will leak out.*

5. Transfer the sealed coverslips to a heated stage under the fluorescence microscope. To attach the coverslip to the stage, spread a thin layer of conductive glue on the stage and place the coverslip sandwich over it.
6. To get good thermal contact between the stage and coverslip slowly push the coverslips back and forth across the thermal glue with tweezers, until you see a good seal of glue. Do not push down on the sandwich this cases the liquid to leak. Do not push up or the two coverslips may slide apart. **(Note 25&26)**
    - *Note 25: When the vesicles are first put on the temperature controller there may be a lot of motion from convection currents. Wait a few seconds and this should slow down. If the vesicles keep moving, you may have a leak in the grease or uneven connection with the thermal glue. Try carefully squeezing the sandwich together laterally and/or moving the sandwich around the plate to get a better connection with the glue. If matters don't improve, grab a new plate.*
    - *Note 26: Some of the success in electroformation is just practice. Commonly the first 5-10 tries don't yield many vesicles. If your first few batches don't work, try again with an easier system like 100% Egg PC and go back to phase separated system once you can consistently make Egg PC vesicles.*

Finding transition temperature

1. Starting with the temperature stage at 50-60°C, cool the system down and take a sweep of temperatures every 5-10 °C to determine what range you start to see phase separation (polka dots of a different phase appear). **(Notes 27 -30)**

- *Note 27: You can view vesicles in the eye piece or with the imaging software. Be sure the light source is bright enough to capture clear images and remember that the vesicles are floating in all directions. You may have to increase the frame rate to prevent pictures from being blurry. It will take practice to get clear pictures.*
- *Note 28: You are looking for phase separation in giant spherical unilamellar (1-bilayer thick) vesicles. Do not count vesicles with bright pieces of crud around or inside of them, vesicles within vesicles or vesicles that are not spherical (ex. hot dog shaped).*
- *Note 29: If the system is low in cholesterol (< 30%) and phases are not circular or do not merge, the system may have a gel/liquid phase (See* Figure *2a).*
- *Note 30: Depending on composition of vesicles, drastic temperature changes (greater than 10°C in less than 30 seconds) can lead to vesicle popping. Do not lower the temperatures too quickly.*

2. After you've taken a sweep, get a fresh coverslip sandwich with vesicles and go to lowest temperature you swept BEFORE you saw phase separation. Slowly lower 1-2 degrees at a time until you start to see phase separation. Wait 1-2 minutes at given temperature for the system to reach thermal equilibrium.
3. Once you first see phase separation, sweep across your sample randomly, and count the number of phase separated and non- phase separated vesicles at a given temperature. You'll want to count at least 20 vesicles to get an idea of the percentage of vesicles that are phase separated in the sample. **(Notes 31 – 33)**

- *Note 31: Out of focus bright crud can look like phase separation, but it should resolve as you change the focus. Try varying the temperature to see if it goes away at high temperatures and appears at lower temperature. If it does not disappear and reappear, then it's not a phase.*
- *Note 32: For unsaturated lipids like DOPC, light exposure can cause photo-oxidation and change phase behavior. For systems with double bonds, use as little light as possible (ex. use more ND filters and increase the bin number and/or exposure time using the imaging software to make up for less light). Switch to new sample plates more often.*
- *Note 33: Visible phases will be at least a few microns in diameter*

4. Continue to count the percent of phase separated vesicles at several different temperatures spaced 0.5°C or so apart. Try to have 5 temperature points between which 10 and 90% of the population is phase separated. This may not be possible if the range is quite narrow. **(Note 34-37)**
    - *Note 34: Avoid looking at vesicles close to the coverslip sandwich edge (where the grease it) or near bubbles.*
    - *Note 35:The temperature at which phases disappear can appear to be higher than the temperature they appear, due to hysteresis. I take % phase separated at a higher temperature, increase the temperature above the transition temperature and lower again to desired temperature.*

- *Note 36:* Cycling temperature above and below the transition several times can cause the vesicles to become flaccid. Often, domains in flaccid vesicles do not merge. As a result, it can seem like the transition temperature is shifting.. *To be safe, switch to a new plate after cycling 3-4 times.*
- *Note 37: When they are first made, vesicles are taut, but get more unstable over time, and take on strange geometries, like hotdogs instead of spheres. Don't observe vesicles for more than 4 hours after electroformation or when you start to see these weird geometries (whichever comes first).*

5. Try to repeat this with a different batch (made from a different plate) of the same composition, to ensure batch to batch consistency.
6. Plot % phase separated versus temperature. It should be a sigmoidal function spanning 0% phase separated at high temperatures to 100% phase separation at lower temperatures. The reported transition temperature is the temperature at which 50% of the vesicles in the population are phase separated. The uncertainty in the measurement is the span of temperatures between where 10% and 90% are phase separated. **(Notes 38&39)**
    - *Note 38: The differences in transition temperature come from slight compositional differences in the vesicles. How composition differences affect transition temperatures depends where it is in the phase diagram.*
    - *Note 39: For well-behaved systems (ex. most canonical raft systems), the error should be within 1-2 °C. For more difficult systems, systems which don't readily form vesicles or where there is more compositional variation, it may be greater.*

Mapping phase diagrams

1. For each starting composition you should have a transition temperature at which 50% of the vesicles have phase separated.
2. Print out a Gibbs Phase triangle with 10% marks and record the transition temperatures at a given composition. By convention the high-Tm lipid is in the bottom right corner, the low-Tm is in the bottom left corner, and cholesterol is at the top.
3. To decide what compositions to check, fan outwards varying in steps of 10 mole % from a starting point near the center of phase diagram (ex. 40/40/20). Keep fanning outward until you see no phase separation or reach a binary axis.
4. Once you have plotted your temperatures verify that it is well behaved **(Note 40)**
    - *Note 40: Features of ternary phase diagram: 1.) To date, our group has never observed liquid-liquid phase separation phase separation of GUV's at the lipid/chol binary axes. 2.) Above 66% is inaccessible for vesicles containing most PC-lipids. This value of the cholesterol solubility is smaller for vesicles rich in DiPhyPC and most PE-lipids, and is not known for all lipid types. 3.) At very high % of the high melting temperature the vesicle is found in one solid phase is one solid phase 4.) At low %cholesterol (usually <20 mole %) there is a solid-liquid coexistence region. The solid domains appear dark and are usually non-circular 5.)There may be a 3 phase region between solid-liquid and liquid-liquid, however this it is difficult to confirm via fluorescence of GUV's. If circular domains merge at the edges but do not coalesce to one bigger phase, they may be in a three phase region. 6.) At temperatures above the solid/liquid or three-phase region there is a liquid-liquid*

region. At high fractions of high-T_{melt} lipid the vesicles are mostly dark phase. At high fractions of the low-Tm lipid, the vesicles are mostly bright phase. 7.) In the liquid/liquid phase separating regime, there should only be one maximum transition temperature (one mountain peak). If you see more than one, rerun the temperatures around the peaks.

5. To get more specific feature information like phase boundaries, you can take data at smaller compositional changes than 10%. However composition range in a batch of GUV's is usually a few mole %.
6. You can plot phase diagrams by hand or use software like Matlab to make surface plots.

Figure 34 Plating lipids.

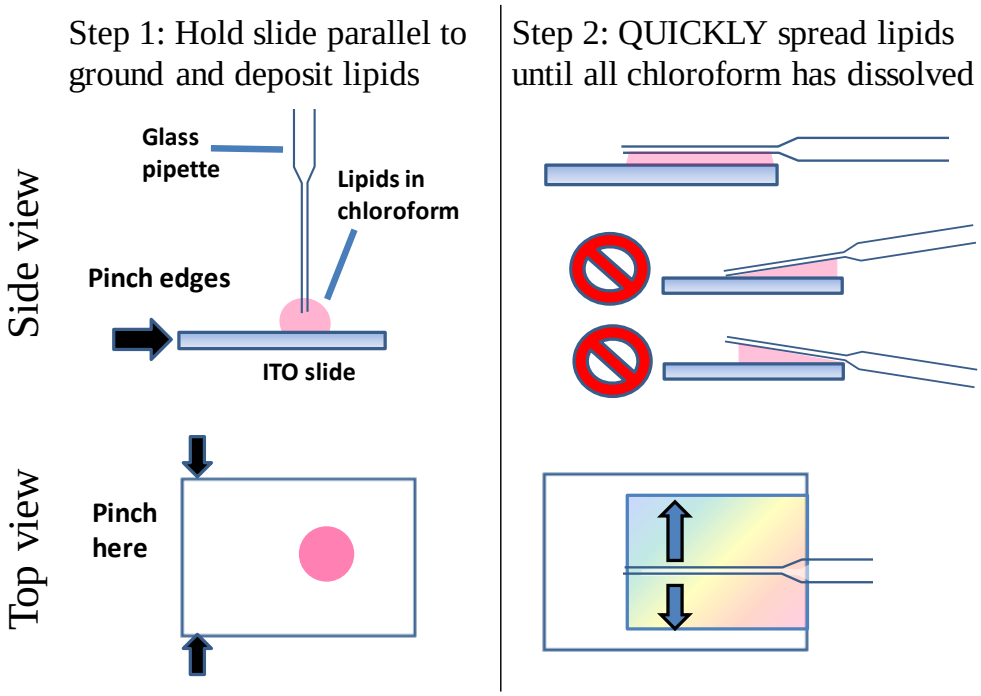

Figure 35 Making electroformation chambers

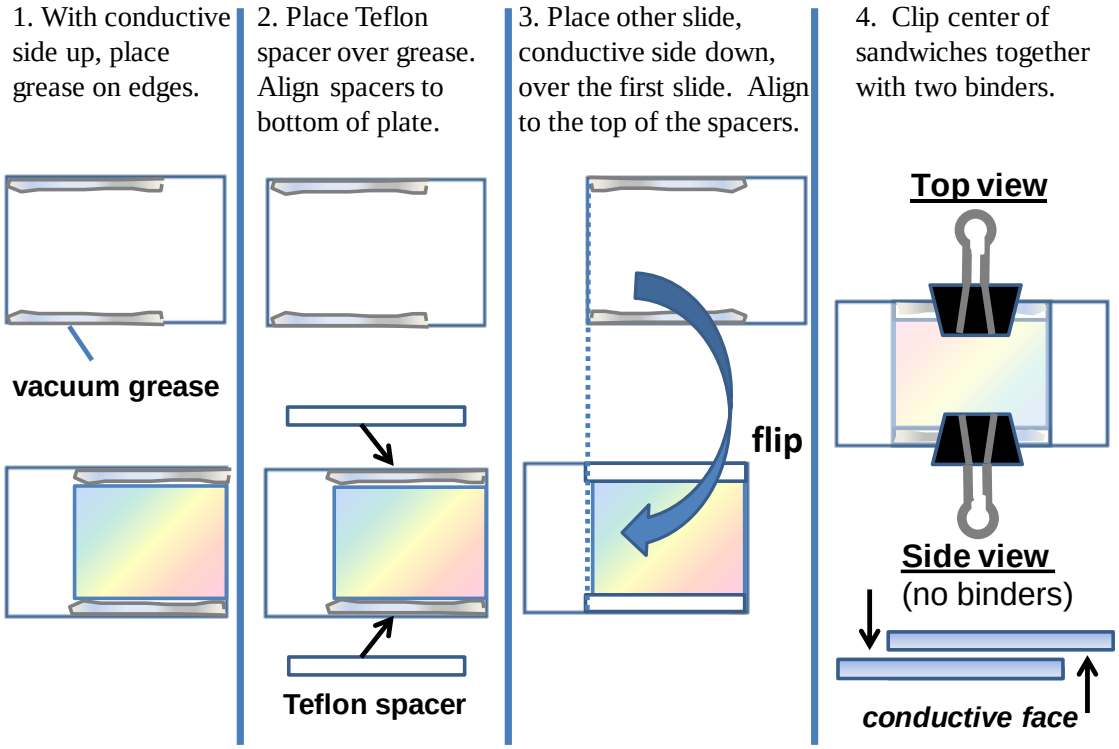

Figure 36 Attaching chambers to bus bars. (A) With black binder clips, clip the conductive sides of the ITO to the aluminum bus bars. (B) Using the voltmeter, check that the conductivity between the ITO slide and bus bars is less than 150 Ohms. (C) Up to four chambers can be clipped to a set of bus bars.